UNIVERSITEIT VAN PRETORIA
UNIVERSITY OF PRETORIA
YUNIBESITHI YA PRETORIA

DESIGN AND IMPLEMENTATION OF A CONTINUOUS POLYTETRAFLUOROETHYLENE DEPOLYMERISATION SYSTEM:

Moving from batch to semi-automated continuous TFE production

Anya Bezuidenhoudt

University of Pretoria
MEng (Chemical Engineering) Dissertation

UNIVERSITEIT VAN PRETORIA
UNIVERSITY OF PRETORIA
YUNIBESITHI YA PRETORIA

DESIGN AND IMPLEMENTATION OF A CONTINUOUS POLYTETRAFLUOROETHYLENE DEPOLYMERISATION SYSTEM

Moving from batch to semi-automated continuous TFE production.

Author: Miss Anya Bezuidenhoudt

Supervisor: Prof PL Crouse

Sub-supervisor: Mr PW Sonnendecker

Dissertation submitted in fulfilment of the requirements for the degree Master of Engineering (Chemical Engineering) at the University of Pretoria.

Faculty of Engineering, Built Environment & IT
Department of Chemical Engineering

November 2016

Synopsis

At the University of Pretoria's Fluoropolymer Laboratory, an important long-term project is the development of a waste polytetrafluoroethylene (PTFE) depolymerisation process where TFE can be produced, purified and polymerised to reproduce pure PTFE. At the start of this project, the process consisted of a batch depolymerisation system, a sub-zero distillation column, and a polymerisation reactor system. The batch depolymerisation system could not produce enough gas per session to operate the downstream processes efficiently. The main aim of this investigation was to adapt the batch depolymerisation system to enable continuous depolymerisation by designing, implementing and testing a continuous PTFE screw feeder. With the screw feeder in place, the operating limits, with regard to temperature, pressure, and Teflon® PTFE 807N feed rate, were determined. The effects of temperature and pressure on the tetrafluoroethylene (TFE), hexafluoropropylene (HFP) and octafluorocyclobutane (OFCB) fractional composition were examined and the optimum operating conditions to maximise these products were determined statistically.

An investigative approach was used in designing the hopper system. The optimum hopper wall angle and Teflon® PTFE 807N feed mixture was determined experimentally by testing four hopper angles, pure Teflon® PTFE 807N, and two Teflon® PTFE 807N mixtures (Teflon® PTFE 807N mixed with larger, compressed Teflon® PTFE 807N, particles in a 70:30 wt % and 50:50 wt % ratio) and two motor speeds. At all of the hopper angles and Teflon mixture configurations, rat-hole formation prevented the feeder from producing a constant flow rate. A hopper wall angle of 20° (to the vertical) together with plain Teflon® PTFE 807N were selected, as these two variables together helped to delay the formation of rat-holes the most. A stirrer was inserted in the hopper to negate the rat-holing problem.

The continuous feeder was successfully designed, manufactured, calibrated, and installed. The feeder consists of a wedge-shaped hopper with a constant pitch, a tapered shaft screw and is capable of providing a maximum Teflon® PTFE 807N flow rate of approximately 20 $g \cdot min^{-1}$ for up to 40 min. Experimental test runs of the continuous depolymerisation system indicated that the minimum operating reactor temperature was 650 °C due to heat transfer and or rate of reaction limitations. The maximum flow rate of Teflon® PTFE 807N was determined to be 11 $g \cdot min^{-1}$ for the current reactor system. The maximum operating temperature and pressure were limited to 750 °C and 40 kPa, respectively, to avoid operating conditions that could lead to the increased production of PFIB.

A three-level full factorial experimental design was used to determine the temperature and pressure effects on the fractional distribution of TFE, HFP, and OFCB under steady operating conditions. For pressure control purposed no carrier gas was used. The PTFE flow rate and

experimental run time were kept constant at 11 g·min^{-1} and 15 min, respectively. The pressure in the system was regulated manually by constricting the flow of product gas out of the system.

A maximum TFE mole percentage of 97 % was achieved at operating conditions of 650 °C and 2 kPa. The maximum HFP mole percentage (31 %) was observed at operating conditions of 750 °C and 20 kPa. A maximum of 55 % was observed at 750 °C and 40 kPa for OFCB.

Statistical analysis of the continuous depolymerisation results indicate that TFE formation is highly sensitive to changes in pressure, with higher TFE yield fractions achieved at low pressures. The production of OFCB is highly sensitive to pressure, whereas the formation of HFP is equally affected by pressure and temperature changes. However, changes in pressure have a larger effect on the HFP production than temperature when operating at pressures lower than approximately 20 kPa. At higher pressures the sensitivity has the inverse affect, with temperature having a larger effect. As opposed to TFE, an increase in temperature and pressure leads to an increase in the HFP and OFCB concentration. To achieve a TFE mole percentages of 95 % and higher, the operating temperature of the system has to be kept in the range of 650 °C – 720 °C, together with a system pressure of 2 kPa or less. Within the operating range of 730 °C – 750 °C and 35 kPa – 40 kPa a mole percentage of 50 % and higher can be expected for OFCB. A mole percentage of 19 % and higher can be expected for HFP in the operating range of 744 °C – 750 °C and 32 kPa – 40 kPa.

It was determined through a kinetic analysis of the system, that the residence time of the product gas in the reactor has a large effect on the production of HFP, with an increase in residence time leading to a sharp increase in the HFP concentration and a decrease in the OFCB and TFE concentrations. Analysis of the determined product specific kinetics indicate that the predominant HFP production pathway at low residence times (< 3 s) is via the reaction of TFE with difluorocarbenes. At higher residence times the dominant reaction pathway is the dissociation OFCB.

Acknowledgements

The author would like to express her sincere gratitude and appreciation to:

My parents, who have always supported and motivated me through everything.

Paul Sonnendecker for his expertise, guidance, and support in building and commissioning the feeder system and his help in solving the unsolvable.

My supervisor, Prof PL Crouse, in providing me with the opportunity to work on this project and his guidance throughout.

The National Research Foundation (NRF) for financial support.

The Fluorochemical Expansion Initiative (FEI) for financial support.

Mr IJ van der Walt at Necsa for his advice on designing and operating the process.

Summary of contents

Contents

List of figures

List of tables

Nomenclature list

Symbol	Description	Unit
d_{crit}	Critical hopper width	
D_{OD}	Outside diameter	(mm)
D_{ID}	Shaft diameter	(mm)
E_{act}	Activation energy	(kJ·mol^{-1})
F	Flight thickness	(mm)
ff	Flow factor	
g	Gravitational acceleration	(9.8 m·s^{-2})
i	Degree of filling factor	
k	Rate coefficient	
k_0	Pre-exponential factor	
m	Shape factor	
n	Motor speed	(rpm)
n_1	Reaction order	
n_{system}	Molar flow rate	(mol·s^{-1})
P	Pitch length	(mm)
P	Reactor pressure	(kPa)
Q	Flow rate	(g·min^{-1})
R	Universal gas constant	(8.314 J·mol^{-1}·K^{-1})
t	Time	(s)
T	Temperature	(°C; K)
$V_{reactor}$	Reactor volume	(m^3)
x	Conversion	
x_i	Actual factor value	
x_H	HIGH factor value	
x_L	LOW factor value	

Symbol	Description	Unit
X_1	Temperature coded value	
X_2	Pressure coded value	
Y_1	TFE response function	
Y_2	HFP response function	
Y_3	OFCB response function	
	Greek	
β	Response function constants	
θ_p	Hopper wall angle	(°)
μ_s	Coefficient of static friction	
ρ_b	Bulk density	(g·cm^{-3})
σ	Stress	
σ_1	Major principal stress	
σ_c	Unconfined yield strength	
φ_e	Angle of internal friction	(°)
φ_x; φ_w	Angle of wall friction	(°)

List of abbreviations

Abbreviation	Description
CSTR	Continuous flow stirred-tank reactor
DEM	Discrete Element Method
FCC	Face Centered Composite
HFE	Hexafluoroethane
HFP	Hexafluoropropylene
KBr	Potassium brominde
$LiTaO_3$	Lithium Tantalate
MIR	Mid-infrared
OFCB	Octafluorocyclobutane
PFIB	Perfluoroisobutene
PFR	Plug Flow Reactor
PT	Pressure sensor
PTFE	Polytetrafluoroethylene
PWM	Pulse Width Modulation
RSM	Response Surface Methodology
SCCM	Standards Cubic Centimetres per Minute
TC	Temperature sensor
VFD	Variable Frequency Drive

1 Introduction

Fluoropolymers are important synthetic materials in science and industry and are used to meet a variety of severe specifications required by modern engineering. The star of all of the industrial fluoropolymers is polytetrafluoroethylene (PTFE) due to its wide range of unique and extraordinary characteristics, which include chemical inertness, insolubility, and a wide operating temperature range. Fluoropolymers, including PTFE, are regarded as high - value products due to the high market demand and the difficulties associated with the production and handling of the monomer tetrafluoroethylene (TFE), the main building block of PTFE and related copolymers. According to a report released by Zion Research in December 2015, the global PTFE market was valued at approximately 4 billion US dollars in 2014 and is expected to be worth around 6.5 billion US dollars by the year 2020.

Due to the non-melt-processability of PTFE resin, a large amount of waste is generated annually, most of which is either incinerated, landfilled, or ground up and ram extruded to produce lower quality tubes and profiles (Simon & Kaminsky, 1998; van der Walt, 2007). These destructive or re-use methods pose economic and environmental issues, particularly when considering the evolution of extremely toxic gases (*eg* perfluoroisobutylene (PFIB)) during the incineration of PTFE. In recent years, methods of PTFE recycling have been investigated, with the main focus on the thermal decomposition of PTFE. This process produces high-value monomers, which include TFE, hexafluoropropylene (HFP) and octafluorocyclobutane (OFCB) (Lewis & Naylor, 1947). Due to the transport and handling restrictions and difficulties of TFE, it has become commercially unavailable (Hercules *et al*, 2014), leading to the requirement of safe, on-site production methods. Since TFE is produced during the decomposition of PTFE, waste PTFE can in principle be used to produce new, high molecular weight PTFE in a multi-unit operation process.

At the University of Pretoria's Fluoropolymer Laboratory, an important long-term project is the development of a waste PTFE depolymerisation process where TFE can be produced, purified and re-polymerised to reproduce pure PTFE. This process consisted of a batch depolymerisation system, a low-temperature distillation column, and a polymerisation reactor system at the start of the project. The batch depolymerisation system was capable of pyrolysing 30 grams of PTFE per session. However, several of these batch runs were required to produce enough raw products to operate the distillation column optimally. This was time-consuming. The batch system also posed controllability issues due to the difficulty in regulating the system pressure, leading to a large variation in the distribution of TFE, HFP, and OFCB in the product stream. Hence, a need arose to adapt the batch system to enable

continuous depolymerisation capable of steady operation under safe, repeatable and controllable conditions.

The main aim of this investigation was to adapt the current batch depolymerisation system to a continuous system by designing, implementing and testing a continuous PTFE screw feeder. With the new feeder in place, the operating limits of the system were determined along with the various operating conditions, regarding temperature and pressure, which would optimise the selectivity of the three main depolymerisation products, namely TFE, HFP, and OFCB. Hence, this report is divided into two parts. Part 1 focuses on the design considerations, testing and implementation of the continuous screw feeder, as well as the operating limits of the continuous system. Part 2 focuses on the experimental determination and discussion of the temperature and pressure effects on the selectivity of TFE, HFP, and OFCB. A brief kinetics analysis of the system is also included.

The main objectives and limitations for each section are as follow:

Part 1: Continuous feeder design, manufacture, and design implementation.

To achieve a successful continuous feeding system the following main objectives and design limitations had to be adhered to:

- The feeder system had to be designed to feed Teflon® PTFE 807N.
- The screw feeder had to be able to operate under vacuum conditions.
- The hopper must have a capacity of at least 1 kg Teflon® PTFE 807N.
- Due to structural stability requirements and in-house manufacturing restrictions, the minimum screw outside diameter was limited to 21.5 mm.
- The screw feeder feed rate was limited by the capacity of a 50 L holding cylinder available for gas collection.
- Due to the unknown effect that forces inside the hopper system may have on the compression of PTFE into the screw, no specific flow rate range was specified for the screw at the onset of the project.
- The PTFE mass flow rate of the feeding system had to be repeatable and relatively constant over a minimum period of 30 min at various motor speeds.
- After feeder implementation, the operating limits regarding temperature, pressure, and PTFE feed rate had to be determined experimentally.

Part 2: Product selectivity analysis: Continuous PTFE depolymerisation.

The main objectives and operating limitations for this section are as follows:

- Experimentally determine temperature and pressure effects on the selectivity of TFE, HFP, and OFCB.
- Statistically analyse the data to select conditions that would favour the production of single and two component systems.
- The maximum operating temperature and pressure for the depolymerisation system were limited to 750 °C and 40 kPa, respectively. These limits were selected as a precaution to avoid conditions that could lead to an increased production of PFIB.
- The total reaction time was limited to 15 min due to gas storage constraints.

Part 1. Continuous feeder design, manufacture and design implementation

In this section, the steps taken to develop the continuous PTFE screw feeder and the alterations made to the current batch system to implement said feeder, are covered. To design an efficient storage hopper using the method developed by Andrew Jenike (1964), the bulk solid flow properties need to be characterised by determining four essential parameters. These parameters are the bulk density, ρ_b, the effective angle of internal friction, φ_e, unconfined yield strength, σ_c, and angle of wall friction, φ_x. However, due to equipment limitations, only the bulk density of Teflon® PTFE 807N could be determined, consequently, it was decided to take an investigative approach in designing the hopper system.

Summary of contents

2 Screw feeder design literature

2.1 Screw feeders

The first screw type conveyor was invented by Archimedes in 287 BC. It consisted of a helically shaped pipe with its lower end placed in water. As the pipe is rotated the water rises up the pipe. Today the same principle of moving material by a helical screw is implemented to transport all sorts of materials, especially solids. The workings of a screw conveyor are quite simple: As the screw is rotated, the material that is resting between two adjacent flights (see Figure 1) is promoted to slip down the face of the 'rising' side of the flight, causing the material to move forward at the rate of one pitch per rotation of the screw. This is true if we assume that the material does not spill over the centre of the shaft to fall back into the preceding pitch space (Bates, 2000).

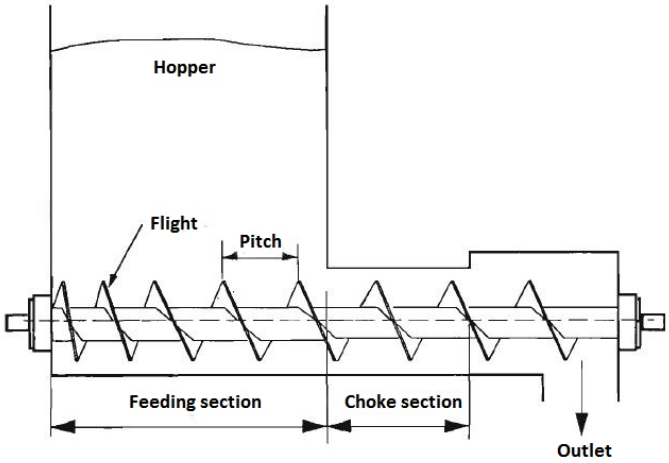

Figure 1: General screw feeder setup (from Bates (2000)).

A wide variety of screw type solid handling devices exists in the industry. All of these devices operate using the same principle but are divided into different categories depending on the main application of the device. These categories include 'screw feeders', 'screw elevators', 'hopper discharge screws', 'metering screws', and 'screw conveyors'. Screw conveyors and screw feeders operate on the same principle, but the cross-sectional fill percentage and mode of transport for the two devices differ. The cross-sectional fill in screw conveyors is typically less than 45 %, whereas screw feeders have a 100 % fill, as depicted in Figure 2. This is due to the screw feeder's inlet being flooded with material as it is fed from the storage hopper. Screw conveyors operate in gravity mode, whilst screw feeders operate in flooded mode. The most important region of a screw feeder setup is the interface between the screw and the storage hopper. Generally, the screw feeder is placed inside the storage hopper so that the screw's first few flights are completely covered with material. The main benefits and limitations of screw feeders are listed in Table 1 (Bates, 2000).

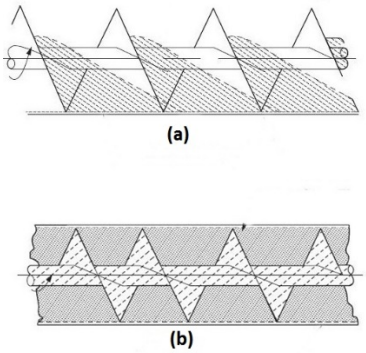

Figure 2: Difference in cross-sectional fill in (a) screw conveyor with less than 45 %, and (b) screw feeder with 'flooded' fill (Bates(2000)).

Table 1: Operating benefits and drawbacks of screw feeders (McGlinchey, 2008)

Screw feeders	
Operating benefits	**Operating drawbacks**
Screw feeders are always enclosed, protecting the material from contamination and external factors.	Compared to other types of feeders, they are mechanically inefficient.
Screw feeders can operate at extreme temperature and pressure conditions.	When running empty or under light load conditions as well as starting under full conditions, high power loads may be experienced.
They have a compact cross section because they only have one working element.	Material build up may occur around the centre shaft that causes clogging of the screw, especially with sticky or stringy material.
They can be controlled to operate over a wide range of capacities.	The screw can damage the material being transferred.
Inlets and outlets of various sizes can be fitted intermediately with ease.	Screw feeders are not self-cleaning, hence, maintenance is required on a regular basis.
By varying the material of construction, they can be used in applications that require the transfer of highly corrosive, hot or abrasive materials.	A poor screw feeder design can cause arching, bridging and rat-hole formation in the hopper.
The feeder design can easily be adjusted to accommodate any type of material, including wet, damp, cohesive, sticky, or lumpy material.	The transport efficiency is low in comparison to belt conveyors.
Simple to design, construct and operate and can operate in inclined positions.	The feeder is limited by the size and structural stability of the screw.

Screw feeders are generally divided into two groups: bin discharge feeders and metering screws. There is no definitive difference between these two groups as both are designed to discharge material from a storage hopper. The prime function of bin discharge feeders is to provide a constant reliable feed from a storage unit. Metering screws are designed with the main purpose of providing a reliable, predictable and controlled bulk solid feed rate from a storage hopper. The feed rate is accurately controlled by varying the power input to the screw, therefore, adjusting the screw's rotational speed. Rotational speeds can be fixed or variable, with typical speeds ranging from 15 rpm to 100 rpm. Depending on the material properties and the effect of the screw on the material, the output volume varies linearly with rotational speed. It is important to note that the static material density and the material density in transit might differ significantly due to the forces acting upon the material during screw operation; therefore, it is important to calibrate the screw before operation.

Several shapes of screws can be used in a screw feeder (Figure 3). The simplest and most economic shape is a uniform pitch screw (Figure 4). However, these screws have one major disadvantage; material extraction from the hopper only takes place from the first one to two exposed pitch lengths in the hopper, the rest of the exposed screw length in the hopper needs to shear through the stationary material. This leads to an increase in power requirement. To counteract this effect, one needs to spread the extraction length along the screw axis. This is achieved by using a variable or stepped pitch construction (Figure 3). Care should be taken in selecting a pitch since too small a pitch could cause the material to get stuck in the grooves and rotate with the screw instead of being transported along. A rule of thumb is that the ratio between the pitch length and the screw diameter should be between one-third and unity. At larger ratios, the transfer efficiency of the screw diminishes.

Fernandez, Cleary, and McBride (2011) implemented the Discrete Element Method (DEM) to simulate the effects that different screw geometries have on the flow achieved inside a wedge-shaped storage hopper. Six different screw geometries were studied and are depicted in Figure 4.

The results obtained after running the simulation for 80 s are depicted in Figure 5. The distribution of the colour mapping inside the storage hopper gives a clear indication of the drawdown of material achieved inside the storage hopper. It is clear that the standard uniform pitched screw produced the worst drawdown pattern since the material is only extracted from the far end of the screw, with no material flow in the hopper outlet region. It is clear from these results that a semi-even drawdown pattern is achieved in the hopper wherever some form of tapered screw configuration is used.

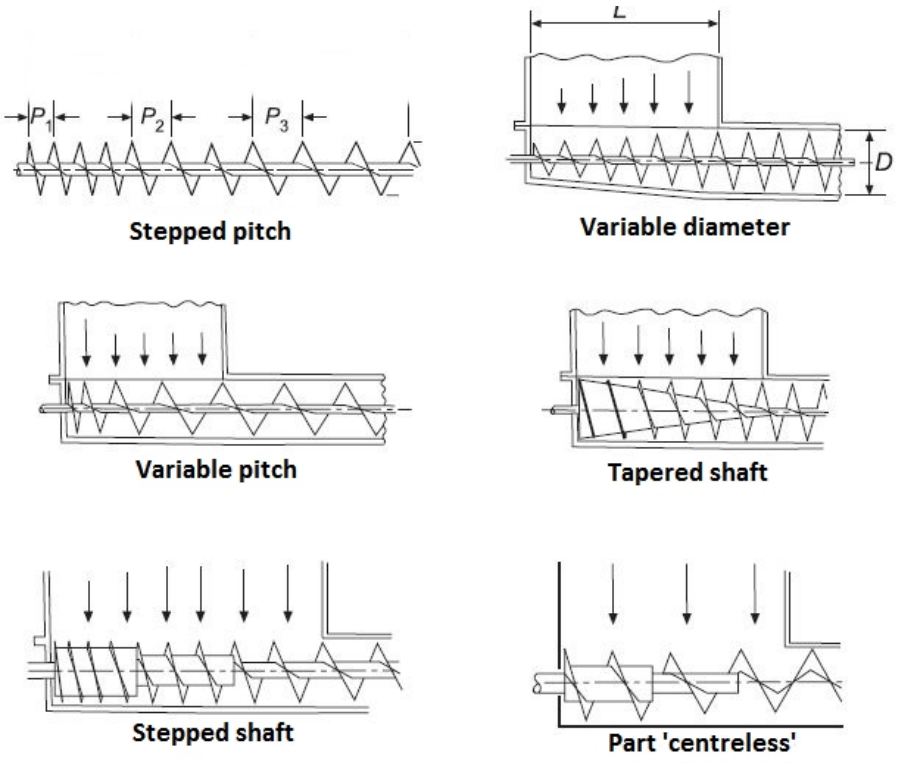

Figure 3: The six main forms of screw feeders (Bates (2000)).

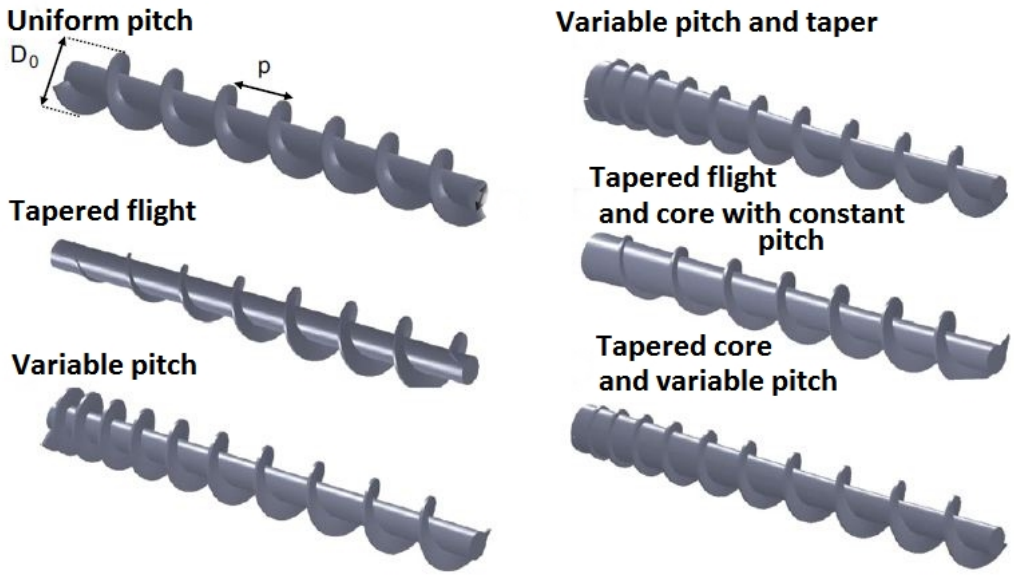

Figure 4: Six different screw geometries investigated by Fernandez, Cleary, and McBride (2011).

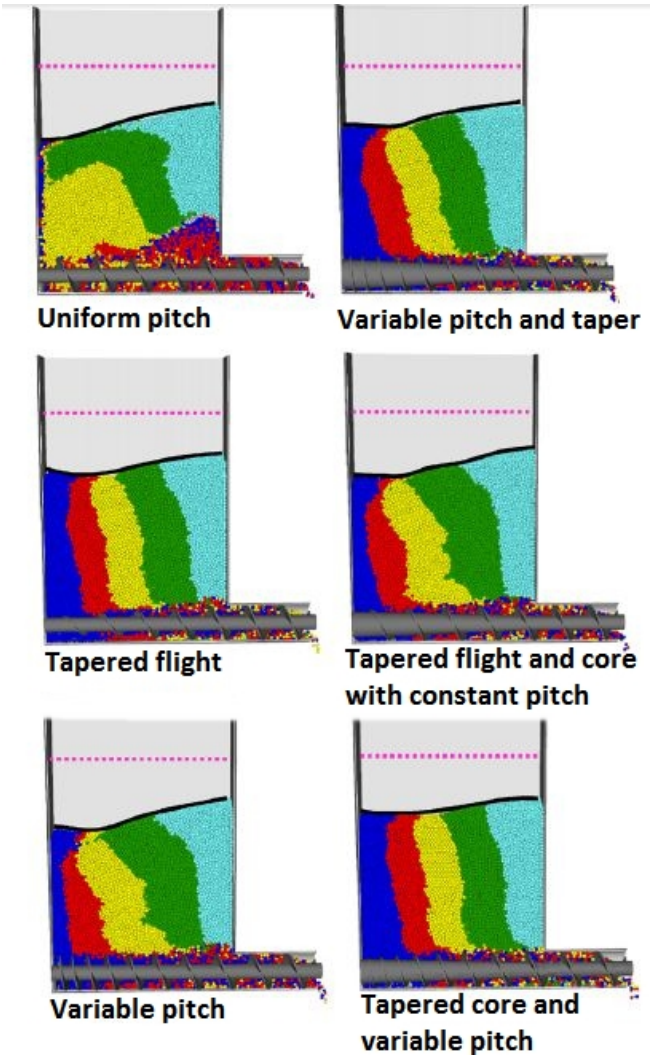

Figure 5: Results of the simulation performed by Fernandez, Cleary and McBride (2011) to determine the effect that different screw geometries have on the flow pattern in a storage hopper.

2.2 Storage hoppers

2.2.1 Hopper internal flow and associated flow problems

Metering screws are used to provide a reliable, predictable and controllable flow rate of material to a process. In order to achieve this, two main conditions have to be satisfied: the flow of material should be continuous and smooth during all conditions of operation; the screw feeder should be filled with material in a continuous, consistent and uniform manner. These two conditions can only be achieved if the flow regime inside the storage hopper is taken into account.

In 1964 Jenike (as quoted by Bates, 2000) studied the flow in hoppers and defined two major flow patterns: mass flow and funnel flow. A third flow pattern was later identified, namely expanded flow, which is a combination of the two major flow patterns (Figure 6). Jenike

(1964) (as quoted by Bates, 2000) defined mass flow as the flow pattern in which all of the material is in motion during extraction (Figure 6(a)). However, this does not imply that all of the material at any given cross-section throughout the hopper is moving at the same velocity. Funnel flow (Figure 6(b)) is described as the flow pattern in which some of the material is stationary and some of the material is in motion during extraction. The easiest way to distinguish between the two patterns is the presence or absence of wall slip at the boundaries, as wall slip at all boundaries is always present in mass flow patterns. The main advantages of mass and funnel flow are compared in Table 2.

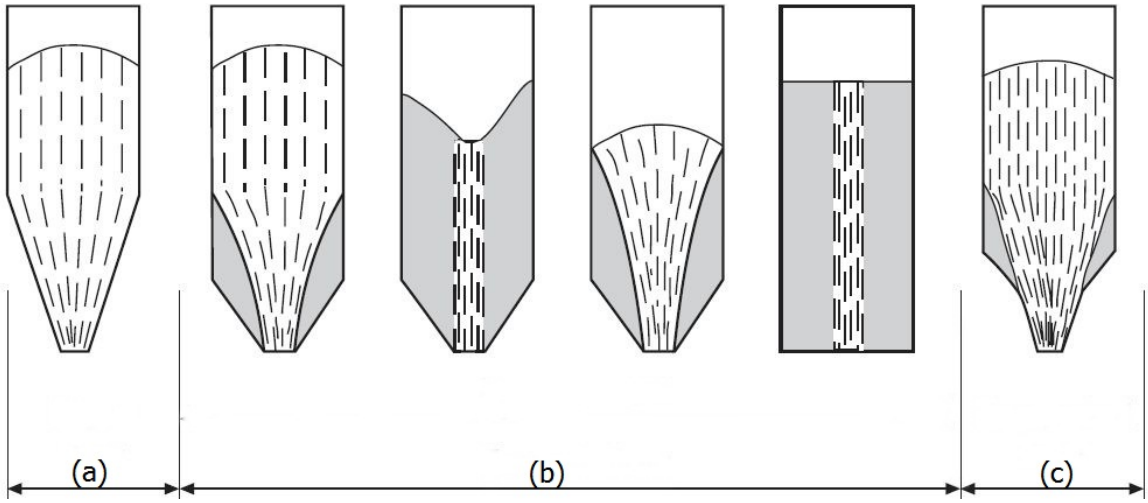

Figure 6: Different types of flow patterns in hoppers. (a) Mass flow, (b) Funnel- or core flow, and (c) Expanded flow (Bates (2000)).

Table 2: Comparison between mass and funnel flow in a hopper (Amoros *et al*, 2000).

Mass flow	Funnel Flow
Eliminates the possibility of flow obstructions.	Less headspace is required for the same storage capacity.
Minimises the effects associated with size segregation.	The hopper walls need to withstand less pressure.
There are no dead spaces in the hopper.	The walls are subjected to less abrasion.
Uniform and controllable flow are achieved.	Dead spaces of no material movement are always present.
No irregular density changes of the material are experienced.	Material size segregation could occur.
The total available storage capacity is used.	

The flow pattern in the hopper is not the only factor that should be taken into account when designing a screw feeder system. Other common problems associated with flow in a hopper are (Chase, *sa*):

- *Ratholing/piping* (Figure 7(a)): Rat-holing occurs when the material inside the hopper forms a hole or pipe in the middle of the hopper with the material on the sides of the hopper exit remains stagnant or is stable enough that no flow occurs.
- *No flow due to arching or doming* (Figure 7(b)): The material inside the hopper is cohesive enough to form a dome or arch over the hopper outlet.
- *Flushing* (Figure 7(c)): Flushing occurs when the material is compacted inside the hopper in such a way that air struggles to penetrate through the particles. This causes a decrease in material discharge.
- *Incomplete emptying*: Dead spaces inside the storage hopper prevent complete discharge of the loaded material.
- *Segregation*: Particles of different sizes and densities tend to segregate due to vibrations leading to a non-uniform material discharge as smaller particles will trickle down through the void spaces between larger particles.

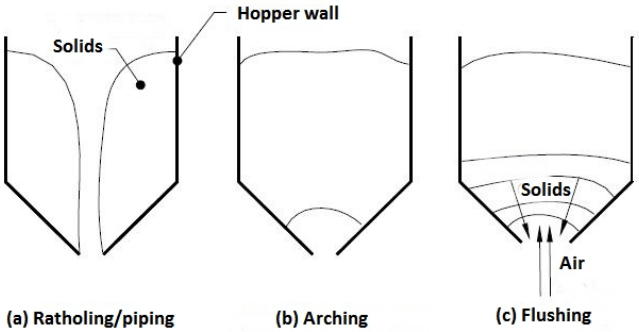

Figure 7: Common problems associated with storage hopper particle flow (Chase, *sa*).

Choosing between designing a hopper for mass flow or funnel flow all depends on the material. A free-flowing, non-fibrous solid with no elastic spring back tendencies would not require flow at the walls to be present; therefore, a funnel flow hopper design would be sufficient. By contrast, a mass flow design is recommended for materials that are fibrous, cohesive and compressible (Diamondback Technology, 2005).

2.2.2 Storage hopper design

Jenike (1964) developed a fundamental hopper design procedure that is used extensively in industry and is described in Schulze (2008). The main objectives of this procedure are to determine the minimum hopper outlet size that would prevent arching and the optimal hopper wall angle, θ_p (Figure 8). To design an efficient storage hopper the bulk solid flow properties need to be characterised by determining four essential parameters. These

parameters are the solid's bulk density, ρ_b, the effective angle of internal friction, φ_e, unconfined yield strength, σ_c, and angle of wall friction, φ_x.

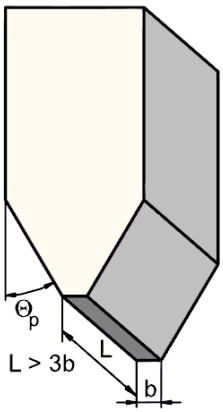

Figure 8: Wedge hopper design parameters (Schulze (2008)).

Jenike's approach is based on the calculation of stresses in hoppers. He derived two partial differential equations by applying equilibrium conditions to an infinitesimal volume element of bulk solid in a hopper. These two equations are functions of the bulk solid properties and the hopper slope. A solution for these two equations only exists for a specific combination of parameters, θ_p, φ_e, and φ_x. It is only under these specific conditions at which mass or funnel flow will occur. Using these equations, Jenike theoretically determined the mass flow and funnel flow boundaries for a conical hopper as illustrated in Figure 9. Figure 10 illustrates the mass flow boundaries for wedge-shaped hoppers. This diagram, however, is not based on theoretical considerations but rather on practical experience from Jenike's work; therefore, caution should be taken when using Figure 10 (Schulze, 2008: 295 – 300).

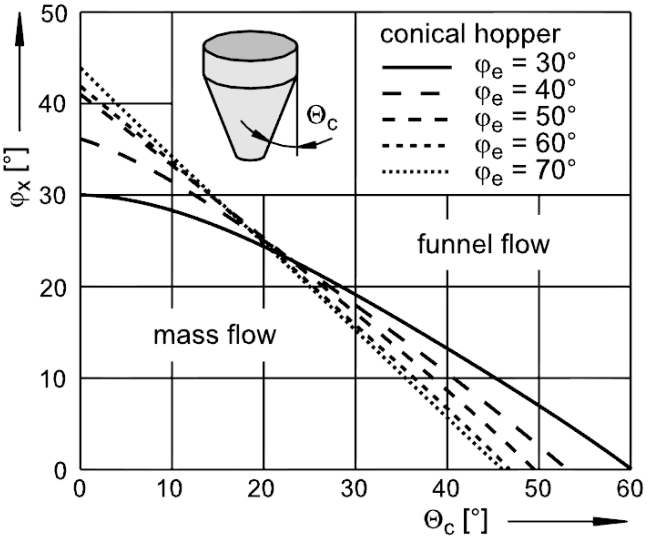

Figure 9: Mass flow diagram (conical hoppers) (Schulze, 2008: 298).

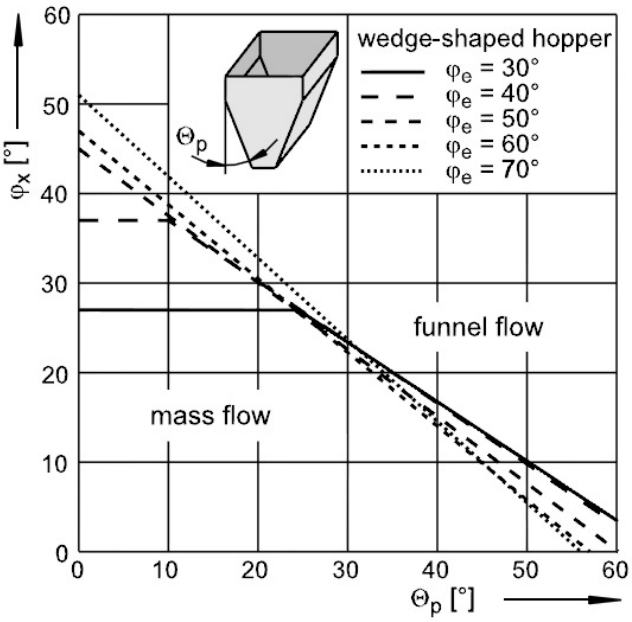

Figure 10: Mass flow diagram (wedge-shaped hopper) (Schulze, 2008: 299).

After the hopper slope has been determined the minimum slit width of the outlet, which will avoid arching, is determined. For this hopper, stresses are considered. As described in Schulze (2008) the most important stress to consider is the major principal stress, σ_1, as seen in Figure 11. For each major principle stress, the unconfined yield strength, σ_c, can be measured. The relation between these two stresses is known as the flow function. Arching occurs when the force that the bulk solid transfers to the hopper walls is big enough to support the weight of the bulk solid. Jenike calculated this stress, represented as σ_1', by assuming that the arch has a smooth shape with a constant thickness and that the arch only carries its own weight. Following further assumptions, Jenike developed Equation (1) to calculate the critical slit width, represented by $2r \cdot \sin\theta_p$ in the equation.

$$\sigma_1' = \frac{2r \cdot sin\theta_p \cdot g \cdot \rho_b}{1 + m} \quad (1)$$

In the equation, m is a shape factor: m equals zero for wedge-shaped hoppers and unity for conical hoppers. A stable arch is only possible when the unconfined yield strength, σ_c, is greater than the stress present in a stable arch, σ_1'. This is represented in Figure 11 as all of the points below the point of intersection between σ_c and σ_1' on the graph. The intersection point represents the height in the hopper at which the hopper width is equal to the critical width, d_{crit}, which has to be exceeded to avoid arching (Schulze, 2008: 301).

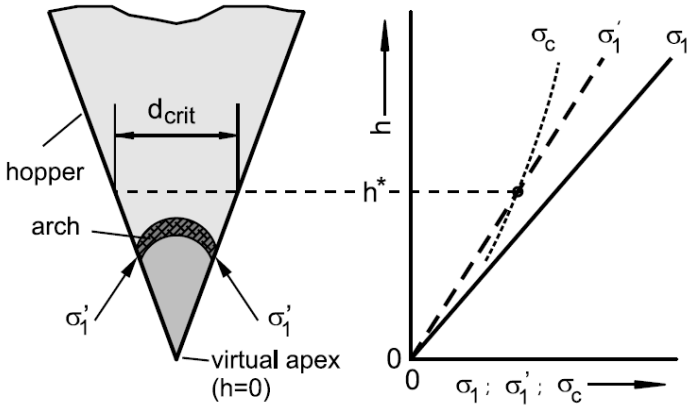

Figure 11: Model for determining the minimum outlet size, d_{crit} (Schulze, 2008: 299).

Since this method of determining the critical hopper width in not practical, Jenike developed a procedure based on the fact that the ratio σ_1/σ_1' always remains constant inside the hopper. This ratio is called the flow factor, *ff*:

$$ff = \frac{\sigma_1}{\sigma_1'} = const = (1+m)\cdot s\left(\theta_p, \varphi_x, \varphi_e\right)\cdot \frac{\sin\varphi_e}{\sin\theta_p} \qquad (2)$$

Here *s* is the differential equation used to derive Figure 9 and Figure 10. The flow factor is dependent on the solid properties (φ_x, φ_e) and the hopper shape (m, θ_p). To simplify the calculations Jenike developed graphs relating the flow factor to the hopper slope and angle of wall friction as seen in Figure 12. Reference graphs are available for different effective angles of internal friction for different hopper shapes, starting at 30° up to 60° in increments of 10°.

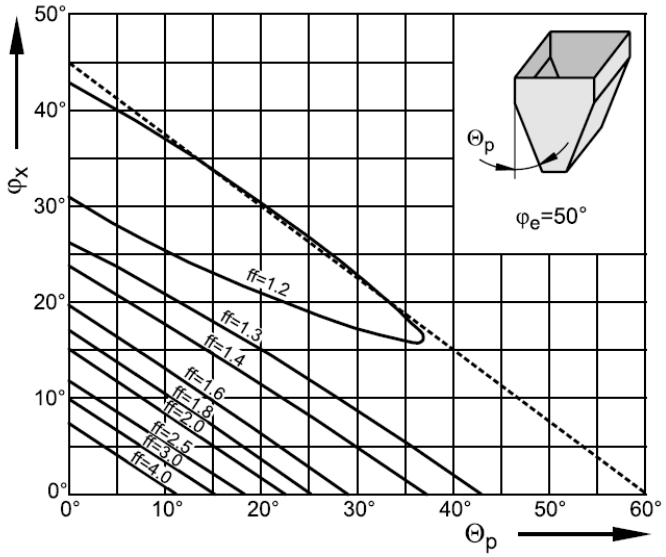

Figure 12: Flow factor for wedge-shaped hoppers and φ_e=50° (Schulze, 2008: 316).

Now that the flow factor for a certain hopper configuration can be calculated, σ_1' can be calculated using Equation (2) and (3) and can be plotted. From this graph the intersection point $\sigma_{c,crit}$ is determined and used in Equation (4) to calculate the critical outlet opening width for a wedge-shaped hopper. To avoid arching inside a wedge-shaped hopper, the wedge outlet opening width should be larger than the critical width, d_{crit}, and the outlet opening length should at least be three times the chosen width (as indicated in Figure 8).

$$\sigma_1' = \frac{\sigma_1}{ff} \tag{3}$$

$$d_{crit} = \frac{\sigma_{c,crit}}{g \cdot \rho_b} \tag{4}$$

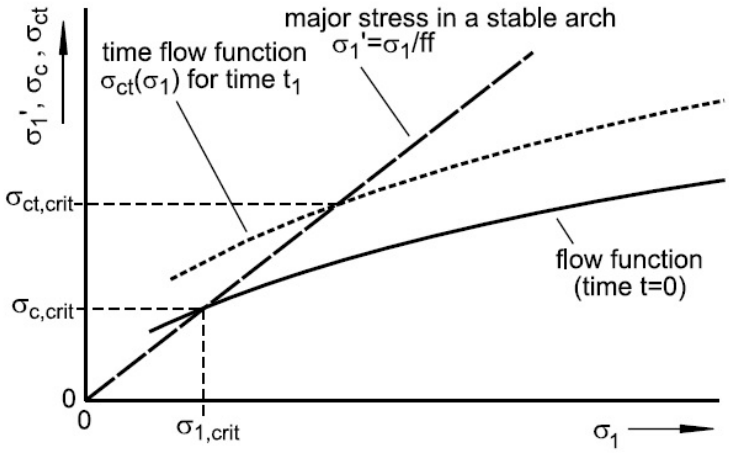

Figure 13: Flow function and time flow functions: major stress in a stable arch, σ_1' (Schulze, 2008: 303).

3 Batch and continuous PTFE depolymerisation literature

The design of a screw feeder is highly dependent on not only the bulk material properties of the material, but also on the general layout of the system. Therefore, some background is required on the feed PTFE, Teflon® PTFE 807N in particular, and the in-house batch depolymerisation system. In this section, the above mentioned will be covered, along with a comparison of the current batch depolymerisation system with the continuous depolymerisation systems described in the literature.

3.1 Polytetrafluoroethylene

Polytetrafluoroethylene (PTFE) was discovered by accident by the E.I. DuPont de Neumors (DuPont) (now known as Chemours) scientist Roy Plunkett in 1938, when tetrafluoroethylene spontaneously polymerised in a cylinder, and was commercialised by DuPont in 1946 under the trade name Teflon (van der Walt, 2007). PTFE has a very diverse application spectrum ranging from non-stick cookware to applications in highly corrosive and high-temperature environments due mainly to its extraordinary properties. Some of the most important properties are:

- PTFE is chemically inert
- It exhibits excellent thermal stability over a wide range of temperatures
- It has excellent lubricity
- It is hydrophobic
- It is insoluble in all known solvents and resistant to all acidic and alkaline substances (Rae & Dattelbaum, 2004)

TFE is polymerised using emulsion or suspension polymerisation to produce the perfluorinated straight-chain high molecular weight polymer with a formula $–(CF_2–CF_2)_n–$. The short and extremely strong carbon-fluorine bond is what imparts the majority of PTFE's characteristic properties. The well-known carbon-hydrogen bond has an energy of 413 $kJ{\cdot}mol^{-1}$ which is much smaller than that of the carbon-fluorine bond (484 $kJ{\cdot}mol^{-1}$). This carbon-fluorine bond is not as susceptible to van der Waals forces as hydrocarbons, making PTFE more resistant to chemical attack. Furthermore, the extremely small fluorine atoms attached to the carbon backbone forms a protective sheath surrounding the carbon chain. This sheath shields the carbon atoms from chemical attack and confers chemical inertness and stability. It reduces the surface energy of PTFE resulting in a low coefficient of friction and is the reason for PTFE's characteristic non-stick property (Gangal, *sa*).

PTFE has a very high melt viscosity (1 GPa·s up to 10 GPa·s) which is why PTFE is non-melt processable. PTFE has a working temperature range of -185 °C up to 260 °C. Above 260 °C,

PTFE starts to degenerate and around 340 °C, PTFE changes from a white crystalline material to a transparent amorphous gel (Gangal, *sa*). According to Collins, Fiveash, and Holland (1969), PTFE starts to show signs of thermal decomposition at temperatures of 300 °C under atmospheric pressure and in an inert atmosphere; however, this temperature lowers to 280 °C in a vacuum. The general physical properties of PTFE are listed in Table 3.

Table 3: Physical properties of PTFE.

Density	($g \cdot cm^{-3}$)	2.2 to 2.3
Melting point	(°C)	First melting point: 342; Second melting point: 327
Dielectric constant	(at 1 kHz)	2
Dynamic coefficient of friction		$4x10^{-2}$
Surface energy	($dyne \cdot cm^{-1}$)	18
E_{act}	($kJ \cdot mol^{-1}$)	339
Melt viscosity	(Pa·s)	10^9 to 10^{11}

3.2 Teflon® PTFE 807N

3.2.1 General bulk solid properties of Teflon® PTFE 807N

Teflon® PTFE 807N was procured from DuPont to be used as raw material for this investigation. The general material properties for Teflon® PTFE 807N are listed in Table 4 below.

Table 4: DuPont Teflon® PTFE 807N physical properties as determined by DuPont (DuPont, *sa*)

Average particle diameter	µm	600
Standard specific gravity		2.156
Bulk density	$g \cdot cm^{-3}$	0.95
Tensile strength (using 76 mm test disk)	MPa	26
Melting peaks		
Initial	°C	344
Second	°C	327

3.2.2 Bulk solid density determination

To verify the data presented by DuPont for Teflon® PTFE 807N, the bulk density was measured using a gas pycnometer with a 3.5 cm^3 cup size. The results are shown in Table 5.

Table 5: Bulk density determination for PTFE.

Measured mass (g)	Calculated bulk density ($g \cdot cm^{-3}$)
3.271	0.935
3.289	0.940
3.167	0.905
Average	Average
3.241	0.927

3.3 PTFE depolymerisation kinetics

The depolymerisation kinetics of PTFE has been studied since the late 1950s and 1960s. More recent studies focused on the side reaction kinetics, for example, the reaction kinetics of a TFE and octafluorocyclobutane (OFCB) mixture (Atkinson & Atkinson, 1957), instead of the total process kinetics starting with PTFE as a reagent. Many researchers (Siegle *et al,* 1964; Anderson, 1964; Cox, Wright & Wright, 1964; Morisaki, 1978; Jun *et al,* 1995; Consena & Font, 2001; van der Walt, 2007) have studied the overall kinetics of PTFE depolymerisation, but up to date no kinetic study has been performed to determine the product-specific kinetic data starting with PTFE as reagent. The experimentally determined activation energies and pre-exponential factors available in the literature for the overall depolymerisation of PTFE are listed in Table 6.

Table 6: Experimentally determined PTFE depolymerisation activation energy and pre-exponential factor values.

Source	Temperature range (°C)	Atmosphere	Sample size (mg)	Reaction order	Pre-exponential factor	Activation energy ($kJ \cdot mol^{-1}$)
Siegle *et al*, 1964	360 - 510	Vacuum	30 - 100	First	$3x10^{19}$ s^{-1}	347.50
Jun *et al*, 1995	510 - 600	Helium		First		327.41
Anderson, 1964	25 - 620	Vacuum	9 - 11.5	First	$4x10^{20}$ min^{-1}	322.38
van der Walt, 2007	500 - 620			0.54	$1.78x10^{13}$ s^{-1}	260.00
Cox, Wright & Wright, 1964		Vacuum		First	10^{19}	318.20
Morisaki, 1978	450 - 790	Helium	10	First		361.74
Consena & Font, 2001	80 - 800	Nitrogen	3 - 4	First	$4.122x10^{21}$ s^{-1}	349.10

3.4 Converting the in-house batch-depolymerisation system to continuous

The thermal decomposition of perfluoropolymers like PTFE differs from that of polyolefins in that the depolymerisation reaction dominates during thermal decomposition (Lonfei, Jingling & Siiuman, 1986). The most basic method of PTFE-depolymerisation is by means of heating the polymer to above its thermal degradation temperature using a furnace in an inert atmosphere at pressures varying between ambient and absolute vacuum. However, steam (Schottle *et al,* 1995) and radiation methods (Schulze, Bolwin & Schnurnberger, 1995; Ferse *et al*, 1978) have been studied. According to the literature, a mixture of product gases are produced during depolymerisation depending on the operating condition. The most well-known depolymerisation products include the monomer TFE, HFP, OFCB, octafluoro-1-butene (1-OFB), octafluoro-2-butene (2-OFB) and highly toxic perfluoroisobutene (PFIB).

Only a handful of continuous PTFE depolymerisation systems have been reported (Cox, Wright & Wright, 1964; Meissner *et al*, 2004; van der Walt, 2007; Simon & Kaminsky, 1998; Ichida & Homoto, 2008; Schottle *et al,* 1995). When one compares all of these setups, a common layout for a continuous depolymerisation system becomes evident.

By combining the continuous pyrolysis equipment of Simon and Kaminsky (1998), Meissner *et al* (2004), van der Walt (2007), Ichida and Homoto (2008) and Schottle *et al* (1995), the general depolymerisation system in Figure 14 was developed. Each of the individual systems will be discussed in short, including a general comparison with the current in-house batch-depolymerisation system (see Figure 15).

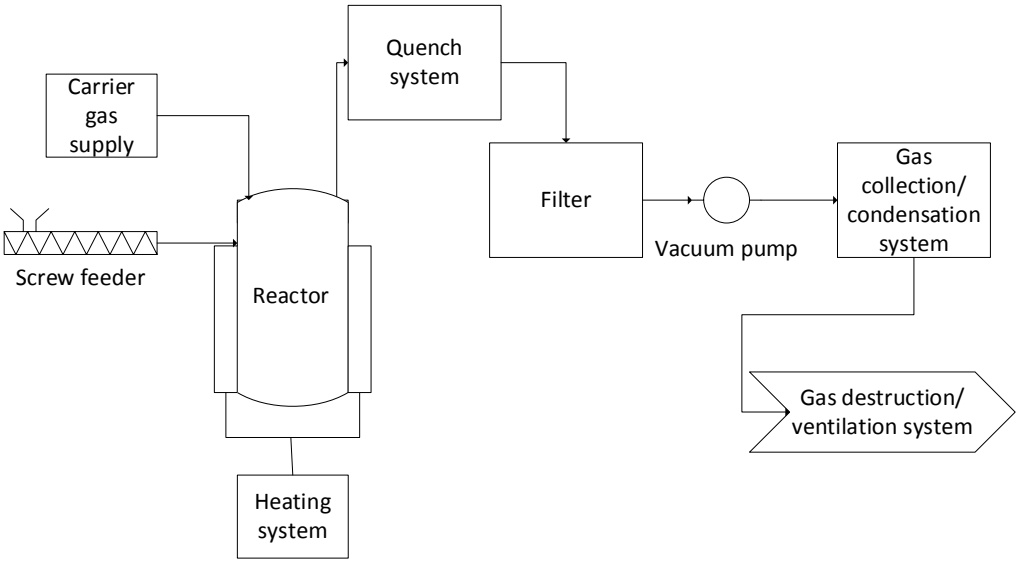

Figure 14: A general layout of a continuous laboratory scale PTFE depolymerisation system.

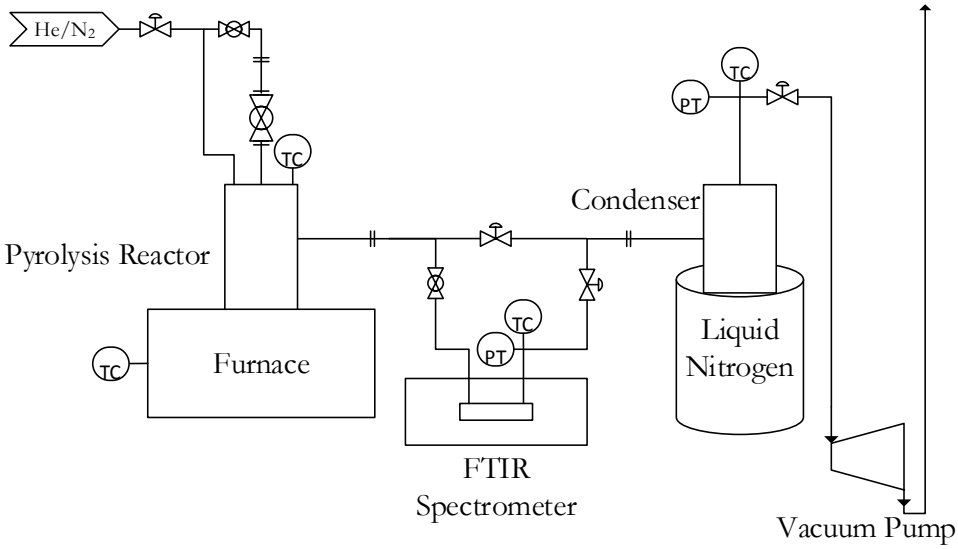

Figure 15: The in-house batch depolymerisation system capable of pyrolysing up to 30 g of PTFE at various operating temperatures and pressures.

3.4.1 Carrier gas

Various carrier gases can be used depending on the purpose of the depolymerisation system. Generally, nitrogen or helium is used to perform PTFE depolymerisation under reduced pressure conditions. The inert carrier gas can be replaced by steam as described by Ichida and Homoto (2008) or used as a fluidising gas in a fluidised bed reactor (Simon & Kaminsky, 1998). The main disadvantage of using steam is the production of hydrogen fluoride as a by-product. Care should be taken when selecting a carrier gas as the gas could affect the products produced during depolymerisation as detailed in section 10.2.2.

The in-house batch depolymerisation system can be operated with or without a 200 SCCM flow of nitrogen or helium depending on the operating conditions. Generally, helium will be used if the evolved gases are condensed using liquid nitrogen.

3.4.2 Screw feeder

In all of the continuous systems described in the literature (Cox, Wright & Wright, 1964; Meissner *et al*, 2004; van der Walt, 2007; Simon & Kaminsky, 1998; Ichida & Homoto, 2008; Schottle *et al,* 1995), a screw feeder connected to a storage hopper was used to provide a continuous flow of PTFE into the reactor at various flow rates (5 g·min^{-1} to 50 g·min^{-1}). Screw feeders are generally the best option for systems operating under vacuum conditions. This is one of the main reasons why a screw feeder was selected as a continuous feeder for the current investigation.

In the batch system, a PTFE feed tube is loaded with a measured amount of PTFE before an experimental run. A ball valve separates the feed tube and the reactor. When the reactor

reaches temperature, the ball valve is opened and the PTFE drops into the reactor. The reactor system is capable of pyrolysing up to 30 g PTFE per session.

3.4.3 Heating system

Heat can be supplied to the system using various methods depending on the type of reactor used. The most common methods are an electrically heated furnace and electrical resistance coils. The in-house batch reactor is heated with a resistive furnace.

3.4.4 Reactor

Various reactors can be used to pyrolyse PTFE. Van der Walt (2007) investigated four types of reactors: a drop tube reactor, rotary kiln reactor, a paddle reactor and a vibrating reactor. Ichida and Homoto (2008) patented a process that used a rotary kiln reactor in a steam atmosphere, whereas Simon and Kaminksy (1998) used a fluidised bed reactor containing quartz sand to depolymerise PTFE in a steam atmosphere. The reactor used does not necessarily need to be a complicated piece of apparatus, as Meissner *et al* (2004) proved by using a nickel pipe as a reactor.

Pyrolysis of PTFE is achieved in a simple stainless steel drop tube reactor in the in-house batch system. The reactor can be operated at temperatures up to 850 °C within a pressure range between ~1 kPa (abs.) and atmospheric pressure (~86 kPa (abs.)).

3.4.5 Quench system

The reactions during PTFE depolymerisation occur both in the melt and in the gas phase. To prevent the gas-phase reactions from continuing when the products leave the reactor, a quenching or cooling system is required to rapidly cool the gas at the reactor exit. Meissner *et al* (2004) achieved this by cooling the reactor exit with water. Van der Walt (2007) implemented an annular water-cooled, double-tube, self-cleaning quench probe. Both of the above-mentioned methods are non-invasive and do not contaminate the products gas. Schottle *et al* (2005) opted to use the invasive method of injecting a spray of water directly into the gas stream. No cooling system was implemented in the in-house batch system since the gas residence time between the reactor and the condenser was deemed short enough.

3.4.6 Filter

A suitable filter is used to remove any particles that might still be present in the product gas. This is essential especially when a measuring instrument (*eg* FTIR, GC-MS) is connected in line with the product stream. Most continuous depolymerisation systems in the literature (Meissner *et al*, 2004; Simon & Kaminsky, 1998; Schottle *et al,* 1995) make use of a cyclone separating system. Glass wool was inserted in the reactor outlet of the in-house batch system to prevent any particles from entering the rest of the system.

3.4.7 Gas collection or condensation

In all of the continuous depolymerisation processes, a gas collection or condensation system is used to collect samples of the evolved gas. Generally, the product gas is either collected or compressed into a sample cylinder via liquid nitrogen traps or a compressor. The product gas is stored for a short period under reduced pressure for analysis purposes only, however, no mention was made of storage methods for an extended period of time.

During pyrolysis in the in-house batch system, the product gas was condensed in the condenser using liquid nitrogen. After operation the product gas was evaporated and collected in sample cylinders for analysis.

3.4.8 Gas destruction or ventilation

All of the studied depolymerisation systems used one of two methods for disposing of the product gas. The first method involved burning the product gas in a flare and venting the exhaust gas. Alternatively, the product gas is diluted using an inert gas (to below the lower flammability limit of all possible components present) and vented. The later method was implemented in the in-house batch system.

3.5 The in-house batch-depolymerisation: additional information

The semi-automated batch-depolymerisation system is remotely controlled and monitored by software written in National Instruments™ LabVIEW Full Development Suite 2015. A typical batch depolymerisation run would be executed as follows: PTFE is measured and loaded into the PTFE feed tube (with 1” bore) before the experiment starts. The tube is sealed using a vacuum flange. At initialisation, the system enters a series of flush and evacuation cycles to remove any oxygen or impurities in the system. The software then performs a vacuum check to establish if the system has any leaks. If the system is deemed leak-tight, the reactor is heated to a pre-specified reaction temperature. If a reaction pressure is specified the system is pressurised using either helium or nitrogen. The PTFE in the feed tube is isolated from the reactor with a ball valve. Once the reactor reaches temperature, the ball valve is opened initiating the reaction. The evolved product gas either flow directly to the condenser where it is condensed using liquid nitrogen or it flows through the inline Perkin Elmer Spectrum Two™ spectrometer to the condenser, depending on the experimental requirements (Figure 16). Samples taken at certain intervals during an experimental run are analysed using an at-line GC-MS (see Appendix C.4.2).

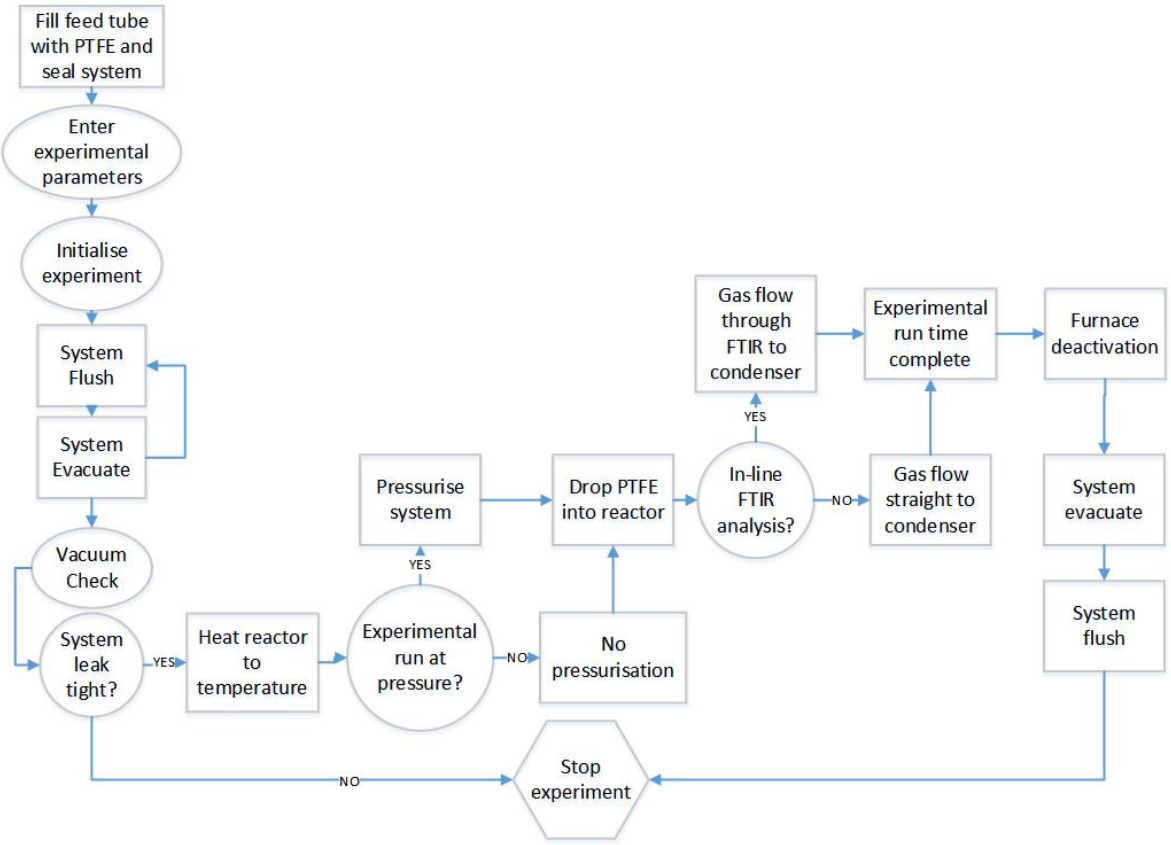

Figure 16: Process block diagram illustrating the normal operation of a batch depolymerisation run.

4 Initial screw feeder design

4.1 Initial screw feeder design considerations

4.1.1 Screw feeder design objectives, specifications, and limitations

For the hopper and screw design to be fully specified, the following criteria had to be met:

- To be able to compare the depolymerisation results to historic batch results, the feeder system had to be designed to feed Teflon® PTFE 807N. However, since the system will be used in future to depolymerise waste PTFE, the feeder had to be designed and manufactured in such a way that it can easily be adapted to accommodate irregular ground scrap material.
- The batch system is situated under an extraction hood, hence, spatial restrictions had to be considered.
- The screw feeder had to be able to operate under vacuum conditions to eliminate any pressure fluctuation complications in the system.
- The hopper had to have a capacity of at least 1 kg Teflon® PTFE 807N.
- Due to structural stability requirements and in-house manufacturing restrictions, the minimum screw outside diameter was limited to 21.5 mm.

- A 50 L holding cylinder was available for product gas collection, hence, the screw feeder feed rate and total reaction time were limited by the cylinder capacity.
- Due to the unknown effect that forces inside the hopper system may have on the compression of PTFE into the screw, no specific flow rate range was specified for the screw at the onset of the project. The literature indicates (Anderson, 1964; Cox, Wright & Wright, 1964; Siegle *et al*, 1964; Morisaki, 1978; Jun *et al*, 1995; Consena & Font, 2001; van der Walt, 2007) that the thermal decomposition of PTFE may be approximated by a first order reaction rate and is therefore not affected by the initial mass of PTFE in the reactor. The reactor's ability to handle the flow rates provided by the feeder is only dependent on the operating temperature and heat transfer rates achieved in the reactor. Consequently, the screw sizing design was only limited by the equipment available and structural stability.
- The PTFE mass flow rate of the feeding system had to be repeatable and relatively constant over a minimum period of 30 min at various motor speeds.
- The flow profile of PTFE in the hopper should be such that no severe rat-holing or arching occurs. These phenomena could affect the flow of PTFE into the reactor.
- After feeder implementation, the operating limits regarding temperature, pressure, and PTFE feed rate had to be determined experimentally.

4.1.2 Screw feeder speed control

The screw was operated using a reversible, geared AC induction motor, with the general properties as stated in Table 7. A variable frequency drive (VFD)(Delta VFD004EL 230V Class) was used to vary the motor speed. To prevent excessive overheating of the motor during operation, the minimum operating speed was limited to 40 % of the maximum output speed, 35 rpm, which equates to 14 rpm.

Table 7: MC244PT80B5 induction motor general information.

Gear ratio	80	
Delivered power	49	W
Input rpm no-load	2800	rpm
Output rpm no-load	35	rpm
Rated torque	7.9	Nm
Voltage	230Δ	Vac – 50 Hz
Current	0.52Δ	VAC

The VFD output frequency was limited by the motor frequency range (0 Hz to 50 Hz). The VFD was programmed to follow a linear relationship between frequency and voltage as indicated in Figure 17. Motor speed can be estimated using the ratio between the VFD frequency output range and the motor speed range as illustrated in Equation (5). To verify the actual

motor speed at each frequency a switch with a roller at the end was installed. As the motor shaft turns the switch is activated after each revolution. The switch signal was 100 ms.

$$RPM_i = RPM_{max} - \frac{RPM_{max}(Frequency_{max} - Frequency_i)}{Frequency_{max}} \quad (5)$$

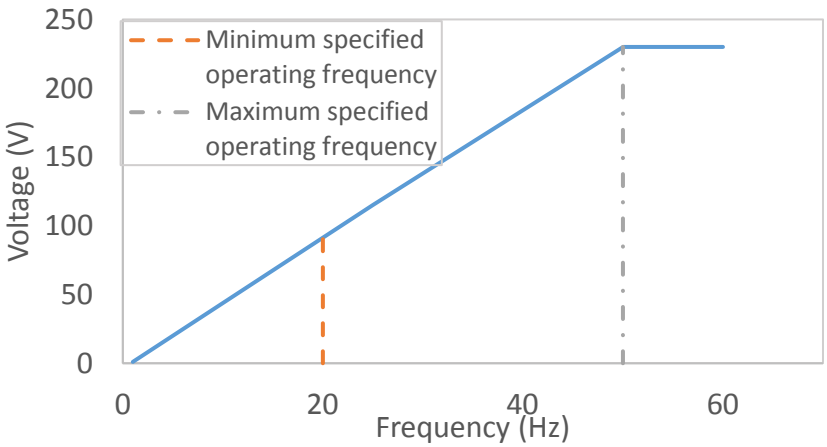

Figure 17: VFD programming correlation between frequency and voltage.

4.1.3 Planned system alterations

The batch-depolymerisation system is described in Figure 18. As mentioned previously (section 3.1), PTFE starts to degenerate above 260 °C. To avoid any feeding problems associated with this, the feeder should not operate in an atmosphere that exceeds a temperature of 250 °C. The screw feeder had to be installed where the PTFE feed tube is located in Figure 18.

As gases evolve during and experimental run, a pressure differential could develop between the hopper (1) headspace and the reactor (4). This may cause PTFE to be sucked back into the hopper. To negate this, the hopper headspace and reactor had to be connected directly. The process flow diagram for the planned installation of the screw feeder is indicated in Figure 19.

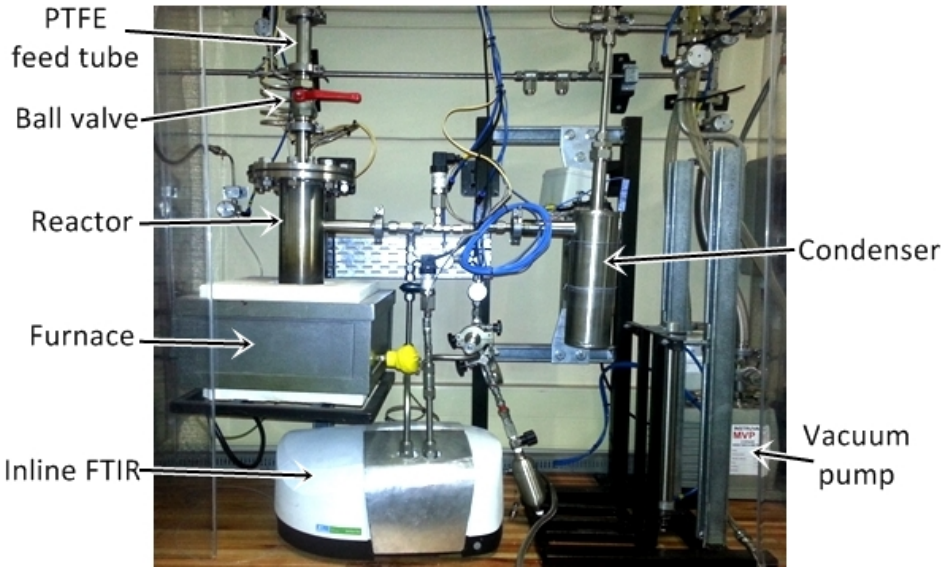

Figure 18: The batch depolymerisation system available in the Fluoropolymer laboratory.

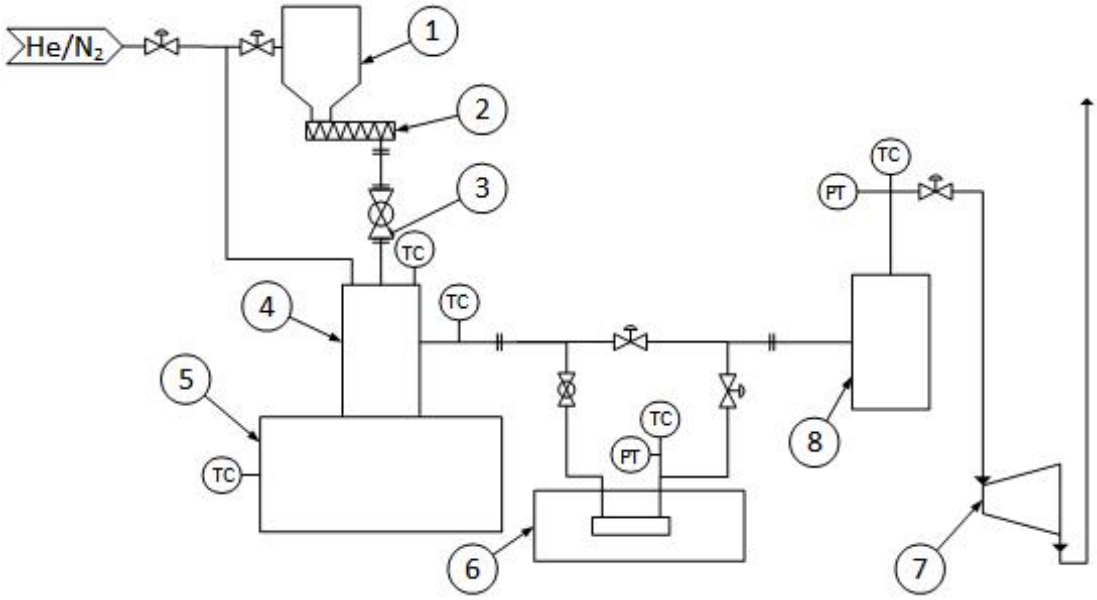

Figure 19: Planned installation of the screw feeder: (1) hopper, (2) screw feeder, (3) ball valve, (4) pyrolysis reactor, (5) furnace, (6) FTIR spectrometer, (7) vacuum pump, (8) condenser.

4.2 Initial hopper design

An investigative approach was followed to design the storage hopper. The literature indicated there are three variables that affect the flow achieved inside a hopper: the hopper outlet dimensions, the hopper wall angle, and the material particle properties (especially the particle size distribution). The hopper outlet dimensions were already specified by stipulating the minimum screw outside diameter (21.5 mm). Hence, the optimum hopper wall angle and the optimum PTFE feeding mixture had to be determined experimentally. An initial testing hopper was required to determine these two variables experimentally. The design of this

hopper is discussed in this section. The steps followed to determine the optimum hopper angle and PTFE feeding mixture are detailed in section 5.1.1.

4.2.1 Hopper shape and flow pattern selection

In conjunction with a screw feeder, there are only three hopper shapes to consider: wedge-shaped hoppers, chisel-shaped hoppers, and racetrack-shaped hoppers (see Figure 20). A wedge shape was selected purely due to the construction difficulties that accompany the other two shapes.

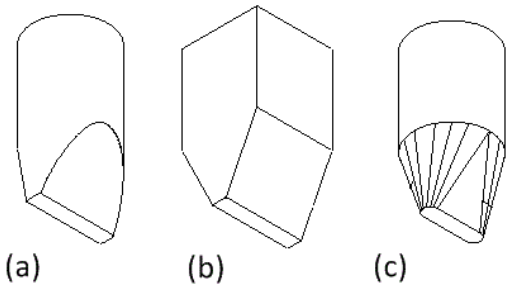

Figure 20: Three hopper shapes: (a) chisel shaped hopper, (b) wedge-shaped hopper, and (c) racetrack shaped hopper (Schulze (2008)).

Since Teflon® PTFE 807N is highly compressible, fibrous and somewhat cohesive, it was decided to design the hopper for a mass flow regime.

4.2.2 Hopper sizing and minimum wall angle calculations

To complete the Initial hopper design, estimates found in the literature of the effective angle of internal friction, φ_e, and the angle of wall friction, φ_w, (see 2.2.1) of PTFE were used.

The angle of friction can be defined as the maximum angle at which an object can rest on an inclined plane without sliding down. By this definition, the angle of wall friction can be defined as the maximum angle of the hopper wall at which PTFE can resist sliding down. The angle of wall friction is highly dependent on the material of construction of the hopper. In this case, stainless steel was used as construction material. According to Raymond (1985) a good estimate of the angle of wall friction can be calculated using Equation (6):

$$\tan \varphi_w = \mu_s \tag{6}$$

with μ_s, the coefficient of static friction between PTFE and a stainless steel surface. However, the only static friction coefficient available in the literature is that of PTFE on a steel surface, which varies between 0.05 and 0.2 (The Engineering ToolsBox, *sa*). For the purpose of this investigation, the static friction coefficient of steel was assumed to be the same as stainless steel and a conservative coefficient value of 0.2 was used. Substituting this into Equation (6), the angle of wall friction was estimated to be 11.31°.

The effective angle of internal friction is defined as the interparticle kinematic friction angle that exists during steady flow (Raymond, 1985: 910), whereas the angle of internal friction is the interparticle friction angle as a bulk solid starts to slide on itself at the onset of flow. Typically the effective angle of internal friction is larger than the angle of internal friction. These values are sensitive to temperature, time of storage, moisture content, density and the particle size, shape and distribution.

The angle of repose of a material is a property that describes the piling or stacking of the material particles when poured. The angle of repose can be considered as a measure of the internal friction between the particles as a whole and not between the individual particles (Patil, 2009: 1.37). In an ideal situation where the material is truly homogeneous, it can be said that the angle of repose and angle of internal friction are equal. However, in practice, the angle of repose is smaller than the angle of internal friction.

For the purpose of the initial hopper design, it was assumed that the angle of repose is equal to the angle of internal friction and therefore equal to the effective angle of internal friction, φ_e. Hori and Shizuoka-ken (1997) determined the angle of repose for various granular PTFE with varying particle sizes and bulk densities (see Table 8). The two PTFE mixtures that resemble Teflon® PTFE 807N the most is mixtures 6 and 8. Mixture 6 has a bulk density very close to 0.927 g·cm^{-3}, and mixture 8 has a similar average particle size. The angle of repose for both of these mixtures are in between 30° and 40°. Considering a more detailed mass flow diagram for wedge-shaped hoppers (see Figure 21), it can be seen that at an angle of wall friction of 11.31°, the hopper wall angle is practically the same for an effective angle of internal friction between 30° and 40°. An initial angle of repose, and therefore the effective angle of internal friction, of 35° was used.

Table 8: Angle of repose calculated for various granular PTFE mixtures by Hori and Shizuoka-ken (1997).

PTFE mixture number.		1	2	3	4	5	6	7	8	9
Average particle size	(µm)	276	324	234	255	483	400	263	620	185
Bulk density	(g·cm^{-3})	0.78	0.76	0.66	0.72	0.76	0.81	0.63	0.52	0.47
Angle of repose	(°)	35	34	33	34	34	31	40	37	41

Figure 21 can be represented by Equation (7) for $\varphi_w < \varphi_e$ - 3° and $\theta_p \leq 60°$.

$$\theta_p \leq \left(60.5° + \frac{\arctan\left(\frac{50° - \varphi_e}{7.73°}\right)}{15.07°}\right)\left(1 - \frac{\varphi_w}{42.3° + 0.131° \cdot e^{0.06 \cdot \varphi_e}}\right) \quad (7)$$

Using Equation (7) and the estimated values indicated in Table 9, the minimum hopper wall angle, θ_p, was calculated to be 47.8°. Since the hopper wall angle had to be smaller than or equal to the calculated angle, an initial hopper angle of 45° to the vertical was selected.

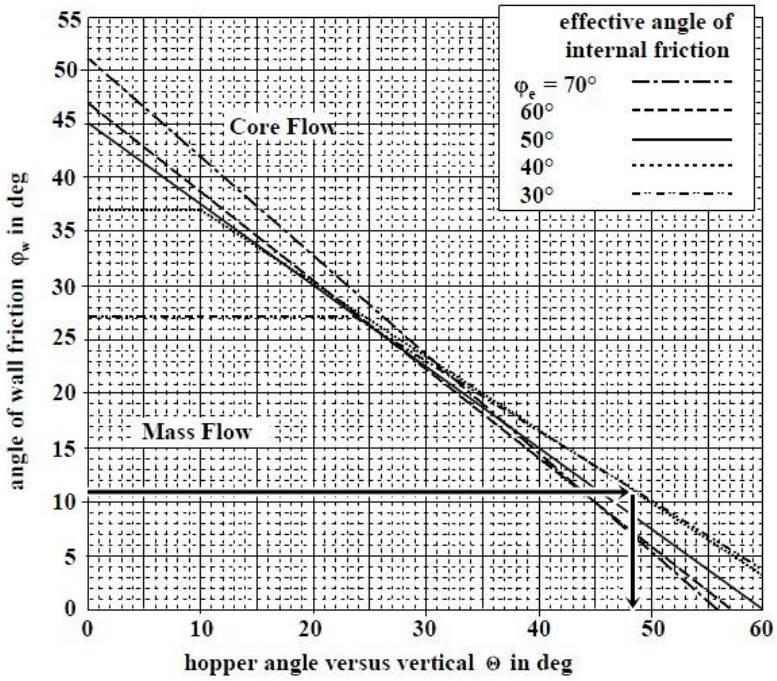

Figure 21: Detailed Jenike mass flow diagram for wedge-shaped hoppers.

Table 9: Estimated values for the particle properties of Teflon® PTFE 807N.

Effective angle of internal friction	φ_e	35°
Angle of wall friction	φ_w	11.31°

To ensure that the screw feeder fits inside the hopper the minimum hopper outlet opening width could be no less than 22 mm. The minimum hopper outlet opening length should at least be larger than three times the outlet opening width, as mentioned in section 2.2.2. Hence, the minimum hopper outlet opening length should be longer than 66 mm. A hopper outlet opening length of 80 mm was selected. The hopper had to have a PTFE holding capacity of at least 1 kg; however, the initial test hopper was designed to have a capacity of 2 kg to accommodate any changes made to the hopper wall angle as discussed in section 5.1.1. This equates to a total hopper volume of 1.6 L. To ensure that the hopper is not filled to the brim the total hopper volume was increased by 25 % to 2 L. The final initial hopper dimensions are indicated in Figure 22.

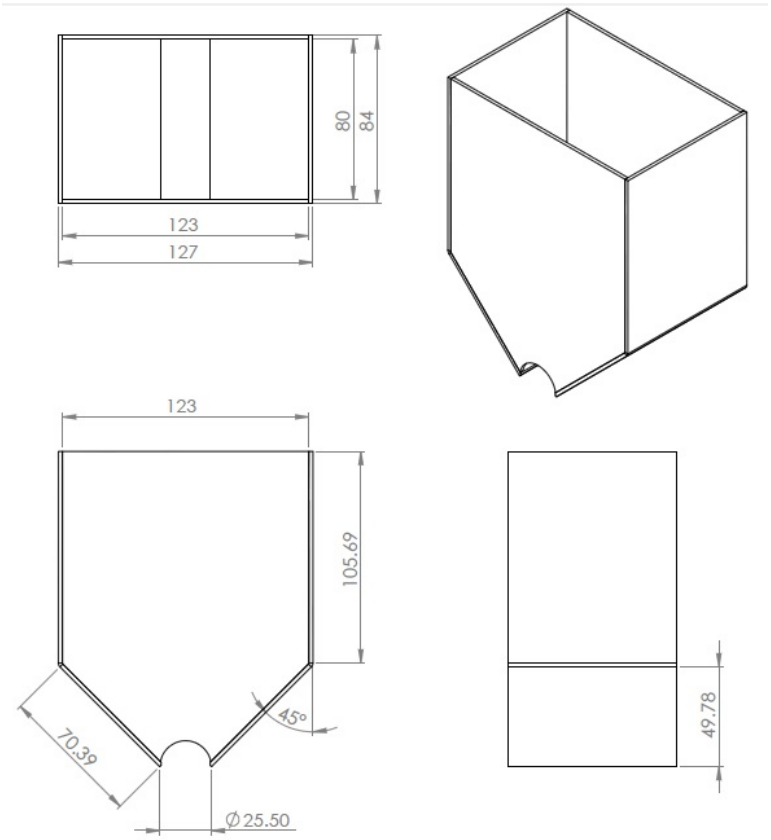

Figure 22: Initial hopper design dimensions. All dimensions are in millimetres.

4.3 Screw selection, design, and manufacture

As shown in section 2.1, a wide variety of screw configurations are available. Following the advice of van der Walt (2015), one of the first screw configurations considered for this application was a ribbon feeder. A ribbon feeder is essentially a shaftless screw as depicted in Figure 23. He suggested this configuration following his experience in feeding PTFE into his continuous depolymerisation setups at NECSA (van der Walt, 2007). They experienced severe PTFE compression inside the screw leading to irregular or no-flow from the feeder, and a ribbon feeder solved this issue. A deeper investigation into this screw indicated that a ribbon feeder with a minimum outside diameter of 21.5 mm, as specified in section 4.1.1, could not be procured commercially and would be impossible to manufacture with the equipment available in the university workshop. Therefore, this design was abandoned.

Figure 23: Ribbon feeder.

To achieve a constant feeder flow rate, an even drawdown in the hopper would be advantageous. Fernandez, Cleary, and McBride (2011) concluded that an even drawdown should be achieved whenever some form of a tapered screw is used. An even drawdown spreads the force acting on individual PTFE particles over the screw surface instead of concentrating the forces at one end as with a uniformed pitch screw. Since Teflon® PTFE 807N particles are very compressible, a uniform drawdown inside the hopper might help reduce the compressive forces and help to produce an even and constant flow rate. Hence, a screw with a tapered shaft was selected.

Considering the pitch selection rule of thumb mentioned is section 2.1, and the specified minimum screw diameter of 21.5 mm, the minimum pitch length should be 7 mm. However, due to limitations on the available equipment, a pitch length of 6 mm was selected with a flight thickness of 4 mm.

The final screw design is depicted in Figure 24. The screw shaft in the hopper was tapered, starting at a diameter of 21.5 mm down to a diameter of 10 mm. The screw shaft at the hopper exit onwards was kept constant at a diameter of 10 mm.

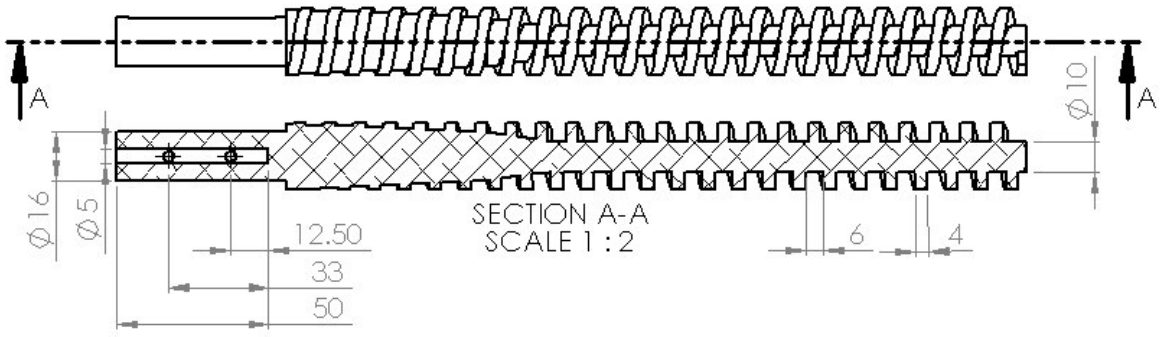

Figure 24: Final screw configuration design

Theoretically, the capacity of a screw feeder can be determined using Equation (8), where Q, is the screw feeder flow rate produced in g·min^{-1}, P, the screw pitch length (mm), F, the screw flight thickness (mm), D_{OD}, the screw outside diameter (mm), D_{ID}, the screw shaft diameter, ρ_b, the bulk density (g·cm^{-3}), n, the motor speed and i, the degree of filling constant. The degree of filling is highly dependent on the material and varies as the material properties and forces inside the hopper vary. When calibrating a screw feeder a value for the degree of filling can be determined experimentally and used together with the equation to predict the screw feeder flow rate.

$$Q = \left(\frac{\pi \cdot (P - F) \cdot (D_{OD}^2 - D_{ID}^2)}{4000}\right) \cdot \rho_b \cdot n \cdot i \qquad (8)$$

Using Equation (8) and an i value of 0.5, the theoretical screw feeder flow rates could be predicted as shown in Table 10.

Table 10: Theoretically calculated screw feeder flow rates with a degree of filling equal to 0.5.

VFD frequency (Hz)	Motor speed (rpm)	Theoretical flow rate ($g \cdot min^{-1}$)
50	37	29.26
40	30	23.74
30	22	17.41
20	15	11.87
10	8	6.33

To determine if the reactor system would be able to handle these flow rates, the overall kinetics of PTFE depolymerisation was examined. The literature indicates (see section 3.3) that the thermal decomposition of PTFE may be approximated by a first order reaction rate and is therefore not affected by the initial mass of PTFE in the reactor. This suggests that the reactor should be able to cope with the feed rates as long as both the conversion and heat transfer in the system are fast enough. The conversion of PTFE at various temperatures was analysed using Equations (9) and (10) and are indicated in Figure 25. The values determined experimentally by van der Walt (2007) (see Table 6 on page 18) were used.

Ideally, to avoid build-up of PTFE in the reactor, complete conversion should be achieved within a minute or two of delivery. Theoretically, the PTFE delivered by the screw in one minute should depolymerise almost completely within that time. As indicated in Figure 25, this only occurs at temperatures higher than and equal to 650 °C. This indicates that for the continuous system, PTFE depolymerisation would be too slow at temperatures lower than 650 °C, and therefore, operation at temperatures lower than 650 °C would not be recommended.

$$x = \sqrt[1-n_1]{1-(1-n_1)kt} \tag{9}$$

$$k = k_0 e^{-E_{act}/RT} \tag{10}$$

Initially, stainless steel was selected as screw construction material. However, limitations on the available equipment, in conjunction with the screw design, limited the construction material to an extruded aluminium round bar.

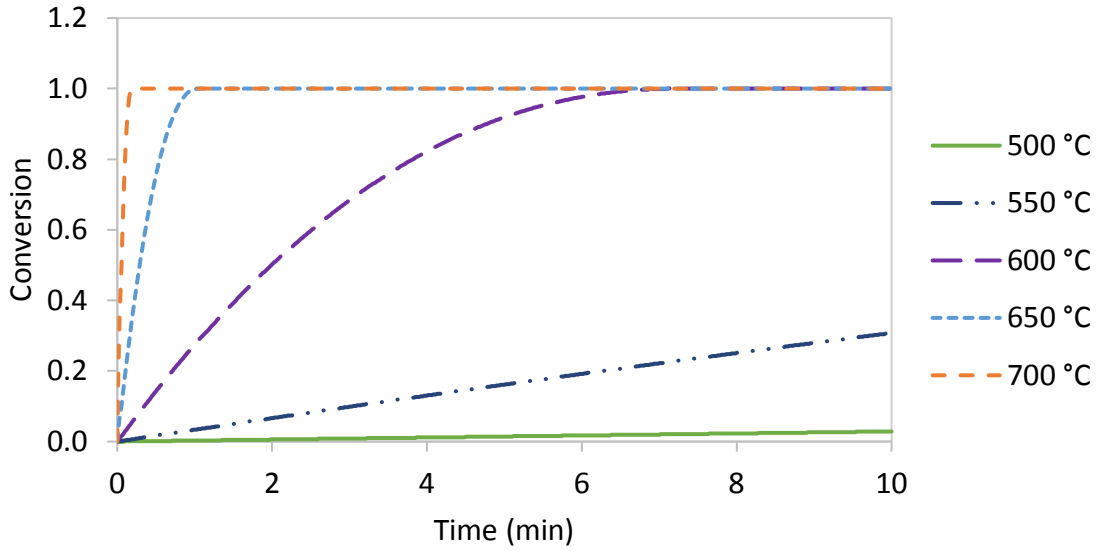

Figure 25: Conversion of PTFE as determined by the kinetic values calculated by van der Walt (2007).

5 Initial feeder system experimental planning, results, and discussion

5.1 Hopper testing experimental method

5.1.1 Variable parameter selection

In order to achieve proper mass flow inside the hopper and to prevent arching or rat-holing problems, two parameters can be varied: the hopper wall angle; particle size and/or particle size distribution of PTFE. Changing the hopper angle will most likely be the most effective parameter. As mentioned in section 4.2.2, the angle of repose, used as an estimate of the effective angle of internal friction, is usually smaller than the actual effective angle of internal friction. This means that the initial hopper design angle might not be steep enough to promote mass flow inside the hopper. Therefore, four different hopper angles were investigated: 45°, 35°, 30° and 20°. The hopper's angles were adjusted to the various selected angles by inserting triangles inside the standard 45° hopper, as indicated in Figure 26.

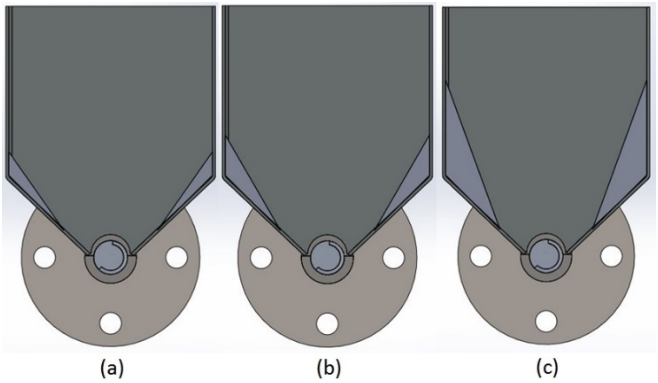

Figure 26: Inserts on the sides of the hopper decrease the hopper angle without affecting the slit width: (a) Hopper angle of 35°; (b) Hopper angle of 30°; and (c) Hopper angle of 20°.

Increasing the particle size or particle size distribution of PTFE could increase its flowability and thereby decrease its effective angle of internal friction, hence increase the hopper angle required to promote mass flow. Increasing the particle size also helps to prevent arching inside the hopper (Diamondback Technology, 2005). For this reason, three different PTFE mixtures were tested:

- DuPont Teflon® PTFE 807N.
- A mixture containing 70 wt % Teflon® PTFE 807N and 30 wt % larger particles (see section 5.1.2).
- A 50 wt % Teflon® PTFE 807N and 50 wt % larger particles mixture (see section 5.1.2).

5.1.2 PTFE particle production method

The larger PTFE particles used to increase the particle size distribution were manufactured following the method described below:

- DuPont Teflon® PTFE 807N was pressed at 15 MPa for 20 s to produce a rigid PTFE disc.
- These PTFE discs were chopped to produce smaller compressed particles.
- The chopped PTFE particles were separated using sieves to produce a mixture with a particle distribution range of 1600 µm to 2000 µm.

5.1.3 Experimental setup

The feeder system setup is depicted in Figure 27 and Figure 28. The hopper and screw designed in sections 4.2 and 4.3 are indicated in the figure. The Parr MagDrive (see Figure 27) connected between the motor and the screw, is a magnetically coupled rotary feedthrough used to seal rotating parts to prevent leakage of gas. Although the MagDrive was not required during the testing stage, it was included to assess its magnetic coupling strength to confirm that it will rotate the screw under the operating conditions.

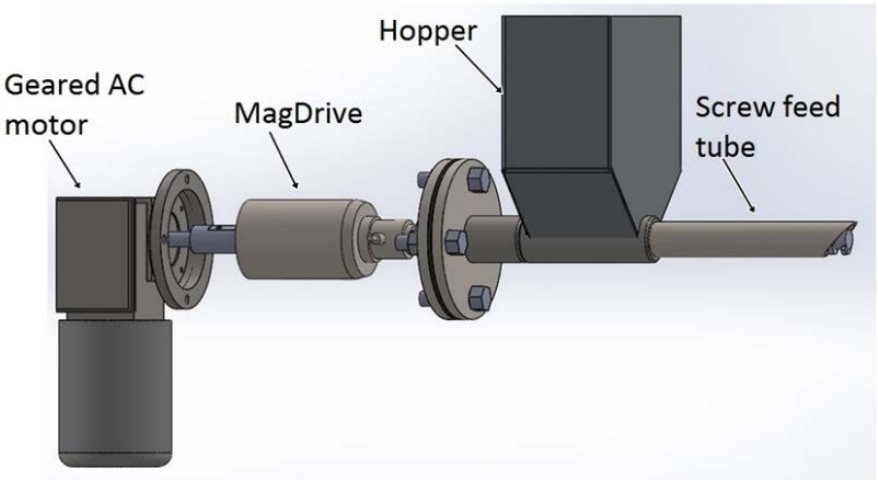

Figure 27: Designed testing feeder system. Support structure not shown.

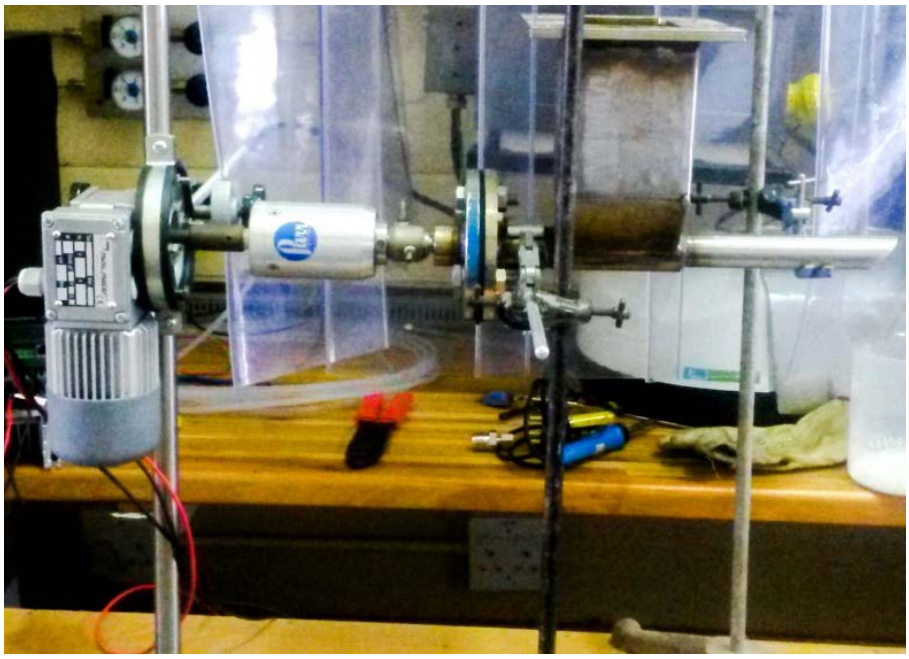

Figure 28: Actual testing feeder system.

5.1.4 Hopper testing experimental planning

The main objectives were to determine the optimal hopper wall angle and PTFE feed mixture that would:

- Provide an expanded or mass flow regime inside the hopper.
- Prevent the formation of arches or rat-holes in the hopper.
- Provide a constant and repeatable flow rate.

The PTFE mass loaded into the hopper and the total run time was kept constant at 400 g and 20 min, respectively. The system was operated at two different motor speeds 21 rpm and 35 rpm, corresponding to VFD frequencies of 30 Hz and 50 Hz, respectively. The four sets of

experimental runs are described in Table 11, Table 12, Table 13 and Table 14. To test the robustness of the system, some experimental runs were repeated at random.

Table 11: Experimental description and layout of the first set of hopper test runs. These runs were performed without any changes in hopper wall angle or particle distribution.

Set number:	One: Operation without any changes				
Description:	The feeder system was set up without any alterations. Therefore, the hopper angle remained 45°.				
Experimental layout					
Motor speed	PTFE mass loaded	Mixture		Hopper angle	Operation time
		Teflon® PTFE 807N	Particulate PTFE		
(rpm)	(g)	(wt %)	(wt %)	(°)	(min)
22	400	100	-	45	20
37	400	100	-	45	20

Table 12: Experimental description and layout of the second set of hopper test runs. These runs were performed with a change in hopper wall angle only.

Set number:	Two: Operation with changes in hopper angle only				
Description:	At a specific frequency, three runs were completed, each at one of the respective decreased hopper angles: 35°, 30°, and 20°.				
Experimental layout					
Motor speed	PTFE mass loaded	Mixture		Hopper angle	Operation time
		Teflon® PTFE 807N	Particulate PTFE		
(rpm)	(g)	(wt %)	(wt %)	(°)	(min)
22	400	100	-	35	20
22	400	100	-	30	20
22	400	100	-	20	20
37	400	100	-	35	20
37	400	100	-	30	20
37	400	100	-	20	20

Table 13: Experimental description and layout of the third set of hopper test runs. These runs were performed with changes in the particle size distribution only.

Set number:	Three: Operation with increase in particle size distribution
Description:	At a specific frequency two runs were conducted, each with one of the respective PTFE mixtures: 70 wt % Teflon® PTFE 807N and 30 wt % particulate PTFE; 50 wt % Teflon® PTFE 807N and 50 wt % particle PTFE. The hopper angle is not changed and remains 45°.

Experimental layout

Motor speed	PTFE mass loaded	Mixtures		Hopper angle	Operation time
		Teflon® PTFE 807N	Particulate PTFE		
(rpm)	(g)	(wt %)	(wt %)	(°)	(min)
22	400	70	30	45	20
22	400	50	50	45	20
37	400	70	30	45	20
37	400	50	50	45	20

Table 14: Experimental description and layout of the fourth set of hopper test runs. These experimental runs were performed with changes in both hopper wall angle and particle size distribution.

Set number:	Four: Operation with change in both parameters
Description:	At a specific frequency, eight runs were conducted. For each of the decreased hopper angles, two runs were completed, each with a different PTFE mixture.

Experimental layout

Motor speed	PTFE mass loaded	Mixtures		Hopper angle	Operation time
		Teflon® PTFE 807N	Particulate PTFE		
(rpm)	(g)	(wt %)	(wt %)	(°)	(min)
22	400	70	30	35	20
22	400	70	30	30	20
22	400	70	30	20	20
22	400	50	50	35	20
22	400	50	50	30	20
22	400	50	50	20	20
37	400	70	30	35	20
37	400	70	30	30	20
37	400	70	30	20	20
37	400	50	50	35	20
37	400	50	50	30	20
37	400	50	50	20	20

5.2 Initial screw feeder testing results and discussion

5.2.1 Initial test runs, complications and system corrections

Before the actual test runs were performed, the feeder system was tested to determine if any alterations were required. Several test runs were performed with Teflon® PTFE 807N at a VFD frequency of 25 Hz.

Initially, PTFE flow was noticed up until 3 min into the run, after which it stopped. Approximately 8 min into a run, the MagDrive would start to slip accompanied with no screw rotation. Closer examination of the screw revealed that PTFE compression in the screw prevented the MagDrive from rotating the screw (see Figure 29). PTFE build-up at the screw exit due to static was also noticed (see Figure 30). To negate the screw clogging, the screw feed tube was shortened to approximately 70 mm past the hopper wall(see Figure 31).

Figure 29: Severe screw clogging

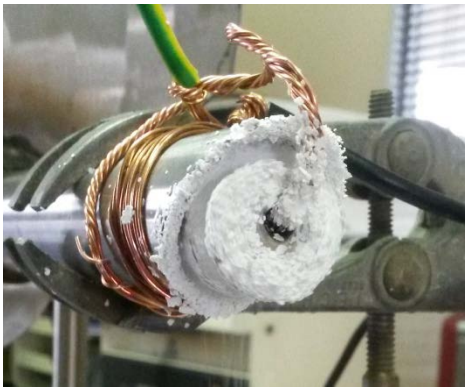

Figure 30: Static build-up at the screw exit.

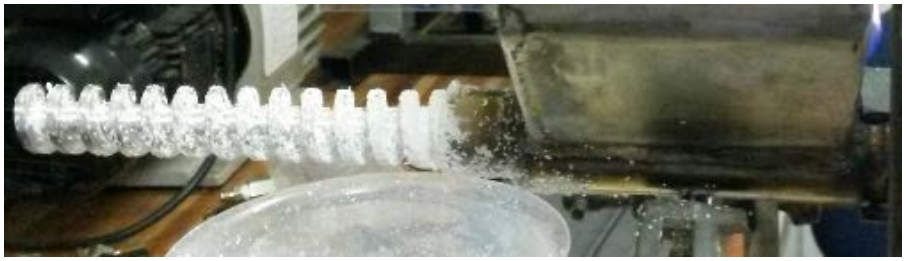

Figure 31: The testing system with shortened screw feed tube.

5.2.2 Motor speed calibration

As mentioned in section 4.1.2, Equation (5) can be used to calculate the motor speed. The maximum motor speed was specified by the manufacturer as 35 rpm at 50 Hz. However test results indicated that the actual maximum motor speed at 50 Hz was 37 rpm. The actual motor speed can now be predicted using Equation (11).

$$RPM_i = 0.74 \cdot Frequency_i \tag{11}$$

5.2.3 Initial hopper testing results

5.2.3.1 Operation without any modifications

The standard hopper with a 45° wall angle was filled with Teflon® PTFE 807N and operated for 20 min at two different motor speeds: 22 rpm and 37 rpm. As indicated in Figure 32, fairly constant and repeatable flow rates were achieved at a lower motor speed (22 rpm) compared to a higher motor speed (37 rpm). At the higher motor speed, rat-hole formation occurred fairly quickly, as indicated by the plateau.

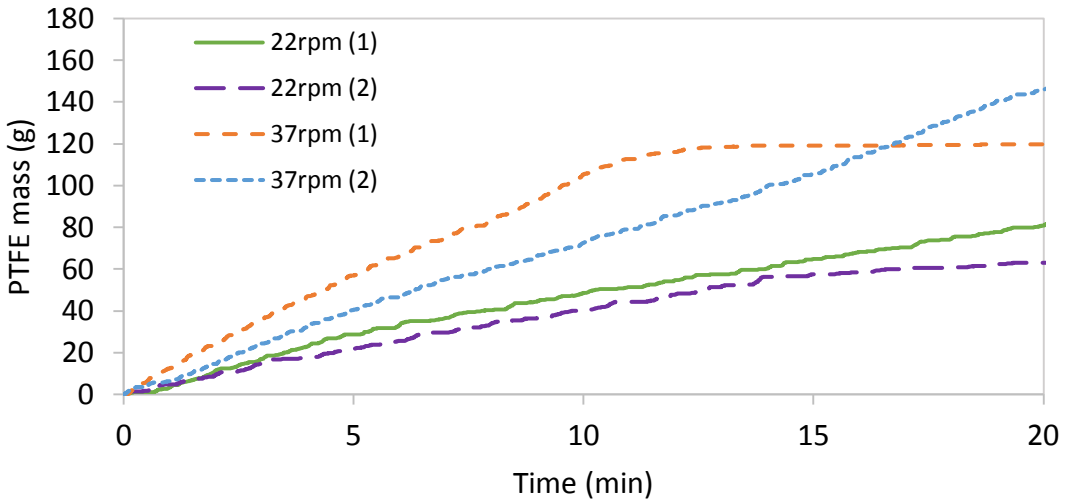

Figure 32: PTFE flow rate achieved with the standard hopper (45° hopper wall angle) at two different motor speeds.

5.2.3.2 Operation with change in hopper angle only

During these experimental runs, the hopper was filled with Teflon® PTFE 807N and operated for approximately 20 min at two different motor speeds: 22 rpm and 37 rpm. Figure 33 indicates that a fairly constant and repeatable flow rate was achieved at a low motor speed (22 rpm). However, even though the flow rates do not give any indication of this, rat-hole formation did occur throughout each of these runs. Examples of these rat-holes are depicted in Figure 34. It is clear that a change in hopper wall angle did not have an appreciable effect on the flow rates.

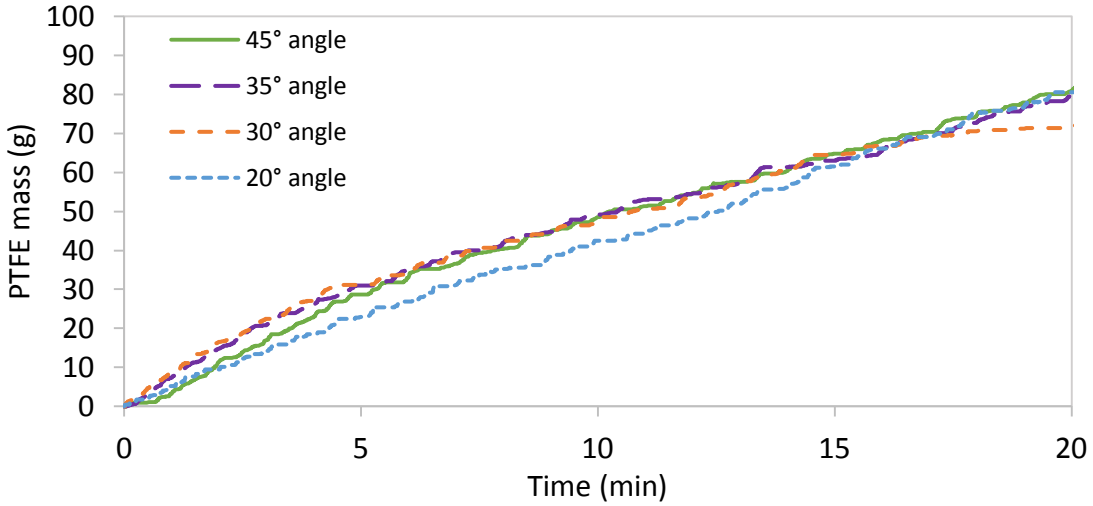

Figure 33: PTFE flow rate profile produced with Teflon® PTFE 807N at 22 rpm and four different hopper angles.

Figure 34: Rat-hole formation experienced in the hopper at two different hopper angles for a motor speed of 22 rpm (30 Hz).

At the higher motor speed, the flow rates were fairly constant for the first 5 min (see Figure 35). However, rat-hole formation severely affected the flow of PTFE as indicated by the plateaus. A decrease in hopper wall angle does seem to delay the effect of rat-holes on the system.

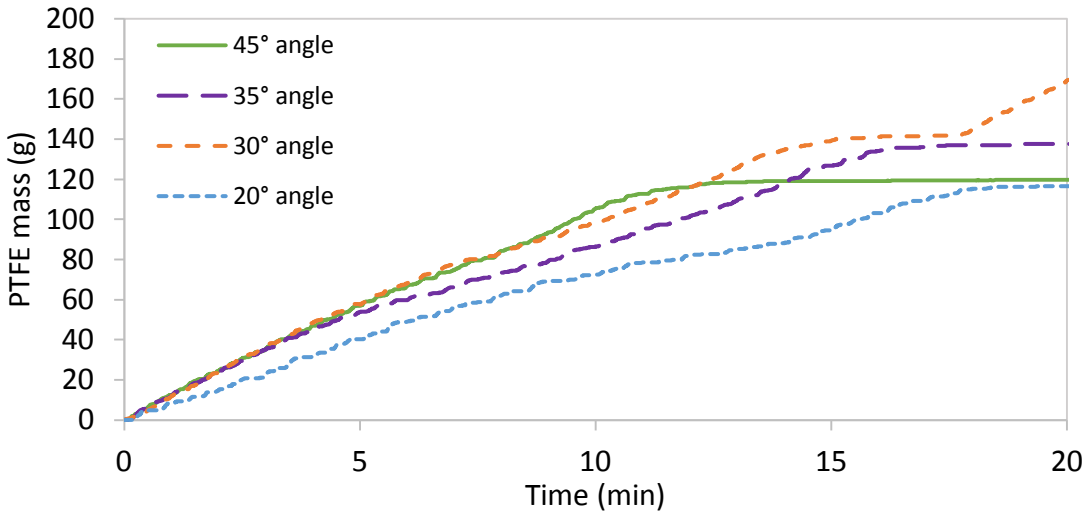

Figure 35: PTFE flow rate profile produced at 37 rpm and at four different hopper angles with Teflon® PTFE 807N.

These results indicate that a constant and repeatable flow rate can be achieved at any wall angle provided that the motor speed remains low. A steeper hopper wall angle will help to delay the effects of rat-holing; however, it will not prevent rat-hole formation.

5.2.3.3 Operation with change in particle size distribution

Figure 36 and Figure 37 indicate that the flow rate profile achieved by using Teflon® PTFE 807N and a 70:30 wt % mixture followed the same trend at both motor speeds. This indicates that there is no clear difference in the effects on screw filling and hopper flow pattern with a slight increase in the particle size distribution. However, with a 50:50 wt % mixture ratio the system becomes unpredictable at both motor speeds. Rat-hole formation affected this mixture at random times, which showed that a 50:50 wt % mixture would not produce a constant and repeatable flow rate. However, the 50:50 wt % ratio mixture aided the rat-hole to collapse in on itself as indicated by the stepping flow rate witnessed in Figure 37.

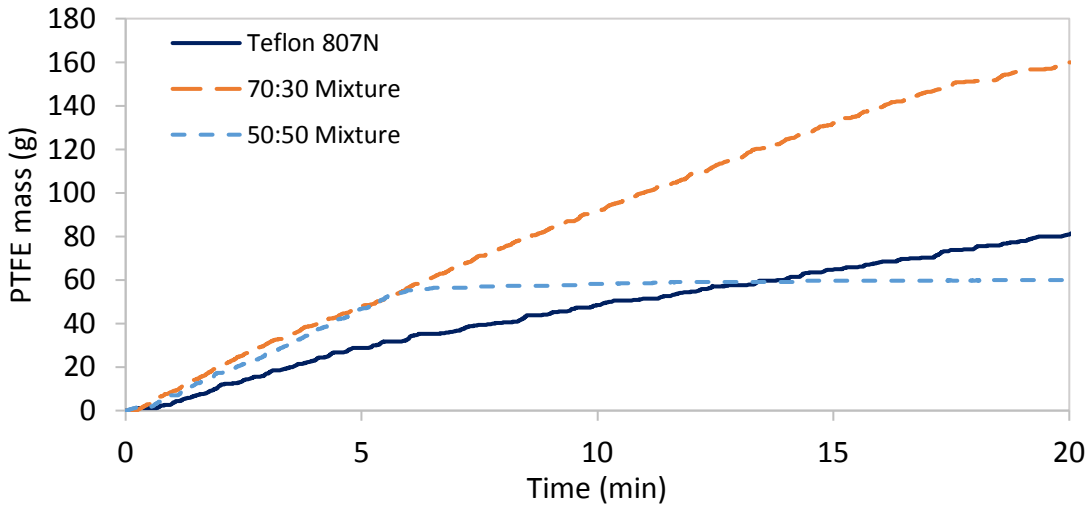

Figure 36: PTFE flow rate profile produced at 22 rpm, a hopper angle of 45° and three different PTFE mixtures.

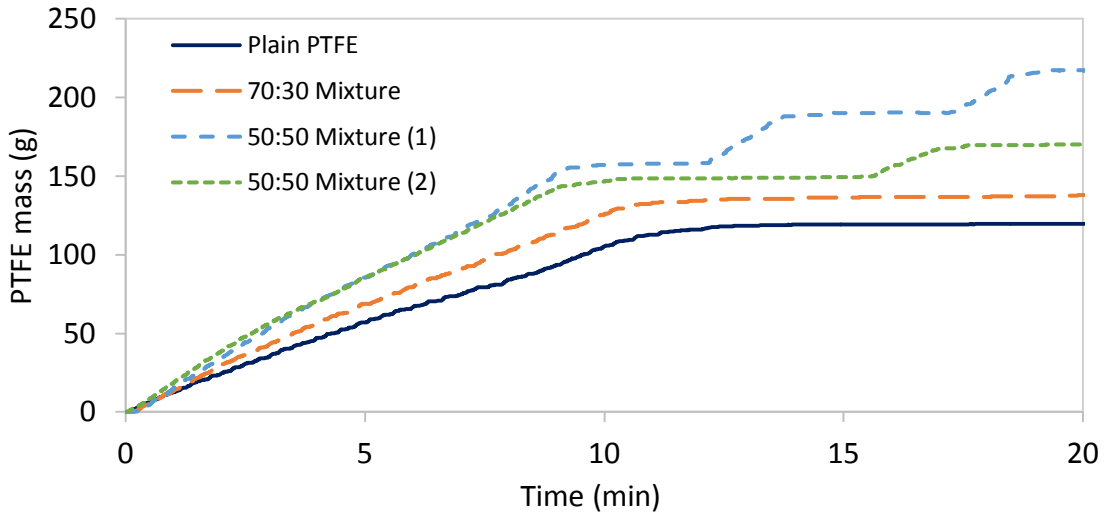

Figure 37: PTFE flow rate profile produced at 37 rpm, a hopper angle of 45° and three different PTFE mixtures.

5.2.3.4 Operation with change in both variables

Comparing Figure 38 and Figure 39, constant and repeatable flow rates were achieved at lower motor speeds, with the exception of runs performed with a 50:50 wt % mixture ratio. Rat-hole formation was present, and a decrease in hopper wall angle seeming to delay the formation. This justifies the statements made previously that a 50:50 wt % ratio mixture might not be suitable to obtain a constant, reliable flow rate.

Figure 38 justifies that a 70:30 wt % mixture produces the same results as those obtained using Teflon® PTFE 807N. A steeper wall angle does not have any clear effect on the flow rates achieved. From this, it was concluded that at lower motor speeds, only the particle size distribution had an appreciable effect on the flow rate. At lower motor speeds, increasing

the particle size distribution would not benefit the system at all, therefore, Teflon® PTFE 807N would be recommended.

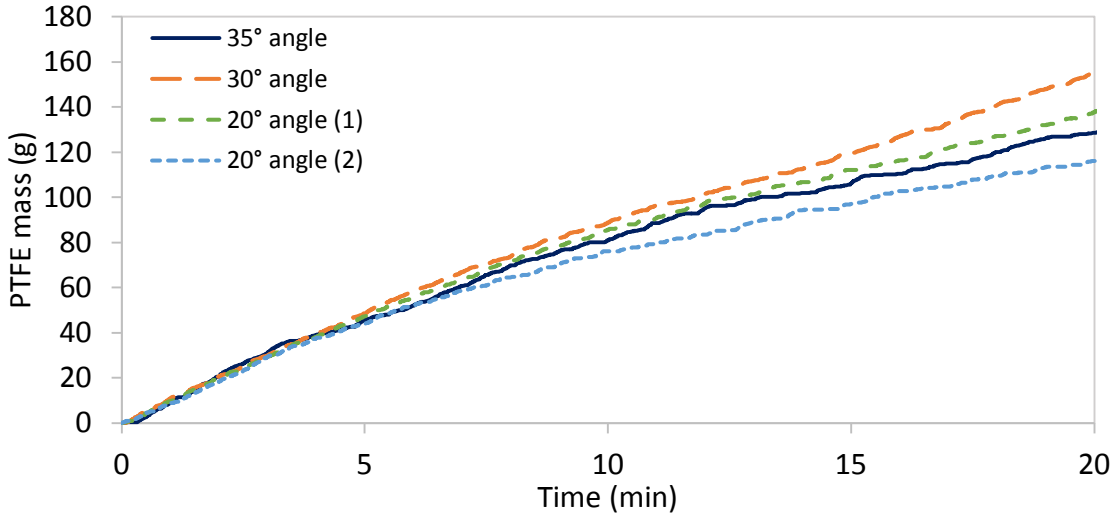

Figure 38: PTFE flow rate profile produced at 22 rpm and a 70:30 wt % % mixture at three different hopper angles.

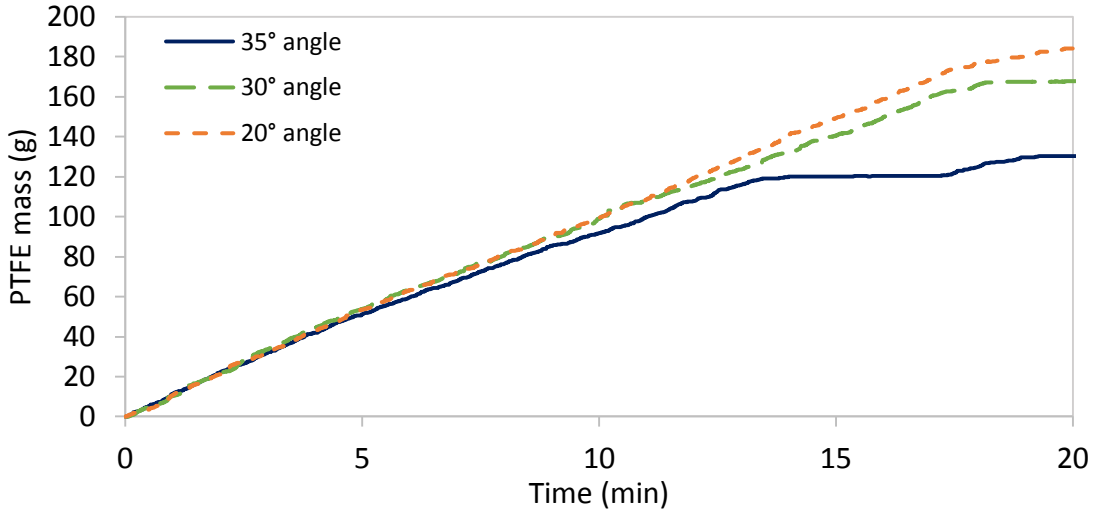

Figure 39: PTFE flow rate profile produced at 22 rpm, a 50:50 wt % % PTFE mixture and at three different hopper angles.

Moving on to Figure 40 and Figure 41, it is once more clear that a 50:50 wt % ratio mixture is extremely rat-hole prone at higher motor speed, with a decrease in the hopper wall angle delaying this formation. Rat-hole formation was also noticed for a 70:30 wt % mixture, however, at later times than compared to a 50:50 wt % mixture. The rat-hole formation in Figure 40 was also delayed by a decrease in hopper wall angle. From these two figures, it was concluded that both the hopper wall angle and the increase in the content of larger particles influence the flow rates achieved at higher motor speeds. It was clear that a steep wall angle helped delay the effects of rat-hole formation experienced at high motor speeds.

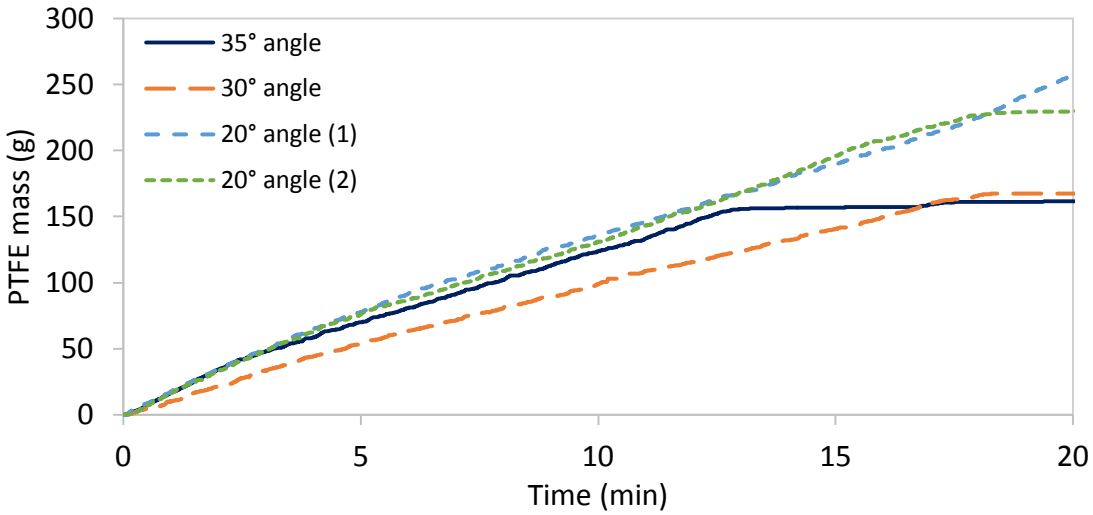

Figure 40: PTFE flow rate profile produced at 37 rpm, a 70:30 wt % % PTFE mixture and at three different hopper angles.

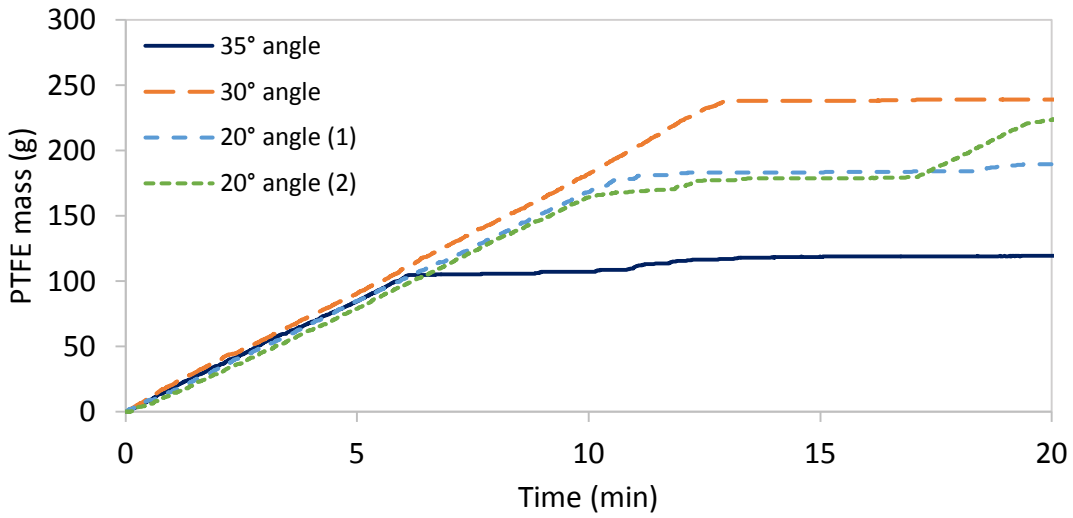

Figure 41: PTFE flow rate profile produced at 37 rpm, a 50:50 wt % % PTFE mixture and at the three different hopper angles.

5.3 Conclusions

The following conclusions were made:

- No optimum PTFE mixture could be selected as all of the mixtures were affected by rat-hole formation under certain circumstances. However, pure Teflon® PTFE 807N would be the best feed material to use.
- Test results for a 50:50 wt % PTFE particle mixture indicate that this mixture is extremely rat-hole prone and does not produce a repeatable flow rate.
- The 70:30 wt % PTFE particle mixture results showed similar trends to those produced when pure Teflon® PTFE 807N was used.
- Following the results for the various hopper angles, it was concluded that an increase in hopper wall angle delayed the onset of rat-hole formation. Therefore, a hopper angle of 20° would be recommended.

6 Final hopper design, calibration, and commissioning

6.1 Amended hopper design

Following the conclusions made in section 5.3, the new hopper was designed with a 20° (to the vertical) hopper wall angle. Since no optimum PTFE particle mixture could be found, the screw feeder would feed Teflon® PTFE 807N.

However, by using these two specifications, no optimal standard hopper design could be achieved that would counteract the rat-hole formation. Rat-hole formation could be negated by using a non-compressible form of PTFE since it was determined to be the compressibility and compaction characteristics of Teflon® PTFE 807N that cause the problem. The particles inside the hopper do not stick to the hopper walls they tend to clump together more. This leads to the conclusion that the angle of wall friction, and therefore the hopper wall angle is not the greatest concern when designing a hopper for Teflon® PTFE 807N. However, it is the angle of internal friction between the particles that cause the problems. It should be kept in mind that the system will be used in future to depolymerise waste PTFE, therefore, the feeder should be designed and manufactured in such a way that it can easily be adapted to accommodate irregular ground scrap material. Waste PTFE particles would be less compressive than Teflon® PTFE 807N and should flow without restrictions in the hopper. For this reason, it was decided not to change the hopper configuration but to include an internal or external agitation method to solve the rat-holing issue.

The easiest solution would be to insert a stirrer in the hopper, but since the system needs to operate under vacuum conditions, a non-invasive method of particle disturbance was initially considered. A vibrator was connected to the outside of the hopper as indicated in Figure 42. Various vibrating methods and intervals were investigated (see Table 27 in Appendix A). This solution did work to an extent, as it helped to collapse rat-holes, but even higher compaction of the Teflon® PTFE 807N particles was noticed. In Appendix A A.1 the results of 15 separate runs can be observed. Analysis of these results led to the conclusion that a vibrator would not help solve the rat-holing issue.

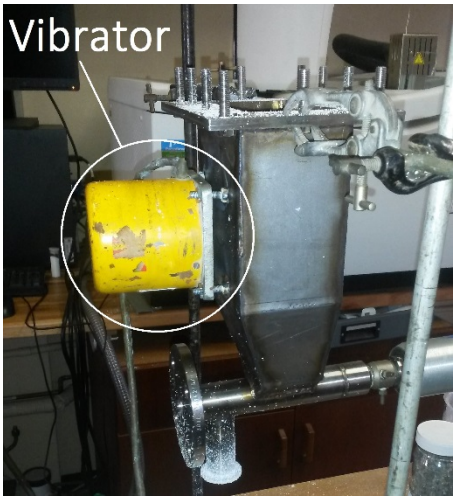

Figure 42: Feeding system with the vibrator attached to the hopper.

It was evident from the vibrator tests that no external method of particle agitation helps with the rat-holing problem. Inserting a stirrer in the hopper was the only viable solution (see Figure 43). Initially, the stirrer was left to stir continuously, but this led to high levels of particle compaction at the hopper, screw interface (can also be seen in Figure 43). The stirrer was programmed to stir for one second every 15 s. This stopped rat-hole formation from occurring completely. However, some particle compaction was still noticed at the bottom of the hopper after a few runs.

Figure 43: System with the stirrer inserted inside of the hopper. One can see the heavily compacted PTFE resulting from over stirring the particles.

The final feeder system is depicted in Figure 44. The stirrer motor shaft and the stirrer shaft are connected through the hopper top flange with a Viton oil seal. To monitor the PTFE level inside the hopper, the hopper top flange was manufactured from clear polycarbonate plate. A viewing glass was inserted at the feeder outlet to monitor the flow of PTFE.

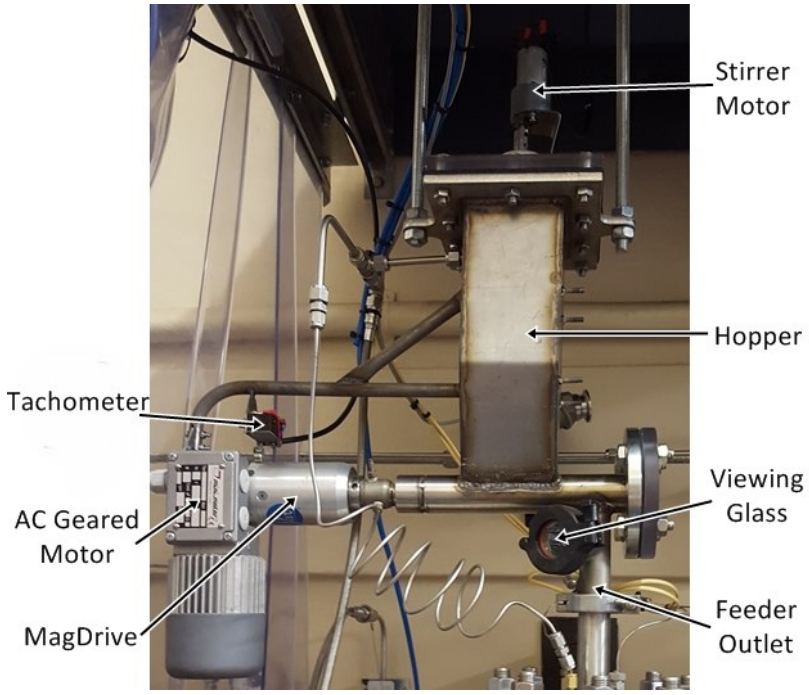

Figure 44: Final manufactured continuous PTFE screw feeder.

6.2 Feeder calibration method

Feeder calibration is required to establish a correlation between the motor speed and the mass flow rate produced by the feeder and to ensure that the flow rate is repeatable and constant over a period of time. The feeder system was calibrated before installation under atmospheric conditions and after installation under vacuum conditions. Since the hopper would have to be subjected to a flush and evacuation cycle as mentioned in section 3.5, the feeder was calibrated under the same conditions to determine the effect of a vacuum on the screw filling. Due to the cost of Teflon® PTFE 807N, the same sample of material was reused for the calibration experiments. After each run, the particles were sieved to remove any large lumps formed during the feeding process and reused.

6.2.1 Alterations made to the system layout

To prevent PTFE from flowing uncontrollably into the reactor during the flush and evacuation cycle, valve V1 (see Figure 45) was inserted in the line connecting the reactor, the hopper, and the inert gas flow. This valve remains closed when the system is flushed and opens during the evacuation cycle to evacuate the hopper bed. To ensure the hopper bed is completely evacuated, the system was evacuated three times, each separated by an equilibration period of 30 s. The ball valve (3) remains closed during the flush and evacuation cycle.

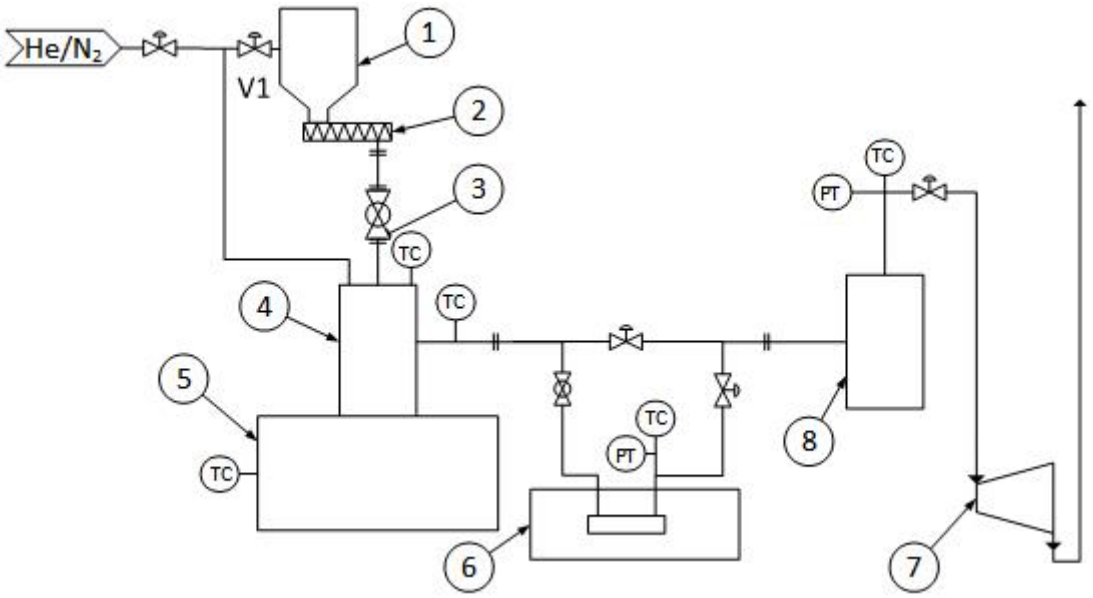

Figure 45: The continuous depolymerisation system with an added valve (V1) before the hopper: (1) hopper, (2) screw feeder, (3) ball valve, (4) pyrolysis reactor, (5) furnace, (6) FTIR spectrometer, (7) vacuum pump, (8) condenser.

6.2.2 System calibration under atmospheric conditions

Feeder calibration was achieved by filling the hopper with 1.2 kg of Teflon® PTFE 807N. The feeder system was operated for 30 min while measuring the PTFE outflow with a computer connected scale. This procedure was repeated five times at VFD frequencies of 50 Hz and 30 Hz, and three times at VFD frequencies of 40 Hz and 20 Hz. The procedure was only repeated three times at 40 Hz and 20 HZ due to time constraints.

6.2.3 System calibration under vacuum conditions

To calibrate the feeder system under vacuum conditions, the feeder was installed in the batch-depolymerisation system where the PTFE feed tube use to be (see Figure 18). The feeder was calibrated by simulating an actual continuous-depolymerisation run without heating the reactor. The system was flushed and evacuated and then subjected to a vacuum test. If the system is deemed leak-tight, the ball valve connecting the reactor and screw opens and a run is initiated. Experimental run time was 10 min. Assuming that the flow rate was constant, the flow rate was determined by weighing the PTFE removed from the reactor. This process was repeated at four different motor speeds corresponding to VFD settings of 50 Hz, 40 Hz, 30 Hz and 20 Hz.

6.3 Calibration experimental results and discussion

The final screw feeding system calibration and determination of the degree of filling constant (i), from Equation (8), for a system at atmospheric pressure and vacuum are discussed below.

6.3.1 Calibration runs under atmospheric conditions

The average calculated flow rate at each of the VFD frequencies are indicated in Figure 46. These values were calculated by averaging the slopes determined for each of the flow rate profiles produced at each of the VFD frequencies. The slopes of those flow rate profiles that deviated from the overall trend formed by the collective were not used to calculate the global average. All flow rate profiles and their corresponding slopes are in Appendix A, Appendix A.2.1.

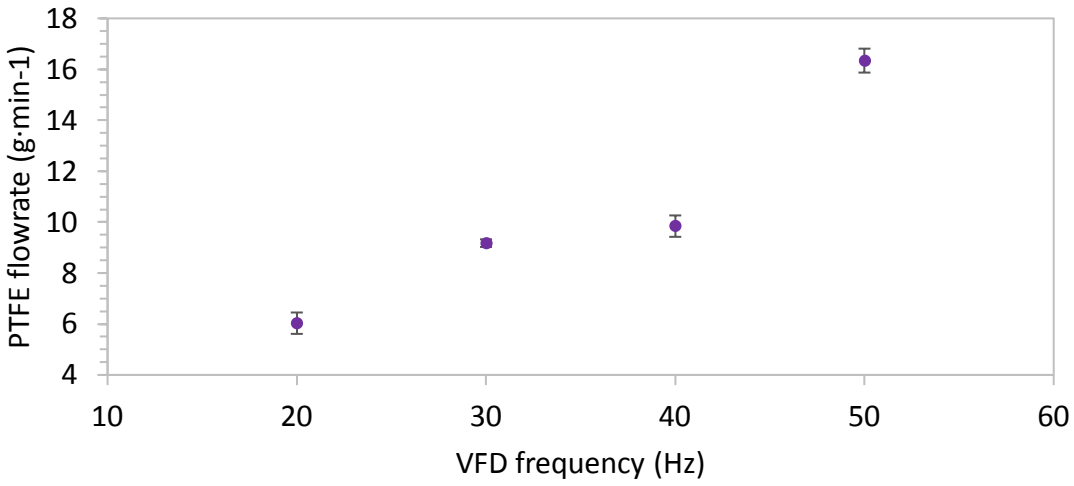

Figure 46: Average calculated flow rate at each of the VFD frequencies.

One would expect that with a constant increase in the motor speed a corresponding relatively constant increase in flow rate would occur. This is true when only the 20 Hz, 30 Hz, and 50 Hz flow rates are considered; however, the flow rate at 40 Hz deviates from this trend. This could be due to the reuse of PTFE particles after each run. It was noticed that when the same batch of PTFE was used for four or more consecutive runs, the flow rate and the flow of particles in the hopper start to change. The particles compress and compact much faster than compared to a fresh batch of Teflon® PTFE 807N.

Since the atmospheric calibration runs are only to determine if the feeder system could provide a constant feed rate, the flow rate at 40 Hz was assumed to be closer to 13 g·min^{-1} than the 9.8 g·min^{-1} seen in Figure 46. The large difference in flowrate noticed at 40 Hz was due to clumping of the PTFE inside the hopper.

The values for the degree of filling constant (i), as seen in Figure 47, was calculated using Equation (12) and the values in Table 15. There is a linear correlation between the motor speed (VFD frequency) and the degree of filling constant. As the motor speed increases, an increase in the degree of filling is noticed. A linear regression was performed on the degree of filling constant values to produce an equation that can be used to predict the degree of

filling at various motor speeds (see Equation (13)). The regression had an R-squared value of 0.996 and standard error value of 0.001. As seen in Figure 47, the predicted degree of filling values correlate well with the actual calculated values, except at 40 Hz. For the purposes of this investigation, the predicted constant value at 40 Hz will be assumed to be accurate.

$$i = \frac{4 \cdot Q}{\pi \cdot 1000 \cdot n \cdot \rho_b \cdot (P - F) \cdot (D_{OD}^2 - D_{ID}^2)} \tag{12}$$

$$i = 0.0011n + 0.238 \tag{13}$$

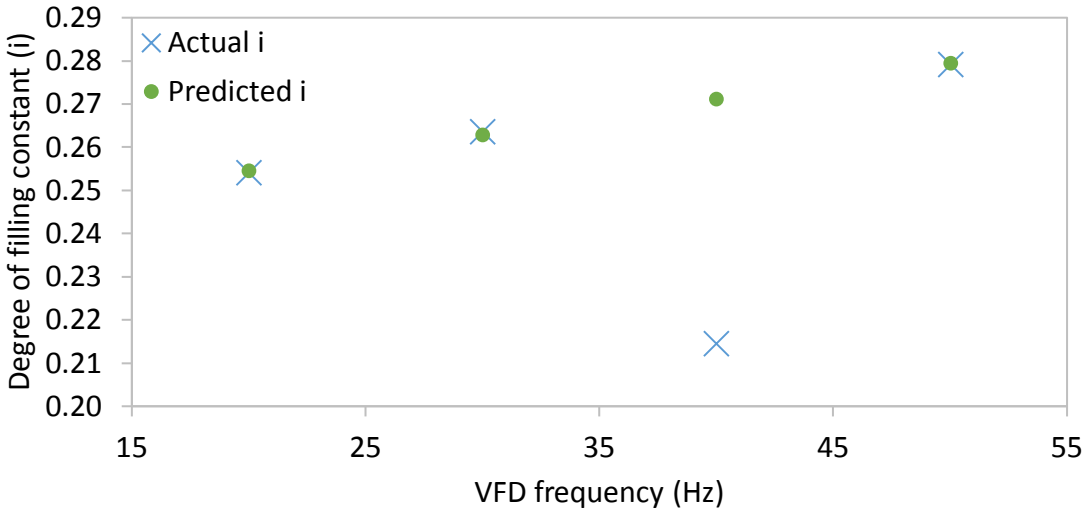

Figure 47: Correlation between the calculated degree of filling constant using the actual flow rate values and the predicted degree of filling constant values using Equation (13).

Table 15: Screw dimension and Teflon® PTFE 807N properties used to determine the screw filling constant (i).

Q (g·min^{-1})	n (rpm)	ρ_b (g.cm^{-3})	P (mm)	F (mm)	D_{OD} (mm)	D_{ID} (mm)
16.342	37	0.927	10	4	21.5	10
9.843	30					
9.175	22					
6.032	15					

6.3.2 Calibration runs under vacuum conditions

The feeder system was operated for 10 min at a specified motor speed (VFD frequency). The flow produced by the feeder was monitored for continuity using a web camera installed in front of the viewing glass (see Figure 44).

The mass measured after each run is indicated in Table 32 in Appendix A. As seen in Figure 48 below, the flow rates increase linearly as the motor speed increase. It was noted that the flow rates under vacuum increased by an average of 20 % from those calculated at

atmospheric pressure. This indicated that either the flush and evacuation cycle or the vacuum operation have an effect on the degree of screw filling achieved in the hopper.

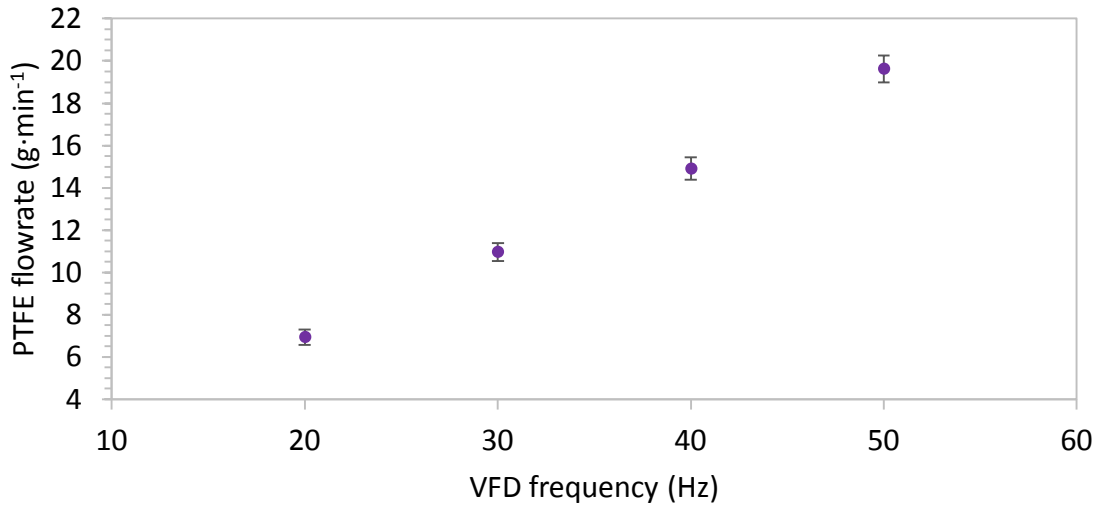

Figure 48: Average flow rate calculated at the four different VFD frequencies for the feeder system under vacuum conditions.

An increase in the degree of filling of approximately 15 % was noticed under vacuum, as oppose to atmospheric pressure (Figure 49). Hence, it is highly recommended to calibrate the feeder system under vacuum whenever any changes are made to the system that could affect the flow rate. The degree of filling under vacuum for this system can be predicted using Equation (14), derived from the actual calculated values.

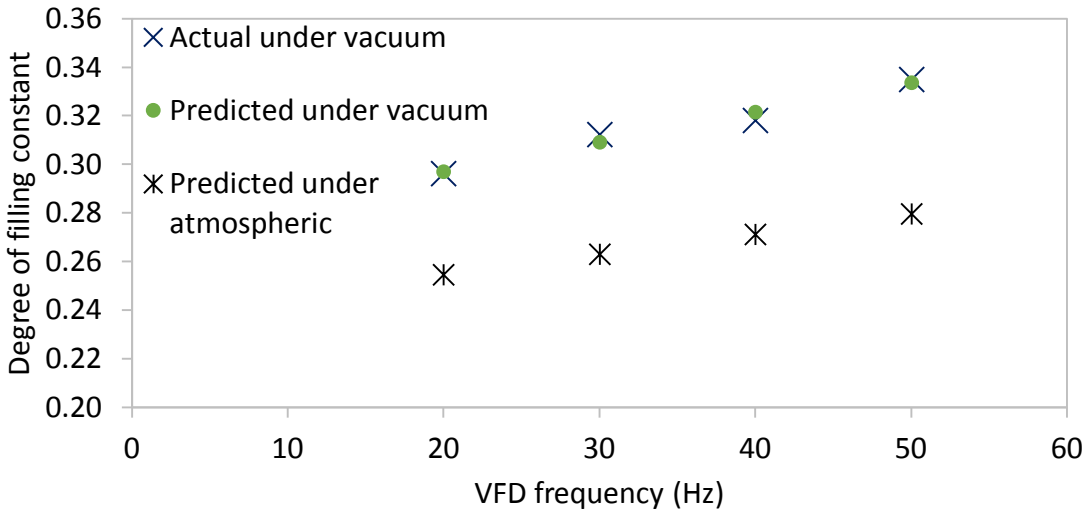

Figure 49: Actual and predicted degree of filling values under vacuum conditions compared to those predicted under atmospheric conditions.

$$i = 0.0017n + 0.2724 \quad (14)$$

7 System operating limits

Preliminary experimental test runs were performed to verify the operating limits of the newly commissioned continuous-depolymerisation system. These runs also helped to establish if any additional system changes were required to accommodate the higher gas volumes. Especially when considering that too much product gas could potentially over saturate the inline FTIR. The following points were investigated:

- The minimum operating temperature of the reactor. It was established in section 4.3 that the PTFE depolymerisation reaction is very slow at temperatures lower than 650 °C. If the reaction is too slow to accommodate the flow of PTFE into the reactor, PTFE build-up occurs. This was not desired as the reactor then need cleaning after each experimental run. Together with the temperature, the heat transfer limitations were assessed.
- The maximum PTFE flow rate also goes hand in hand with the operating temperature. At lower temperatures a lower motor speed, and essentially a lower flow rate, would most probably be preferred. At high temperatures, the system could handle a higher flow rate as the reaction rate is higher.

7.1 Experimental test procedure

7.1.1 Apparatus

Continuous PTFE depolymerisation was achieved in the test setup indicated in Figure 50 below. PTFE was fed into the reactor (4) with the screw feeder (2), where it was depolymerised at a specified temperature. To regulate the reactor pressure, the diaphragm pump (9) was controlled using pulse width modulation (PWM). The evolved product gas from the reactor flowed through an inline FTIR (6) and was pumped to the holding cylinder. The condenser vessel (8) was no longer used to condense the gas, it was kept in the system to aid in removing any debris in the product gas.

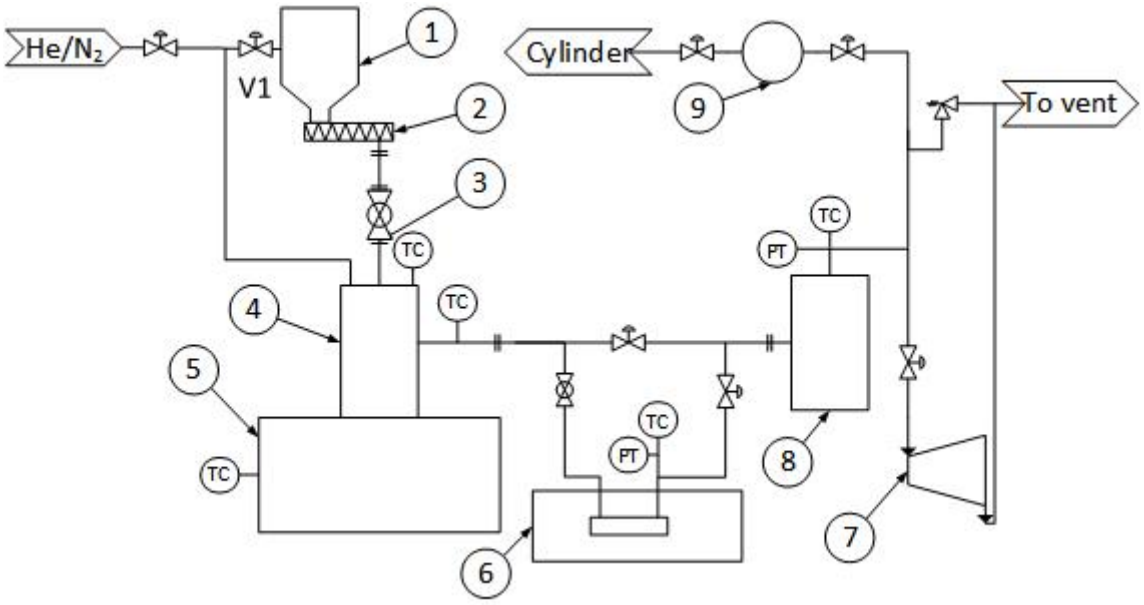

Figure 50: Scheme of the continuous depolymerisation system with the pressure controlled using the diaphragm pump: (1) hopper, (2) screw feeder, (3) ball valve, (4) pyrolysis reactor, (5) furnace, (6) FTIR spectrometer, (7) vacuum pump, (8) condenser vessel, (9) diaphragm pump.

7.1.2 Operating procedure

The entire continuous-depolymerisation system is automated and controlled by an altered version of the software used to control the batch-depolymerisations system as mentioned in section 3.5. The hopper (1) is filled with 1 kg of Teflon® PTFE 807N. The following steps are followed during an experimental run.

Initialisation step

At initialisation, the system enters a flush and evacuation cycle. After which a leak test is performed to ensure the system is leak tight. Once the system is deemed leak tight the reactor (4) is heated to the specified reaction temperature.

Operation step

Once the reactor (4) is at temperature and is deemed stable, PTFE is fed into the reactor. The system is left to operate until enough product gas has evolved to reach the specified reaction pressure. The diaphragm pump (9) is then switched on to control the reactor pressure. Once the specified reaction (10 min) time has elapsed the feeder (3) is switched off.

Finalization step

The system is left to operate for another 10 min at temperature to ensure that all of the PTFE in the reactor (4) has depolymerised. Upon completion of the run, the system is evacuated and flushed to remove any remaining product gas.

7.1.3 Experimental layout

A total experimental run time of 20 min was selected. Continuous-depolymerisation was performed at a feeder motor speed of 22 rpm. These experimental runs were performed at an operating pressure of 10 kPa, and three operating temperatures: 600 °C, 650 °C, and 700 °C.

7.2 Results and discussion

When depolymerisation was performed at a reaction temperature of 600 °C, an extreme rise in pressure was noticed during the 10 min of the finalisation step (section 7.1.2). As predicted by the kinetics, the reaction rate and or rate of heat transfer at this temperature was not fast enough to depolymerise the PTFE as it enters the reactor. Hence, operating the system at 600 °C is not recommended for the current reactor setup. When the reaction temperature was increased to 650 °C, a small increase in pressure was noticed during the finalisation step. Since kinetic data indicated that almost 100 % conversion should be achieved at 650 °C, this increase in pressure could be attributed to weak heat transfer in the reactor. To compensate for this, packing was inserted into the reactor. Although a pressure increase was still noticed when this run was repeated, it was less than previously recorded. At a reaction temperature of 700 °C, no increase in pressure was noticed during the finalisation step, indicating that the reaction rate and heat transfer is sufficient to achieve 100 % conversion. From these experimental runs, it was concluded that the reactor system should not be operated at temperatures lower than 650 °C and with motor speeds higher than 22 rpm.

Throughout the above-mentioned experimental runs, the following problems were noticed concerning the rest of the system and the following alterations were implemented (see Figure 51):

- The PWM controlled diaphragm pump (8) could not keep the system pressure at 10 kPa, not because of the volumetric flow rate of gas but because the pump could not achieve an absolute pressure of 10 kPa. The system was altered by replacing the pump with a larger one and inserting a needle valve (V5) in the system as indicated in Figure 51. Since the new pump could not be controlled using PWM, the system pressure would be controlled by manually operating the needle valve (V5) to constrict the gas flow.
- The evolved product gas saturated the FTIR (6). To resolve this an FTIR sampling system was installed as oppose to continuous, inline sampling. The sampling system consists of valves V2, V3, and V4, a sampling tube (9) and the newly added vacuum pump (10). The new sampling system works as follows: When the reaction is initiated valve V2 opens to allow the evolved product gas to flow into the sampling tube (9). At

the same time, valve V4 opens to evacuate the FTIR system using the new vacuum pump (10). Valve V2 and V4 are closed and valve V3 opens to allow the sample gas to equalise throughout the sampling system. The FTIR is triggered externally and a spectrum collected. This is repeated continuously throughout an experimental run, with a sample spectrum collected every 15 s.

- To avoid PTFE build-up in the reactor (4), the reactor is kept at temperature for another 5 — 10 min after an experimental run. During this time, no PTFE is fed and the evolved gas is diluted with an inert gas and vented.

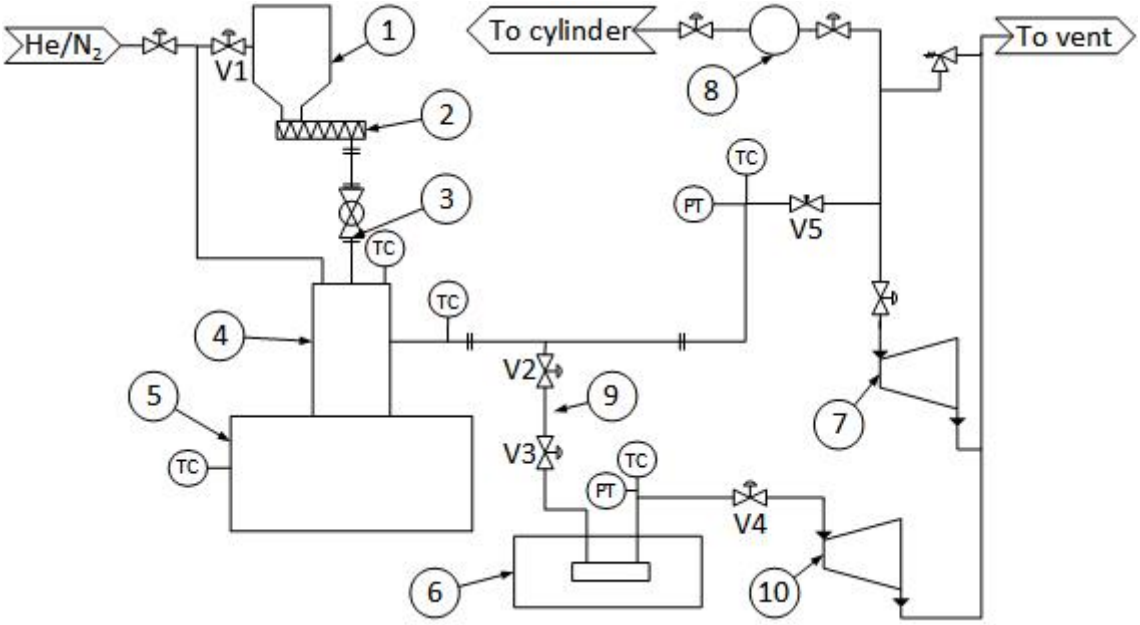

Figure 51: The altered continuous system including the pressure control valve (V5) and the FTIR sampling system: (1) hopper, (2) screw feeder, (4) pyrolysis reactor, (5) furnace, (6) FTIR spectrometer, (7 and 10) vacuum pump, (8) diaphragm pump, (9) sampling tube.

8 Conclusions and recommendations

In conclusion, a continuous PTFE feeder was designed, manufactured, commissioned and tested. This feeder is capable of providing a constant and repeatable flow rate at various motor speeds. The feeder is capable of providing a maximum Teflon® PTFE 807N flow rate of 20 g·min^{-1} for up to 40 min. The feeder consists of a wedge-shaped hopper with a constant pitch, tapered shaft screw. The hopper has a capacity of 1 kg Teflon® PTFE 807N.

Although a constant flow rate was achieved with the current feeder configuration, this feeder is not ideal when working with Teflon® PTFE 807N. Teflon® PTFE 807N is highly compressible and forms rat-holes very quickly inside the hopper, hence the need for a stirrer. A more elaborate hopper and screw design could have been used; however, keeping in mind that this same feeders system will be used in future to convey less compressible ground waste PTFE particles, the design was not altered. The stirrer helped to minimise rat-holing; however, PTFE compression was still present in the lower region of the hopper. Due to this, the full capacity of the hopper could not be used and regular cleaning is required.

The calibration experiments indicated that the flow rates achieved by the feeder are affected by the vacuum system. Therefore, it is highly recommended that the feeder is recalibrated when any changes are made to the feeder configuration.

If the current feeder system is to be used to feed waste PTFE particles, PTFE with a particle size no larger than 2 mm is recommended if the screw dimensions are not altered.

For the current reactor system, it is not recommended to operate the motor at speeds higher than 22 rpm or flow rates higher than 11 g·min^{-1}, especially when operating at temperatures lower than 700 °C. The heat transfer achieved in the reactor, even after the addition of packing, is insufficient to achieve complete conversion of PTFE at temperatures lower than 700 °C for higher PTFE flow rates.

If needed in future the problems associated with heat transfer could be resolved by either decreasing the flow rate of PTFE entering the reactor or changing the reactor design to increase the surface area available for heat transfer. This will not have any effect the minimum allowable operating temperature, but will provide a wider range of PTFE flow rates available for use. The PTFE flow rate could be reduced by either increasing the inner diameter of the screw or replacing the screw feeder motor with a motor with a lower maximum motor speed.

Part 2. Product selectivity analysis: continuous PTFE depolymerisation

The effects of temperature and pressure in continuous PTFE depolymerisation systems have been reported numerous times in the literature (Simon & Kaminsky, 1998; Schottle *et al,* 1995; Meissner *et al*, 2004; van der Walt, 2007; Ichida & Homoto, 2008). Even though the overall effects of these two variables seem to stay the same for every system, the exact distribution of the three main products (TFE, HFP, and OFCB) appear to be system specific. Part two of this dissertation will discuss the methods used to determine the temperature and pressure effects on the fractional distribution of the three main PTFE depolymerisation products for this specific depolymerisation system. These effects were compared to those proposed by Meissner *et al* (2004) and van der Walt (2007). In an effort to investigate the differences in the distributions reported in this investigation with those of Meissner *et al* (2004) and van der Walt, a brief kinetic analysis of the system was performed using the relevant kinetic data available in the literature. This was not one of the main objectives of this investigation, therefore an in-depth kinetic analysis was not performed. The dominant HFP production pathways were investigated by determining the product specific kinetic data for this system.

Summary of contents

9 Main objectives

The main objectives for this section are:

- Experimentally determine temperature and pressure effects on the selectivity of TFE, HFP, and OFCB.
- Statistically analyse the data to select conditions that favour the production of single and two component systems. The small difference between the boiling points of HFP (- 29.4 °C) and OFCB (- 6 °C) compared to TFE (- 76.3 °C) indicate that a mixture containing HFP and OFCB is difficult to separate into its individual components using distillation. Hence, to ease the separation process, a product gas containing mainly TFE, TFE and HFP, or TFE and OFCB is preferred.

10 Literature

10.1 PTFE depolymerisation mechanisms

The mechanism of PTFE depolymerisation has been of interest since its discovery. Lewis and Naylor (1947) first proposed the unzipping or free-radical chain mechanism. This mechanism predicts that the primary depolymerisation products of PTFE are the monomer TFE and difluorocarbene ($:CF_2$). The other well-known depolymerisation products are formed by secondary reactions that depend on the operating temperature, pressure, and the atmosphere present during the reaction (Simon & Kaminsky, 1998). From their experimental data, they proposed that the straight-chained polymer undergoes random carbon-carbon bond breakage to produce free-radical fragments (Equation (15)). Due to the high C-F bond energy, the C-C bonds are broken exclusively (Lewis & Naylor, 1947). These fragments undergo further degradation to produce the monomer TFE and another radical (Equation (16)). The monomer produced is then capable of recombining with other radicals or with itself to produce heavier products such as OFCB and HFP (Equations (17), (18) and (19)).

Initiation reaction: radical formation/random chain cleavage:

$$—(CF_2 - CF_2)_n— \rightarrow R_a—CF_2\bullet + \bullet CF_2—R_b \quad (15)$$

Propagation: monomer formation

$$R—CF_2\bullet \rightarrow R'—CF_2\bullet + CF_2 = CF_2 \quad (16)$$

Propagation: secondary reactions

$$2CF_2 = CF_2 \rightarrow \bullet CF_2—CF_2—CF_2—CF_2\bullet \rightarrow OFCB \quad (17)$$

$$2CF_2 = CF_2 \rightarrow C_3F_6 + \bullet\bullet CF_2 \quad (18)$$

$$CF_2 = CF_2 + \bullet\bullet CF_2 \rightarrow C_3F_6 \quad (19)$$

Morisaki (1978) proposed an elaborate PTFE depolymerisation mechanism which includes the formation pathways of most of the well-known depolymerisation products. Using thermogravimetry and mass spectrometry, he deduced that instead of decomposing to larger (C > 1) free-radical fragments only, PTFE depolymerises to produce difluorocarbenes during the initiation step. These radicals are then free to recombine or react with other depolymerisation products (TFE and HFP), leading to the formation of TFE, HFP, and 1-OFB respectively. Meissner *et al* (2004) proposed a similar mechanism. In both Morisaki and Meissner's mechanisms, two HFP formation reactions were proposed. The first is deemed a secondary reaction where TFE reacts with a difluorocarbene, and the second pathway is categorised as a tertiary reaction since it involves the decomposition of OFCB (produced during a secondary reaction). According to Meissner *et al* (2004), the decomposition of OFCB is the most likely HFP production pathway.

According to van der Walt (2007), another depolymerisation mechanism may be present at high temperatures (700 °C to 900 °C), which involves the polymer chain randomly breaking into fragments. During initiation, the high temperature causes the polymer chain to split randomly into radical fragments of variable length. The monomer molecule is then ejected stepwise from the radical ends. Depolymerisation termination can occur via different steps including direct evaporation, disproportionation, and radical recombination.

From the literature cited, it can be concluded that the process of PTFE depolymerisation may occur via two possible mechanisms which are temperature dependent. The depolymerisation process can be divided up into five steps: Initiation, primary product formation, secondary and tertiary reaction steps and finally the recombination step. The main proposed

mechanisms for each step is summarised below, including all of the possible pathways of product formation.

1. *Initiation*

$$— (CF_2 - CF_2)_n — \rightarrow R_a — CF_2 \bullet + \bullet CF_2 — R_b \quad (20)$$

2. *Primary product formation*

Difluorocarbene $$R_a — CF_2 \bullet \rightarrow \bullet\bullet CF_2 + \bullet CF_2 — R_b \quad (21)$$

TFE Formation $$2 \bullet\bullet CF_2 \rightarrow CF_2 = CF_2 \quad (22)$$

3. *Secondary product formation*

OFCB formation $$2CF_2 = CF_2 \rightarrow \bullet CF_2 — CF_2 — CF_2 — CF_2 \bullet \rightarrow OFCB \quad (23)$$

HFP formation $$CF_2 = CF_2 + \bullet\bullet CF_2 \rightarrow CF_3 — CF = CF_2 \quad (24)$$

4. *Tertiary product formation*

HFP formation $$OFCB \rightarrow CF_3 — CF = CF_2 + \bullet\bullet CF_2 \quad (25)$$

1-OFB or PFIB formation $$CF_3 — CF = CF_2 + \bullet\bullet CF_2 \rightarrow CF_3CF_2CF = CF_2 \; or \; (CF_3)_2C — CF_2 \quad (26)$$

5. *Recombination step*

$$R_a — CF_2 \bullet + \bullet CF_2 — R_b \rightarrow R_a — CF_2 — CF_2 — R_b \quad (27)$$

10.2 Product formation and selectivity

There are three main factors that influence the selectivity of depolymerisation product formation when considering the decomposition of pure PTFE with no additives or catalysts added: temperature, pressure, and the reaction atmosphere.

10.2.1 Temperature and pressure effects

Lewis and Naylor (1947) were the first researchers to investigate the temperature and pressure effects on the products produced during batch-depolymerisation. During their experiments, they investigated the effect of a change in pressure (0.7 kPa to 101.32 kPa) at a degradation temperature of 600 °C and a change in temperature (600 °C to 700 °C) at a

pressure of 5.5 kPa. The experimental data show that an increase in pressure leads to a higher weight percentage of higher molecular weight molecules (i.e. octafluorocyclobutane) together with a decrease in TFE (97 wt % to 16 wt %). An increase in temperature exhibited the same trend; however, the production of TFE was found to be less sensitive to a change in temperature.

Meissner *et al* (2004) investigated several technological parameters that influence the continuous-depolymerisation of PTFE; these include temperature (600 °C – 800 °C), pressure (13.33 kPa – 101.32 kPa), PTFE feed rate (4.17 $g \cdot min^{-1}$ – 16.67 $g \cdot min^{-1}$) and carrier gas flow rate (0 $dm^3 \cdot h^{-1}$ – 200 $dm^3 \cdot h^{-1}$). Their continuous-depolymerisation setup included a vertical and horizontal reactor as seen in Figure 52. PTFE was fed into the vertical reactor where depolymerisation took place at 520 °C. The product gas from the vertical reactor was heated further (600 °C to 800 °C) in the horizontal reactor. The horizontal reactor was divided into two section to enable a change in residence time of the product gas from the vertical reactor.

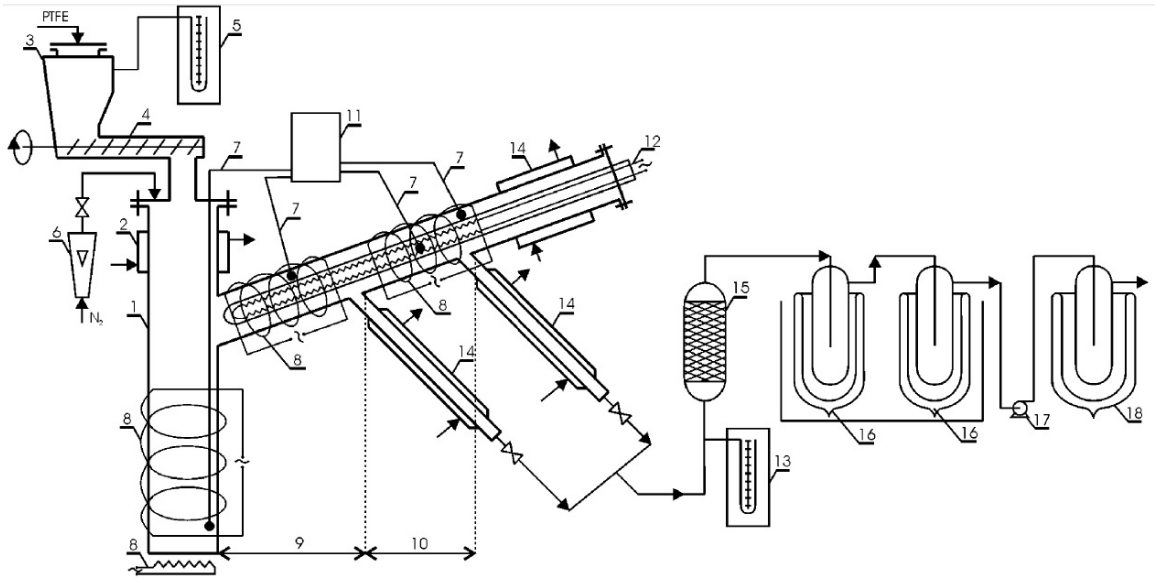

Figure 52: Scheme of the experimental installation used by Meissner *et al* (2004) for the pyrolysis of waste PTFE: (1) vertical reactor, (2 and 14) water condenser, (3) PTFE feeder, (4) feeding screw, (5 and 13) manometer, (6) rotameter, (7) thermocouple, (8 and 12) heating coil, (9) horizontal reactor – first section, (10) horizontal reactor – second section, (11) temperature recorder, (15) dust separator, (16 and 18) freezer, (17) vacuum pump (from Meissner *et al* (2004)).

Using multivariate statistical methods, they set out to determine the parameters that have the highest influence on the production of the various gas products. The response surface equations that describe the effects of the four parameters on TFE, HFP and OFCB formation in both the first and the second section of the horizontal reactor are included in Appendix B. The overall response surface results indicated that the production of TFE was mainly affected by temperature and pressure changes with changes in inert gas flow, residence time and PTFE feed rate being less pronounced. With their reactor setup they managed to achieve a

maximum TFE concentration of 40 wt % at the following conditions: 600 °C, 13.33 kPa, 16.67 g·min^{-1} PTFE feed rate and nitrogen flow rate of 200 dm^3·h^{-1}. However, preliminary studies performed by Meissner *et* al (2004) using a smaller setup indicated that a TFE yield of 98 wt % could be achieved at a temperature of 550 °C and a vacuum of 0.13 kPa.

The overall production of HFP was shown to be highly sensitive to changes in temperature in both the first and second section of the horizontal reactor. They deduced that the residence time of product gas in the horizontal reactor did affect the production of HFP with an increase in the HFP concentration proportional to the residence time. A maximum HFP concentration of 80 wt % was achieved at the following conditions: 750 °C, 53.33 kPa, a nitrogen flow rate of 90 dm^3·h^{-1} and PTFE feed rate of 11.75 g·min^{-1}.

The overall production of OFCB was mainly dependent on temperature. It was found that the residence time had no considerable effect on the production of OFCB. A maximum OFCB concentration of 25 wt % was achieved at the following conditions: 600 °C, 13.33 kPa, PTFE feed rate of 4.17 g·min^{-1} and no nitrogen flow.

van der Walt (2007) used a drop-tube reactor setup to continuously pyrolyse unfilled PTFE in order to study the temperature and pressure effects on the product gas evolution. During these experiments, the temperature was kept constant and the pressure was varied in the range of 5 kPa up to 84 kPa. This procedure was performed at 600 °C, 700 °C, 800 °C and 900 °C. The conditions that produced the highest weight percentage of each of the products are listed in Table 16. His experimental observations followed the same trend as those determined statistically by Meissner *et al* (2004); nevertheless, there exists quite a large difference between the optimum operating conditions for the various gas products. A decrease in TFE was observed with an increase in temperature and pressure, with pressure having the largest effect. The experimental data indicated that an increase in temperature and pressure lead to higher HFP yield. A high TFE concentration, the presence of OFCB, and high temperatures produce advantageous HFP production conditions. These data justify Meissner's and Atkinson and Atkinson's proposal that HFP is produced via the decomposition of OFCB (Equation (25)) instead of the reaction proposed by Equation (24). Other perfluorinated products were produced as well, although in very low quantities. The formation of PFIB increased with an increase in temperature and pressure with high quantities detected at high pressures and temperatures.

Table 16: The operating conditions that would optimise the production of the various products of PTFE depolymerisation as determined by van der Walt (2007).

	Concentration (Vol %)	**Temperature (°C)**	**Pressure (kPa)**
TFE	80 to 94	600 to 900	5

	68	900	82
HFP	61	800	82
	48	720	82
OFCB	27	700	84
HFE	77	920	55

The same trends are observed during most of the experimental data collected in literature. The formation of heavier perfluorinated products is favoured at higher pressures and temperatures, with pressure having the largest effect. Bhadury *et al* (2007) summarised the temperature dependence of the formation of depolymerisation products with a simple diagram (Figure 53).

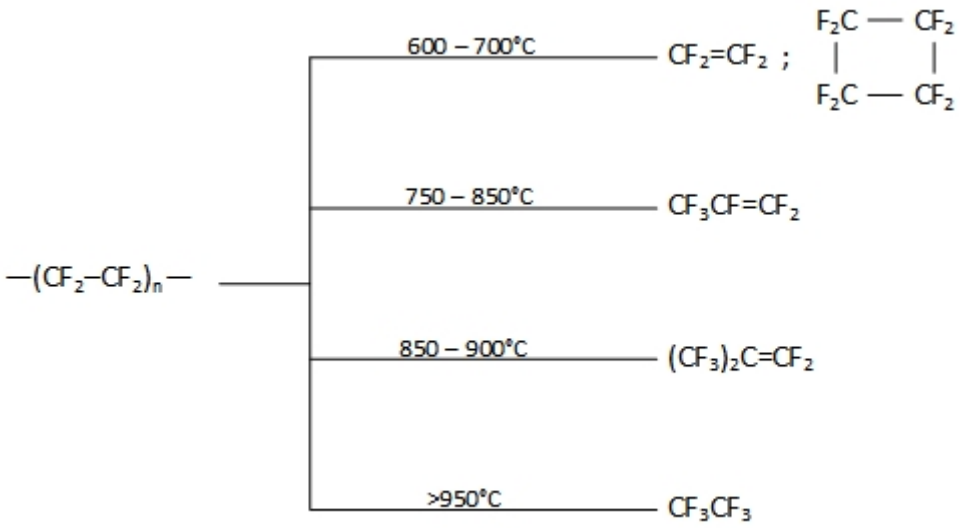

Figure 53: A diagram that summarises the temperature effect on the selectivity of depolymerisation products as suggested by Bhadury and co-workers (2007).

10.2.2 Reaction atmosphere

The reaction atmosphere has a large effect on product formation during depolymerisation. The reaction atmosphere can have an inhibiting, catalytic or no effect on the decomposition as proven by Michaelsen and Wall (1957). During their experiments, it came to light that hydrogen and chlorine atmospheres inhibit the decomposition reaction whereas steam, oxygen, ammonia, and sulphur dioxide accelerate the decomposition reaction. During the depolymerisation of PTFE in these atmospheres other decomposition products like carbon dioxide, hydrogen fluoride (HF) and carbonyl difluoride (COF_2) form in addition to the general decomposition products.

Mesowicz (1987, as quoted by Simon & Kaminsky, 1998) studied the effects of a nitrogen and steam atmosphere on the depolymerisation of PTFE in the temperature range 550 °C to

700 °C and atmospheric pressure. He concluded that steam greatly increases the selectivity of TFE compared to nitrogen. The TFE production can further be increased by increasing the steam flow rate while operating in the lower temperature range (550 °C – 650 °C), together with an increase in HF. This indicates that an increase in steam lowers the partial pressure of the product gases leading to a higher evolution of TFE. Nitrogen and helium atmospheres have no appreciable effect on the product formation.

10.2.3 Apparatus, equipment, and materials

The material of construction of the system can cause contamination in the product gas evolved. For example in the presence of glass or quartz, silicon tetrafluoride, carbon dioxide, carbon monoxide and water are produced due to unwanted side reactions occurring between the depolymerisation gas products and silicon dioxide (Simon & Kaminsky, 1998).

11 Experimental

11.1 Apparatus

PTFE depolymerisation was carried out in the newly commissioned continuous depolymerisation system as described in Appendix C. Teflon® PTFE 807N was used as raw material.

11.2 Experimental design

As indicated by most PTFE depolymerisation investigations in the literature, PFIB is one of the more dangerous product gases produced, in fact classified as a chemical warfare agent (Ganesan, Raza & Vijayaraghavan, 2010). To avoid operating conditions that could lead to the increased production of PFIB, the maximum operating pressure and temperature were limited to 40 kPa and 750 °C, respectively. No carrier gas was used. The Teflon® PTFE 807N feed rate was kept constant at 11 $g \cdot min^{-1}$ (± 0.31 $g \cdot min^{-1}$) by setting the VFD frequency to 30 Hz.

The influence of temperature and pressure on the selectivity of TFE, HFP, and OFCB, was investigated using Response Surface Methodology (RSM) with temperature and pressure selected as input variables following a Face Centered Composite (FCC) design (NIST/SEMATECH, 2012). Meissner *et al* (2004) and van der Walt (2007) confirm that the response surface for each of the depolymerisation products is anything but linear. To incorporate this finding, a three-level full factorial design was followed. All of the experimental points were repeated twice to determine the stability of the system. The three level values for each of the two factors are indicated in Table 17 .

The experimental run time was 15 min. The first 5 min was used to pressurise the system and to allow the system to reach steady state.

Table 17: The levels of the two examined factors.

Level	Coded value	Temperature (°C)	Pressure (kPa)
	X_i	x_1	x_2
High	1	750	40
Center point	0	700	20
Low	-1	650	< 10

11.3 Data analysis

11.3.1 FTIR spectral analysis

Continuous analysis of the pyrolysis product gas was achieved with an inline FTIR. FTIR spectra were generated at intervals of 15 s using Perkin Elmer ® Spectrum Timebase™ software. Spectra were measured between 3000 and 1000 cm^{-1} on gas samples in a gas cell with CaF_2 windows and a path length of 15 mm. The instrument resolution was set on 4 cm^{-1} with a data interval of 1 cm^{-1}. The instrument is fitted with a MIR source, optical KBr beamsplitter and widows and a $LiTaO_3$ source. (Also see Appendix C.4.2.1)

The generated spectra were smoothed and baseline corrected by means of the asymmetric least squares method proposed by Eilers (2003). Spectra were fitted with known spectra from the individual components generated in the lab and solved by means of a Levenberg-Marquardt non-linear solver. The qualitative analysis was determined from Beer's law and previously generated concentration versus absorbance curves generated in the lab (Sonnendecker, 2016).

11.3.2 Statistical analysis

Regression analysis on the fractional distribution of TFE, HFP and OFCB was performed using the regression data analysis package in Microsoft Excel. The effects of each of the independent factors on the response values of the process were estimated using the general quadratic equation represented by Equation (28). This equation comprises a constant, two linear components, two square components, and the cross product representing the interaction effects of temperature and pressure on the response surface. The response functions of the system were described by the following: Y_1 — TFE, Y_2 — HFP and Y_3 — OFCB.

To simplify calculations and determine the significance of each of the variables in Equation (28), the factor values were coded (see Table 17) using Equations (29), (30) and (31),

with x_i as the actual factor value, x_H as the "high" factor value and x_L the "low" factor value. The coded experimental design matrix is given in Table 18.

$$Y_i = \beta_0 + \beta_1 X_1 + \beta_2 X_2 + \beta_3 X_1 X_2 + \beta_4 X_1^2 + \beta_5 X_2^2 \quad (28)$$

$$X_i = \frac{(x_i - a)}{b} \quad (29)$$

$$a = \frac{(x_H + x_L)}{2} \quad (30)$$

$$b = \frac{(x_H - x_L)}{2} \quad (31)$$

After determining the initial response functions for each of the response values, the statistical significance of each of the variables was determined by analysing their F and P - values as well as by comparing the magnitudes of the individual coefficients. The F-value is used to determine of the means between two populations are significantly different whereas, the p-value is the probability that the statistical summary would be the same as or more extreme than the actual observed results.

The response values used in the regression analysis were determined by calculating the mean product-specific mole fraction produced during steady state operation at a specific operating temperature and pressure.

Table 18: The design matrix of the experiments in coded form.

Run number	X_1	X_2
1	-1	-1
2	-1	1
3	1	-1
4	1	1
5	0	-1
6	0	1
7	-1	0
8	1	0
9	0	0
10	0	0
11	0	0
12	-1	-1
13	-1	1
14	1	-1
15	1	1
16	0	-1
17	0	1
18	-1	0
19	1	0
20	-1	-1
21	-1	1
22	1	-1
23	1	1
24	0	-1
25	0	1
26	-1	0
27	1	0

11.3.3 Predicted formation rates from the kinetics available in the literature

In an effort to investigate the differences in the distributions reported in this investigation with those of Meissner *et al* (2004) and van der Walt (2007) further, a brief kinetic analysis of the system was performed using the relevant kinetic data available in the literature. Note that this was not one of the main objectives of this investigation, therefore an in-depth kinetic analysis of the system was not performed.

The PTFE depolymerisation and component specific kinetics available in the literature were combined to determine the predicted formation rates of TFE, HFP, and OFCB. The component specific kinetics (see Table 19) determined by Atkinson and Atkinson (1957) for the thermal decomposition of TFE was used to determine the formation of HFP and OFCB. To determine the formation of TFE, it was assumed that all of the PTFE is converted to TFE during depolymerisation. It was assumed that this reaction will have the same reaction rate as the overall PTFE depolymerisation rates proposed in the literature. The differential equations (equations (35) to (38)) were derived assuming that a steady state is achieved where the difluorocarbene radical concentration remains constant and rate constant k_5 is very small compared to $k_3$and k_4, as proposed by Atkinson and Atkinson (1957). These assumptions were made due to the lack of kinetic data available in the literature for reactions (24) and (34). The predicted formation rates were calculated by solving the differential equations in GNU Octave (Eaton *et al*, 2016). The differential equations were solved using the pre-exponential exponents and activation energies of Siegle *et al* (1964), Anderson (1964), and Consena and Font (2001) (see Table 6 in section 3.3), respectively. The reaction rates predicted by the above mentioned researchers are comparable and therefore the average values of the kinetic parameters were used.

Table 19: The OFCB and HFP formation kinetics determined by Atkinson and Atkinson (1957) and the averaged PTFE depolymerisation kinetics.

Rate constant symbol	Reaction	Pre-exponential factor		Activation energy (kJ·mol^{-1})	
k_{PTFE}	$PTFE \rightarrow CF_2 = CF_2$	1.5x10^{21}	s^{-1}	339.66	(32)
k_1	$2CF_2 = CF_2 \rightarrow OFCB$	10.3x10^{7}	mol^{-1}·s^{-1}	106.27	(23)
k_2	$OFCB \rightarrow 2CF_2 = CF_2$	8.9x10^{15}	s^{-1}	310.03	(33)
k_3	$OFCB \rightarrow CF_3{-}CF = CF_2 + \bullet\bullet\, CF_2$	3.9x10^{16}	s^{-1}	330.50	(25)
k_4	$CF_2 = CF_2 + \bullet\bullet\, CF_2 \rightarrow CF_3 - CF = CF_2$	-	-	-	(24)
k_5	$CF_3 - CF = CF_2 \rightarrow CF_2 = CF_2 + \bullet\bullet\, CF_2$	-	-	-	(34)

$$\frac{dW_{PTFE}}{dt} = -k_{PTFE}W_{PTFE} \tag{35}$$

$$\frac{dN_{TFE}}{dt} = -k_1N_{TFE}^2 + 2k_2N_{OFCB} - k_3N_{OFCB} + \frac{k_{PTFE}W_{PTFE}}{100.02} \tag{36}$$

$$\frac{dN_{OFCB}}{dt} = 0.5k_1N_{TFE}^2 - k_2N_{OFCB} - k_3N_{OFCB} \tag{37}$$

$$\frac{dN_{HFP}}{dt} = 2k_3N_{OFCB} \tag{38}$$

11.3.4 Residence time estimation

In order to relate the measured TFE, HFP, and OFCB mole percentages with the predicted reaction curves mentioned in section 11.3.3, the reaction pressure needs to be accounted for. Assuming the universal gas law holds, the residence time of the gas in the reactor at a constant temperature, constant PTFE flow rate and constant reactor volume is only dependent on the system pressure. To keep the reactor pressure constant the volume of gas leaving the reactor should be equal to the volume of gas evolved during depolymerisation. At a constant temperature and constant molar flow rate, an increase in pressure leads to a decrease in volumetric flow rate. Therefore, the volumetric flow rate at a higher operating pressure is less than at a lower pressure. An increase in system pressure leads to a proportional increase in residence time, since the reactor volume is constant. As a result, the TFE, OFCB, and HFP mole percentages at the three system pressures (< 10 kPa, 20 kPa and 40 kPa) can be plotted against residence time for each temperature. To estimate the residence time it was assumed that the universal gas law holds. It was also assumed that the depolymerisation reaction and side reactions only occur in the reactor and that the reactions stop once the gas has left the reactor. The residence time can be estimated using equation (39):

$$\tau = \frac{P \cdot V_{Reactor}}{\dot{n}_{system} \cdot R \cdot T} \tag{39}$$

In the equation, $\dot{n}_{system}$ is the number of moles of the gas produced per unit time at a specific reactor pressure and temperature, R, is the universal gas constant, T, is the actual reactor temperature, P, is the corresponding reactor pressure and $V_{Reactor}$,is the reactor volume (1.36×10^{-3} m^3). By using the average mole percentage of TFE, HFP, and OFCB produced at a specific reactor pressure and temperature (sections 12.2, 12.3, and 12.4), and the assumption that 0.183 g PTFE·s^{-1} is fed, the average moles of the gas is calculated using equation (40). Although the residence time is calculated to a reasonable degree of accuracy, it is still based on the assumption that all of the PTFE fed per second depolymerises in the same time, this may lead to inaccuracies.

$$n_{system} = \frac{0.184}{\sum_i (n_{fraction_i}) \cdot (MM_i)} \tag{40}$$

12 Results and discussion

12.1 Temperature and pressure control

The median, mean, standard deviation and variance of the actual operating temperature and pressure for each individual experimental run are shown in Table 20. For some of the runs, the total temperature and pressure profiles were not saved due to a program error. Temperature control in the system was good, except for a few instances where the standard deviation exceeded five; however, the overall mean and median for these specific runs remained close to the specified operating temperature. The pressure was controlled manually, within a range of 2 kPa from the specified operating pressure. At the higher pressures of 20 kPa and 40 kPa, this was achieved with ease. However, pressure control at pressures lower than 10 kPa was difficult due to pump inefficacy. The actual measured mean temperature and pressure values for each run was used during the regression analysis.

Table 20: Actual temperature and pressure data logged for the individual experimental runs.

Run nr.	Temperature (°C)	Pressure (kPa)	Actual temperature (°C)			Actual pressure (kPa)		
			Median	Mean	σ	Median	Mean	σ
1	650	< 10 kPa						
12	650	< 10 kPa	651	651	2.2	1.8	1.8	0.2
20	650	< 10 kPa	651	652	4.0	1.6	1.6	0.3
7	650	20	650	650	0.4	20.3	20.3	0.5
18	650	20	651	650	2.6	20.4	20.4	0.4
26	650	20						
2	650	40						
13	650	40	653	652	3.5	39.8	39.9	0.6
21	650	40	648	648	9.0	40.2	40.2	0.8
5	700	< 10 kPa	700	701	2.3	2.5	2.5	0.4
16	700	< 10 kPa	695	694	9.3	3.3	3.3	0.4
24	700	< 10 kPa	701	701	2.4	6.3	6.3	0.3
9	700	20	701	701	1.4	20.3	20.5	1.3
10	700	20	699	700	4.4	20.2	20.2	0.7
11	700	20						
6	700	40	700	700	1.5	40.3	40.2	1.2
17	700	40	700	700	1.1	40.3	40.2	0.6
25	700	40						
3	750	< 10 kPa	749	748	4.1	1.8	1.8	0.2
14	750	< 10 kPa	750	750	2.6	9.3	9.3	0.3
22	750	< 10 kPa	749	747	6.1	8.2	8.2	0.4
8	750	20	750	750	2.6	19.9	19.8	1.0
19	750	20	751	750	1.9	19.9	0.9	0.7
27	750	20	751	751	1.9	20.1	20.1	0.6
4	750	40	751	751	1.2	40.0	39.9	0.7
15	750	40	750	750	1.3	40.3	40.2	0.7
23	750	40	751	751	1.1	39.9	40.0	0.9

12.2 Product distribution produced at 650 °C

As expected, the major depolymerisation products produced at 650 °C were TFE, HFP, and OFCB. Figure 54, Figure 55 and Figure 56, were produced by averaging the data collected for the three experimental runs at the same pressure. The actual fractional distributions used to produce the averaged plots can be viewed in Appendix B.

As seen in Figure 54, very little HFP and OFCB were produced at a reaction pressure of < 10 kPa, with an average of 5 mol % HFP and 4 mol % OFCB. The TFE fraction decreased from an average of 94 mol % at < 10 kPa to 58 mol % and 31 mol % at operating pressures of 20 kPa and 40 kPa, respectively. HFP fraction increased to an average of 13 mol % at an operating pressure of 40 kPa, whilst the OFCB fraction increased to an average of 55 mol %. This was surprising as this high a percentage of OFCB has not been achieved by any of the other researchers, including Meissner *et al* (2004) and van der Walt (2007), at these operating conditions.

No PFIB or HFE was noticed at any of the operational pressures, which can be attributed to the low operating temperature. The deviations from the norm seen in Figure 55, as well as in all of the actual experimental graphs listed in Appendix B, are miscalculations due to noisy FTIR spectra.

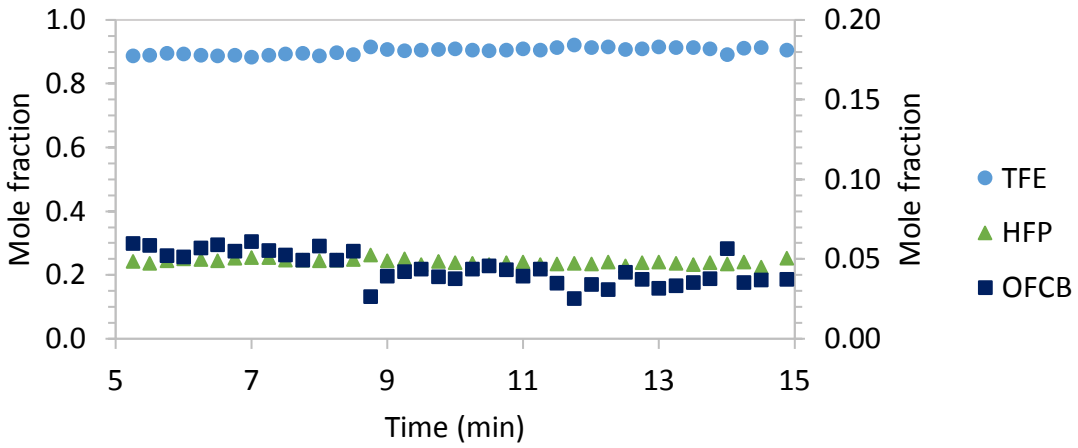

Figure 54: The average fractional distribution of the three main products produced at 650 °C and < 10 kPa during the last 10 min of the experimental run. For clarity, the TFE mole fraction is represented on the primary axis, with the HFP and OFCB mole fractions indicated on the secondary axis.

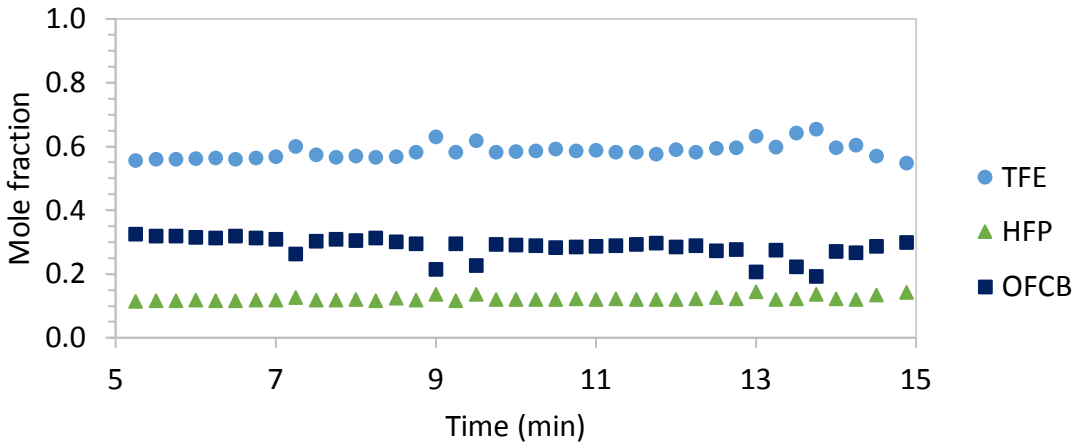

Figure 55: The average fractional distribution of the three main products produced at 650 °C and 20 kPa.

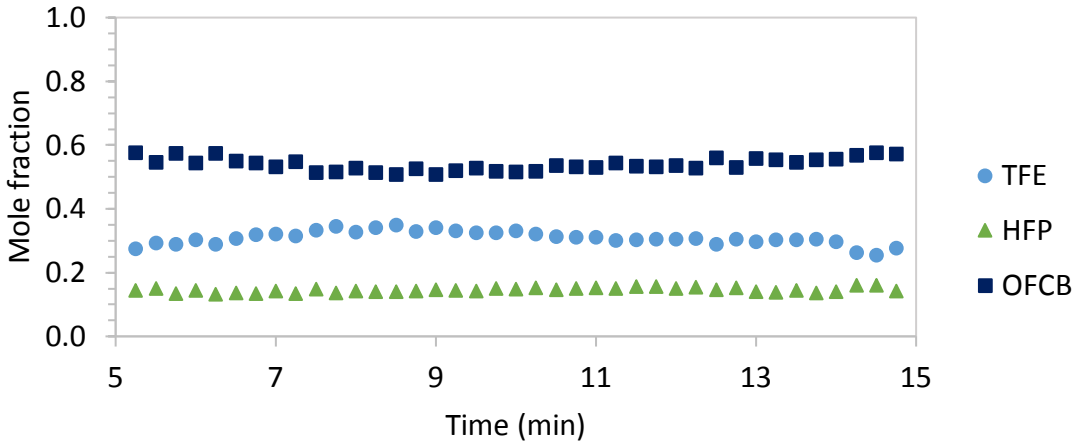

Figure 56: The average fractional distribution of the three main products produced at 650 °C and 40 kPa.

12.3 Product distribution produced at 700 °C

A 50 °C increase in operating temperature did not affect the fractional distribution of TFE, HFP and OFCB as indicated in Figure 57, Figure 58 and Figure 59. An increase in pressure, as seen previously, reduced the TFE fraction from 87 mol % at < 10 kPa to 31 mol % at 40 kPa whilst the OFCB fraction increased from 5 mol % at < 10 kPa to 53 mol % at 40 kPa. As with the 650 °C experimental runs, no HFE of PFIB production was noticed. An increase in pressure clearly led to an increase in the HFP fraction from 7 mol % at < 10 kPa to 15 mol % at 40 kPa.

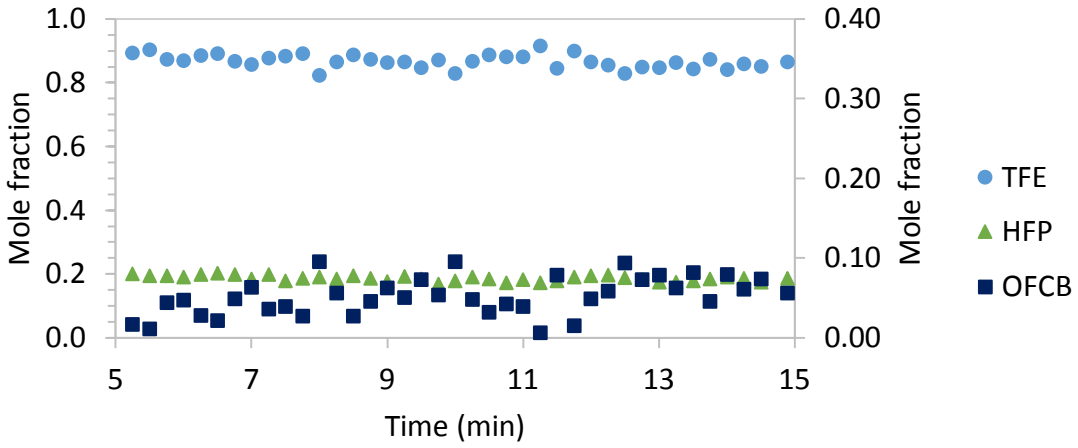

Figure 57: The average fractional distribution of the three main products produced at 700 °C and < 10 kPa. For clarity, the TFE fraction is represented on the primary axis, with the HFP and OFCB fractions indicated on the secondary axis.

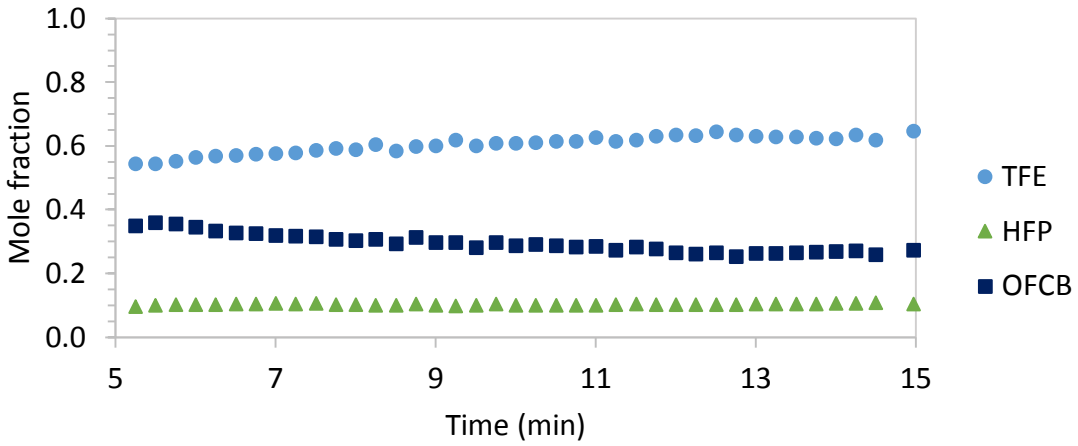

Figure 58: The average fractional distribution of the three main products produced at 700 °C and 20 kPa.

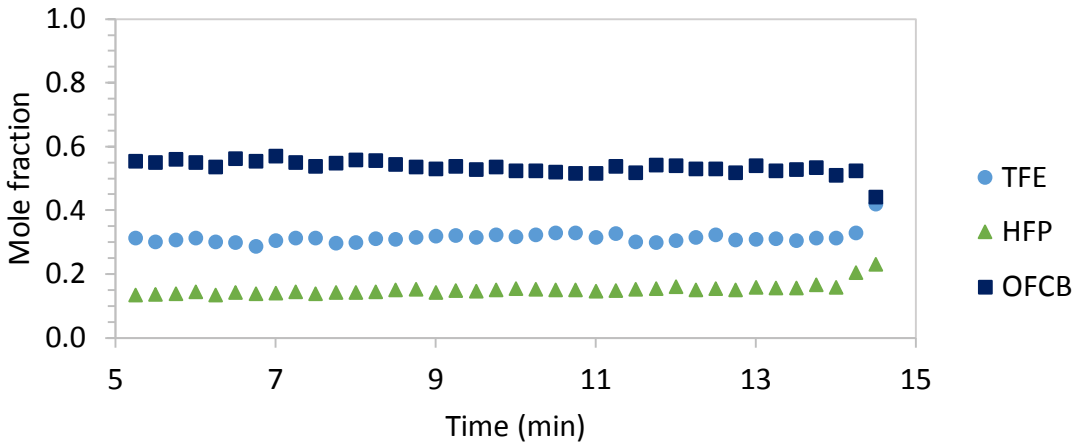

Figure 59: The average fractional distribution of the three main products produced at 700 °C and 40 kPa.

12.4 Product distribution produced at 750 °C

At a higher operating temperature of 750 °C, the TFE mean fraction decreased from 77 mol % at < 10 kPa to 23 mol % at 40 kPa. This is considerably less than the percentages at lower temperatures. Similarly, the OFCB and HFP percentage increased from an average of 13 mol % and 9 mol % at < 10 kPa to 54 mol % and 22 mol % at 40 kPa, respectively. It is clear that all three of these depolymerisation products are strongly affected by pressure, with the higher molecular weight products favoured at higher pressures.

Very low fractions of HFE and PFIB were noticed at all three operating pressures. The HFE percentage stayed constant at 0.6 mol % for all three of the operating pressures, whereas a small increase in the PFIB percentage was noticed with an increase in pressure. PFIB increased from 0.2 mol % to 0.5 mol % at < 10 kPa and 40 kPa, respectively. The percentage values of PFIB and HFE could be underestimated due to the method used to deconstruct the experimental FTIR spectra. All of the product gases evolved, during PTFE depolymerisation, produce strong spectral peaks in the region of 1000 cm^{-1} – 1400 cm^{-1}. Gases present in very small quantities would produce very small spectral peaks. During the deconstruction, these individual spectral peaks could get lost due to peak overlapping, leading to the underestimation of its fractional values.

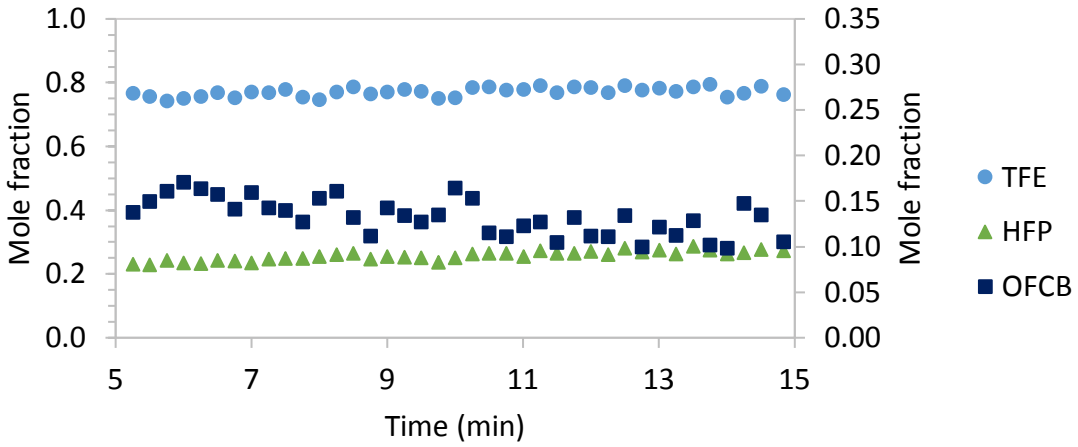

Figure 60: The average fractional distribution of the three main products produced at 750 °C and < 10 kPa. For clarity, the TFE fraction is represented on the primary axis, with the HFP and OFCB fractions indicated on the secondary axis.

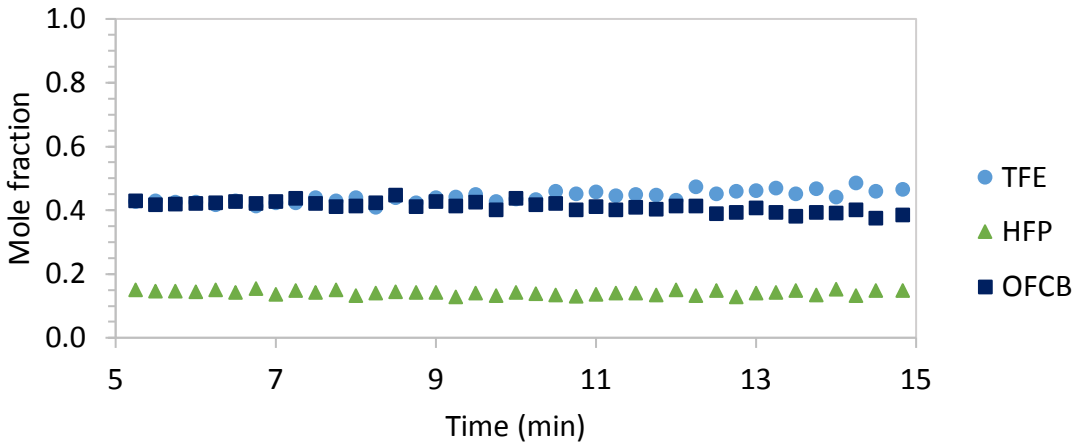

Figure 61: The average fractional distribution of the three main products produced at 750 °C and 20 kPa.

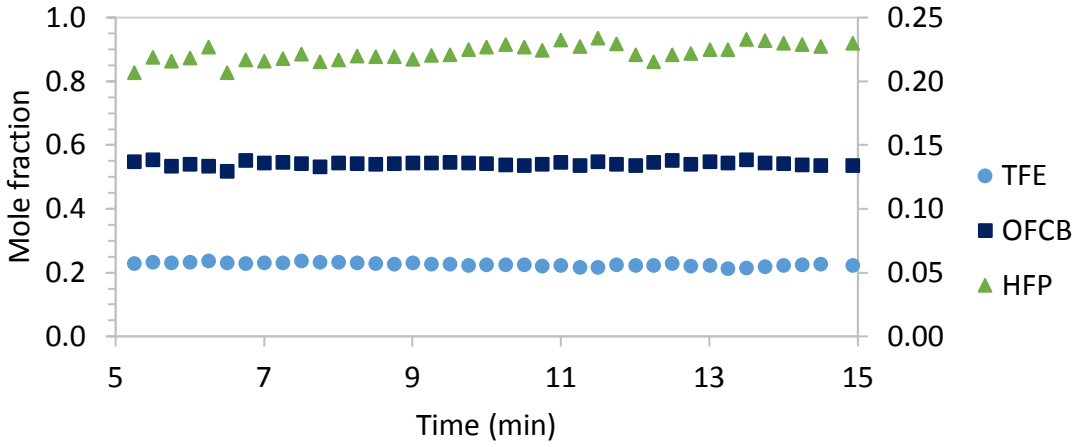

Figure 62: The average fractional distribution of the three main products produced at 750 °C and 40 kPa. For clarity the HFP fraction values are represented on the secondary axis, with the TFE and OFCB fractions represented on the primary axis.

12.5 Statistical analysis of the tetrafluoroethylene yield

The TFE experimental response function values are listed in Table 34 in Appendix B.5. Analysis of the P-values, t-statistic values and the Upper and Lower 95 % confidence interval values of the TFE initial response function indicated that the interaction variable ($\beta_3 X_1 X_2$) was statistically insignificant. The model was refitted with this variable excluded to determine if this would have an effect on the R^2 and adjusted R^2 values. No significant change in the R^2 and adjusted R^2 values were noticed (see Table 21), indicating that the interaction variable of temperature and pressure had no effect on the production of TFE during depolymerisation. The fact that the adjusted R^2 value increased, however slightly, indicated that the prediction model was improved by excluding the interaction variable. Hence, the TFE response surface

could be predicted using Equation (41). This equation was used to plot the TFE response surface in Figure 63.

$$Y_1 = 0.5927 - 0.0642X_1 - 0.333X_2 - 0.0823X_1^2 + 0.1028X_2^2 \quad (41)$$

Table 21: Regression analysis comparison for the TFE response surface.

	Initial regression analysis with $\beta_3 X_1 X_2$ included	Regression analysis with $\beta_3 X_1 X_2$ excluded
R^2	0.961	0.960
Adjusted R^2	0.951	0.953
Significance F	4.57E-14	4.7E-15
Standard error	0.057	0.056

Further evaluation of the magnitude of the individual variables in Equation (41) indicated that TFE production was more sensitive to a change in pressure than a change in temperature. As seen in Figure 63, the TFE fraction decreases faster with an increase in pressure than an increase in temperature. This was substantiated by all of the fractional distribution graphs in the previous sections. To compare the results of this investigation to those of Meissner *et al* (2004), contour plots were produced using the response surface equations of Meissner *et al* (2004) presented in Appendix B.1. The nitrogen flow rate and PTFE feeding rate values used in the equations were 0 $dm^3 \cdot h^{-1}$ and 11 $g \cdot min^{-1}$, respectively.

As seen from Figure 64 and Figure 65 Meissner *et al* (2004) predicted that the TFE concentration is almost equally affected by temperature and pressure in the first section of their horizontal reactor and mainly sensitive to changes in pressure in the second section of the horizontal reactor. Nevertheless, both of these contour plots indicate that the TFE concentration will decrease with an increase in temperature and pressure. This coincides with the data depicted in Figure 63.

From Figure 63 it is clear that a TFE mole fraction of 95 % and higher could be achieved at operating conditions within the temperature range 650 °C and 750 °C, together with a system pressure of 2 kPa or less. Operating conditions of ± 675 °C and < 10 kPa would be the optimum when considering Figure 63. These operating conditions are the same as those predicted by van der Walt (2007). The depolymerisation system of Meissner *et al* (2004) could not be operated at pressures lower than 13.3 kPa, therefore, the response surface equations of Meissner *et al* (2004) cannot be used to predict TFE percentages at pressures lower than 13.3 kPa. However, the response surface of TFE after the first section of the horizontal reactor (see Figure 64) predicts that a TFE percentage higher than 61 mol % can be achieved at

pressures lower than 15 kPa and temperatures lower than 660 °C. This corresponds well with the data represented in Figure 63.

The difference in the pressure and temperature dependence of TFE between Figure 63 and Figure 64 could be attributed to the residence time of the gas in the vertical reactor of Meissner *et al* (2004). As seen from the difference in contours in Figure 64 and Figure 65, residence time can have a large effect. This will be discussed further in section 12.9.

Spontaneous polymerisation of TFE was noticed, with PTFE dust settling on the walls of the piping throughout the system. This could be prevented by lining the piping with any one of the inhibitors mentioned in Appendix C.2. However, caution should be taken as most of the auto-ignition temperatures of these inhibitors are well below the standard operating temperatures of the depolymerisation reactor. Therefore, the piping system further down the line could be lined with an inhibitor but should be avoided close to the reactor.

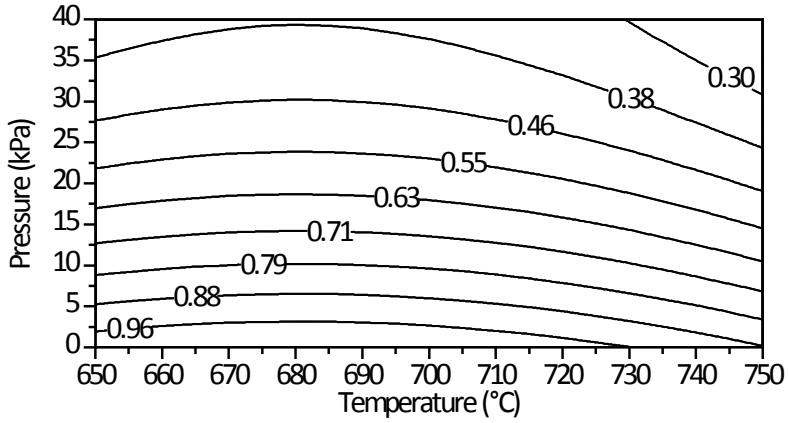

Figure 63: The influence of temperature and pressure on the fractional distribution of TFE.

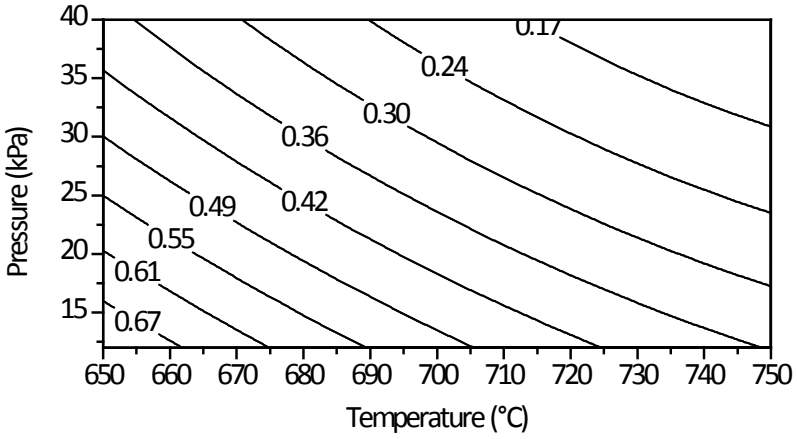

Figure 64: The effect of temperature and pressure on the TFE mole fraction as determined by Meissner *et al* (2004) in the first section of the horizontal reactor. The contour plot was generated using the response surface equations of Meissner *et al* (2004) for TFE (Y_2) presented in Appendix B.1.

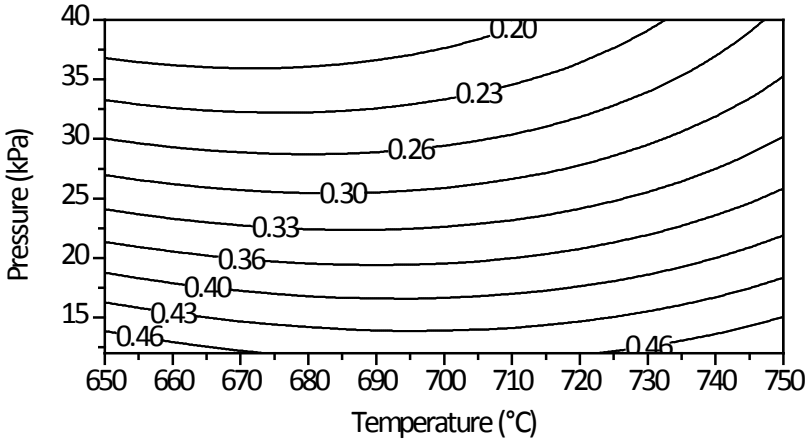

Figure 65: The effect of temperature and pressure on the TFE mole fraction as determined by Meissner *et al* (2004) in the second section of the horizontal reactor. The contour plot was generated using the response surface equations of Meissner *et al* (2004) for TFE (Y_7) presented in Appendix B.1.

12.6 Statistical analysis of the octafluorocyclobutane yield

In contrast to the predictions made by Meissner *et al* (2004), in this system, the OFCB concentration was highly dependent on the operating pressure, as indicated by the density of the contours in Figure 66.

The experimental response function values for OFCB are listed in Table 34 in Appendix B.5. The OFCB concentration was not affected by the interaction variable, therefore, the variable was removed and the response function recalculated. This did not affect the adjusted R^2 value negatively, as seen in Table 22, supporting the conclusion that the interaction variable is statistically insignificant.

$$Y_3 = 0.2853 + 0.0259X_1 + 0.2544X_2 + 0.0508X_1^2 - 0.0601X_2^2 \qquad (42)$$

Table 22: Regression analysis comparison for the OFCB response surface.

	Initial regression analysis with $\beta_3 X_1 X_2$ included	**Regression analysis with $\beta_3 X_1 X_2$ excluded**
R^2	0.956	0.956
Adjusted R^2	0.945	0.947
Significance F	1.55e-13	1.55e-14
Standard error	0.045	0.044

Maximum OFCB fractions of 50 mol % - 55 mol % were observed at operating temperatures of 650 °C – 750 °C and a pressure of 40 kPa. These fractions were almost double than those achieved by both Meissner *et al* (2004) and van der Walt (2007). When considering both Figure 67 and Figure 68 Meissner *et al* (2004) predicted an OFCB percentage higher than 25 mol % at pressures lower than 15 kPa and temperatures lower than 655 °C. In Figure 66, an OFCB concentration of 25 mol % is achieved at 15 kPa and 655 °C, however, this concentration decreases with a decrease in pressure and temperature. The contour plots of Meissner *et al* (2004) for both sections of the horizontal reactor indicate that the OFCB concentration is affected almost equally by temperature and pressure; the residence time has no pronounced effect and that the OFCB concentration decreases with an increase in pressure and temperature. The results in Figure 66 indicate that the OFCB concentration is more sensitive to changes in pressure and that the concentration increases with an increase in pressure and temperature. These results are almost the opposite of those predicted by Meissner *et al* (2004). This difference could be attributed to residence time and is discussed further in section 12.9.

Within the operating range of 730 °C to 750 °C and 35 kPa to 40 kPa a fraction of 50 mol % and higher can be expected for OFCB for the current system. Considering Figure 66, the optimum operating conditions for OFCB would be 750 °C and 40 kPa.

Comparing the response surface of TFE (Figure 63) with that of OFCB, it is clear that an inverse relationship exists. As the TFE concentration decreases with an increase in pressure the OFCB concentration increases. This trend indicates that the dimerisation reaction of TFE is the dominant OFCB production reaction within the temperature and pressure ranges of this investigation.

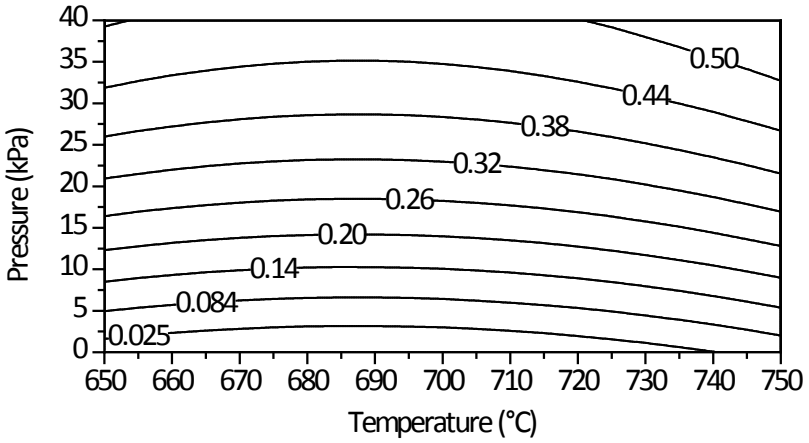

Figure 66: The influence of temperature and pressure on the fractional distribution of OFCB.

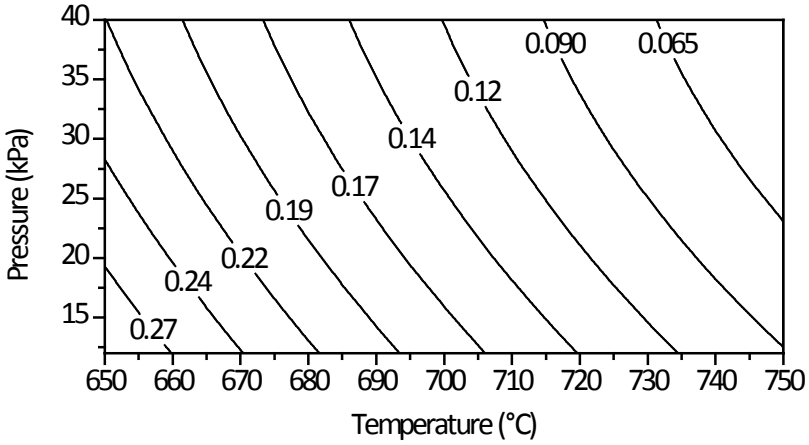

Figure 67: The effect of temperature and pressure on the OFCB mole fraction as determined by Meissner *et al* (2004) in the first section of the horizontal reactor. The contour plot was generated using the response surface equations of Meissner *et al* (2004) for OFCB (Y_4) presented in Appendix B.1.

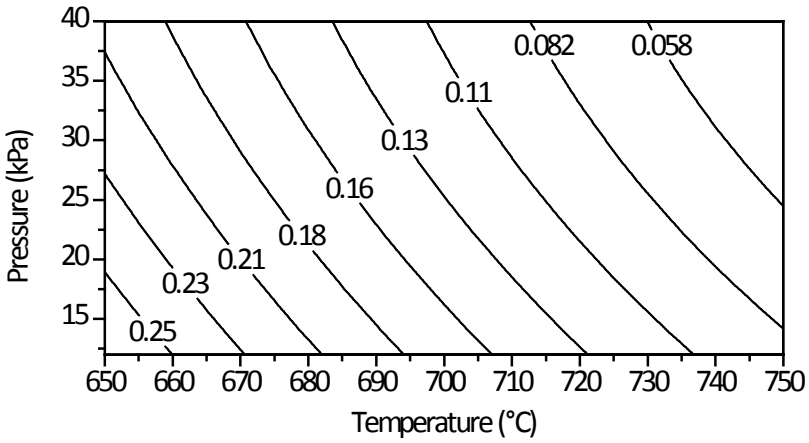

Figure 68: The effect of temperature and pressure on the OFCB mole fraction as determined by Meissner *et al* (2004) in the second section of the horizontal reactor. The contour plot was generated using the response surface equations of Meissner *et al* (2004) for OFCB (Y_9) presented in Appendix B.1.

12.7 Statistical analysis of the hexafluoropropylene yield

The HFP experimental response function values are listed in Table 34 in Appendix B.5. As with TFE and OFCB, analysis of the regression data indicated that the interaction variable has no statistical significance in the HFP response function (see Table 23). The small difference in the magnitude of the coefficients in Equation (43) indicate that the HFP production is affected almost equally by a change in temperature or pressure. However, Figure 69 indicates that there is a point of inflection, where the HFP production becomes more sensitive to changes in pressure than temperature. The density of the contours below a HFP fraction of 13 mol % indicate that the HFP production is much more sensitive to pressure changes in this region. Above the 13 mol % fraction contour, this sensitivity swaps around with the HFP production

now more influenced by changes in temperature. These results were in line with those produced by van der Walt (2007). The contour plots of Meissner *et al* (2004) (Figure 70 and Figure 71) indicate that the HFP production for their system was equally affected by temperature and pressure and an increase in residence time had no pronounced effect.

$$Y_2 = 0.1121 + 0.0314X_1 + 0.0675X_2 + 0.0344X_1^2 - 0.0314X_2^2 \quad (43)$$

Table 23: Regression analysis comparison for the HFP response surface.

	Initial regression analysis with $\beta_3 X_1 X_2$ included	**Regression analysis with $\beta_3 X_1 X_2$ excluded**
R^2	0.795	0.781
Adjusted R^2	0.741	0.742
Significance F	1.34e-06	5.34e-07
Standard error	0.034	0.034

The maximum observed HFP fraction was 25 mol % at operating conditions of 750 °C and 40 kPa, respectively. The HFP surface plot (Figure 69) predicts that HFP would be higher than 19 mol % at pressures higher than 32 kPa and operating temperatures higher than 744 °C. These operating conditions coincide with those proposed by both Meissner *et al* (2004) and van der Walt (2007). However, both Meissner *et al* (2004) and van der Walt (2007) achieved much higher concentrations of HFP (> 64 %). Van der Walt (2007) indicated that a maximum of 64 mol % could be achieved at operating conditions of > 800 °C and 20 kPa. However, at these conditions higher concentrations of PFIB could be produced. The large difference in the HFP concentration measured during this investigation compared to those reported by Meissner *et al* (2004) and van der Walt (2007) could be attributed to residence time and is discussed further in section 12.9.

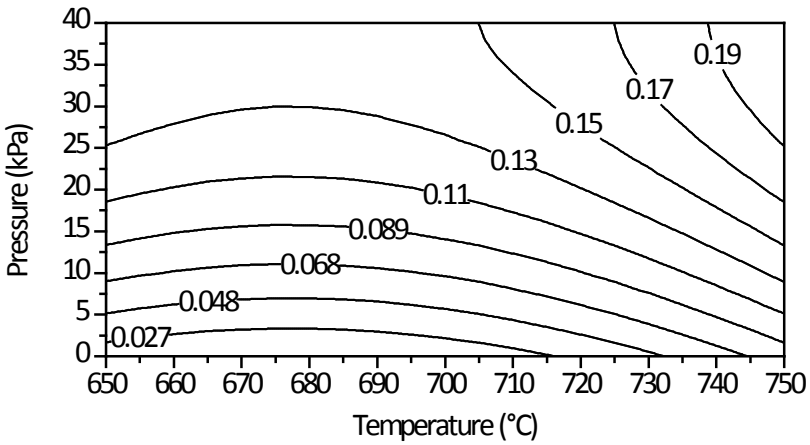

Figure 69: The influence of temperature and pressure on the fractional distribution of HFP.

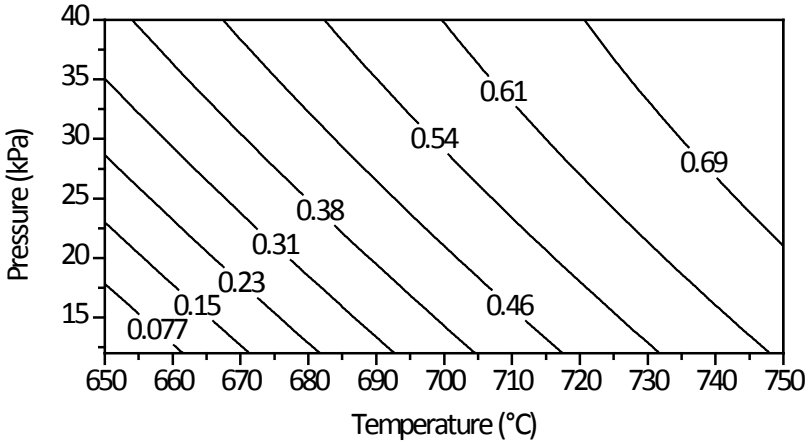

Figure 70: The effect of temperature and pressure on the HFP mole fraction as determined by Meissner et al (2004) in the first section of the horizontal reactor. The contour plot was generated using the response surface equations of Meissner *et al* (2004) for HFP (Y_3) presented in Appendix B.1.

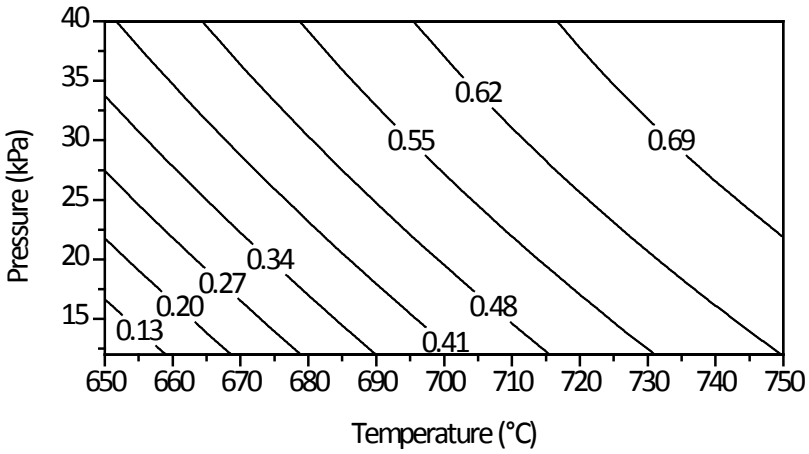

Figure 71: The effect of temperature and pressure on the HFP mole fraction as determined by Meissner *et al* (2004) in the second section of the horizontal reactor. The contour plot was generated using the response surface equations of Meissner *et al* (2004) for HFP (Y_8) presented in Appendix B.1.

12.8 Observations made during failed experimental runs

Throughout all of the above-mentioned experimental runs, the residence time of the evolved product gas was kept constant, at each operating pressure, by achieving steady state in the system. As Meissner *et al* (2004) mentioned, the residence time could have a significant effect on the product distribution. During one of the failed experimental runs the effect of an increase in residence time could clearly be seen, as indicated in Figure 72. These results were recorded during a run operating at 700 °C and 20 kPa. At the start of the run, the PTFE flow became erratic and ultimately ceased due to very low levels of PTFE in the hopper. In an effort to keep the pressure in the system at 20 kPa, the pressure control valve was closed completely. This increased the residence time of the product gas in the system. As can be

seen in Figure 72, this led to a very sharp increase in the production of HFP and PFIB, reaching maximums of 70 mol % and 5 mol %, respectively. A decrease in both TFE and OFCB was observed with the increase in HFP indicating that Reactions (24) and (25) could be occurring simultaneously in the system. As soon as the HFP concentration reached high enough levels PFIB started to increase.

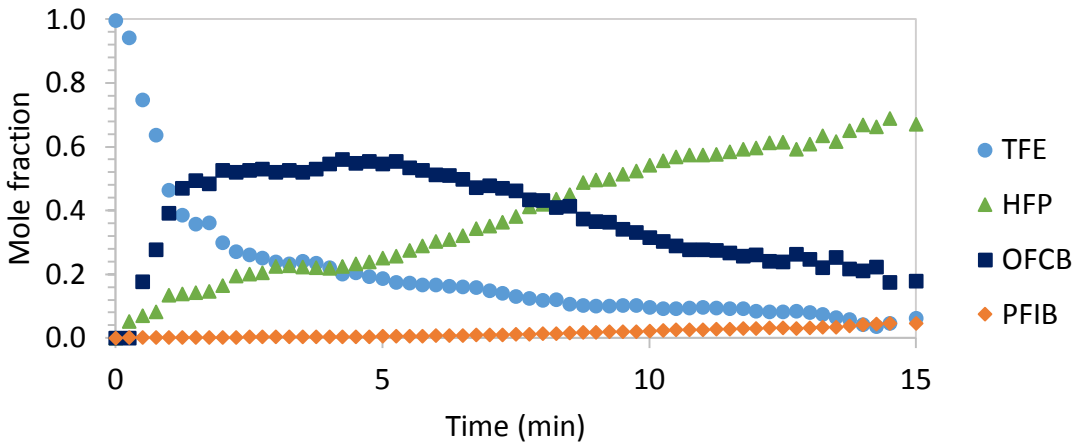

Figure 72: The variation in product distribution due to residence time and no flow of product gas out of the system.

During a second failed experimental run the same effects could be seen (see Figure 73). These results were recorded at operating conditions of 750 °C and 40 kPa. Unlike in the previous experimental run, the PTFE flow seized just before 5 min into the run. The pressure control valve was closed completely in an effort to keep the pressure constant, resulting in an increase in the residence time of the produced gas. 11 min into the run the pressure control valve was opened. As seen in Figure 73, the HFP and PFIB concentration increased during the time that the pressure control valve was closed.

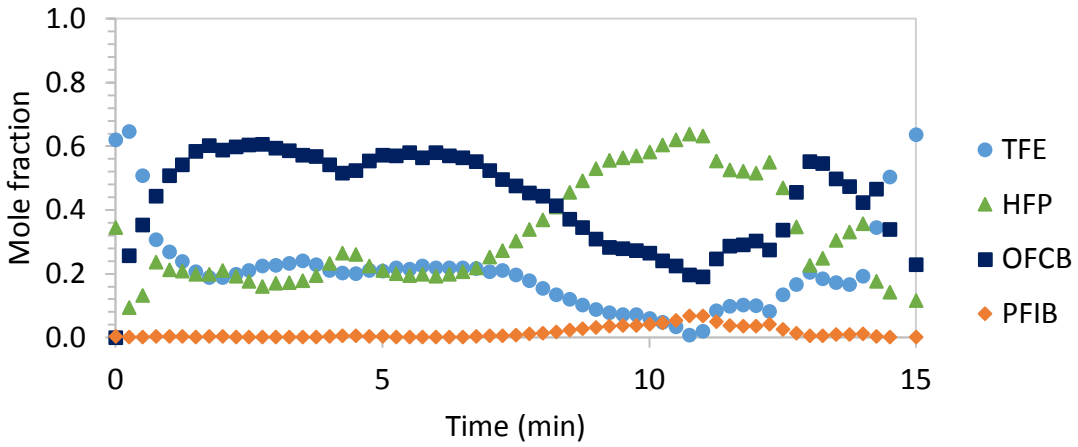

Figure 73: Another example of the effect that an increased residence time has on the production of HFP and PFIB. These results were recorded at operating conditions of 750 °C and 40 kPa.

Not all of the failed experimental runs indicated a sharp decrease in the OFCB concentration as the HFP concentration increased. During one of the experimental runs the stirrer in the hopper malfunctioned and caused the flow of PTFE into the reactor to become erratic. In an effort to keep the pressure in the system constant the control valve had to be closed for very short periods of time and opened again throughout the entire run. This led to sporadic increases and decreases in the product gas residence time. As seen in Figure 74, the HFP, OFCB and TFE concentrations are all very close to each other. Comparing this graph with the fractional distributions recorded for the successful runs at 750 °C and 20 kPa (see Figure 109, Figure 110 and Figure 111 in Appendix B.4.2) it is clear that a slight increase in the residence time increased the HFP concentration to an average of 31 mol %. However, since the pressure control valve was not closed completely throughout the run, the HFP concentration did not increase to the same levels as seen in the previous two cases.

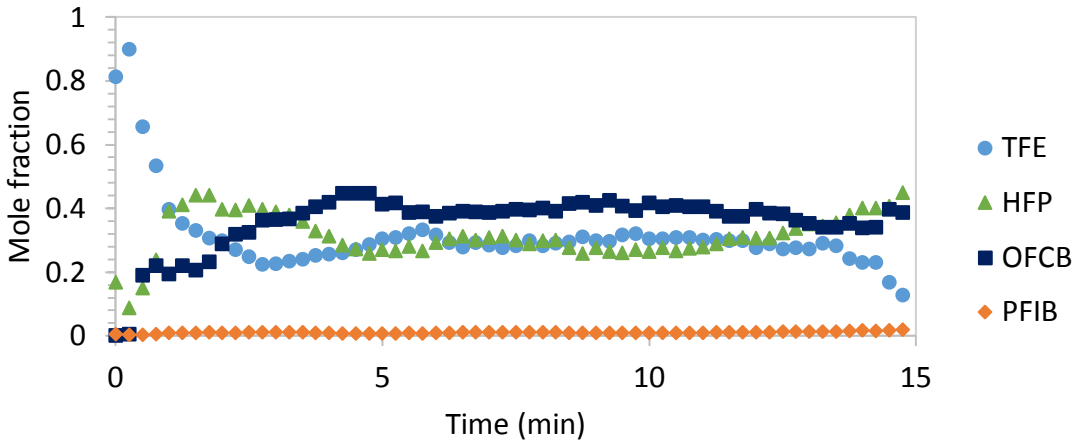

Figure 74: Higher HFP production due to increased residence time at operating conditions of 750 °C and 20 kPa.

These results support the hypothesis that an increase in residence time has a much larger effect on the production of HFP than expected. All of these results suggest that the dominant reaction path for the formation of HFP is through the dissociation of OFCB (Reaction (25)) and not through the pyrolysis of TFE (Reaction (24)); leading to the conclusion that a high concentration of OFCB and an extended residence time are required to achieve high concentrations of HFP. These results are exactly the same as those presented by Atkinson and Atkinson (1957). They proved, through the analysis of batch TFE and OFCB decomposition kinetics, that the dominant reaction pathway in the formation of HFP is via OFCB dissociation.

12.9 Residence time and kinetic analysis

12.9.1 Residence time

The method described in section 11.3.4 was followed to estimate the residence time for the experimental runs performed. The average TFE, HFP, and OFCB mole fractions for each of the experimental runs (runs 1 – 27 in Appendix B) were used to determine the number of moles of the gas and are indicated in Table 24. It is evident from the table that an increase in pressure leads to an increase in residence time at a constant temperature.

Table 24: Residence time calculated at the actual reactor temperature and pressure for all of the experimental runs in sections 12.2, 12.3, and 12.4.

Temperature	Pressure	Actual mole fractions measured			Calculated molar feed rate	Residence time
		TFE	OFCB	HFP		
(°C)	(kPa)	Mol %	Mol %	Mol %	(mol·s^{-1})	(s)
650	2	0.97	0.00	0.03	0.0018	0.2
651	2	0.90	0.05	0.04	0.0017	0.2
651	2	0.95	0.02	0.03	0.0018	0.2
650	20	0.60	0.30	0.11	0.0013	2.7
651	20	0.59	0.26	0.13	0.0014	2.6
650	20	0.60	0.27	0.11	0.0014	2.6
650	40	0.31	0.53	0.16	0.0011	6.3
653	40	0.42	0.44	0.14	0.0012	5.8
648	40	0.31	0.55	0.13	0.0011	6.3
700	2	0.95	0.01	0.04	0.0018	0.2
695	3	0.93	0.02	0.04	0.0018	0.3
701	6	0.87	0.07	0.06	0.0017	0.6
701	20	0.63	0.25	0.11	0.0014	2.5
699	20	0.53	0.36	0.10	0.0013	2.6
700	20	0.64	0.26	0.09	0.0014	2.4
700	40	0.32	0.51	0.16	0.0011	5.9
700	40	0.31	0.54	0.15	0.0011	6.0
700	40	0.43	0.42	0.14	0.0012	5.5
749	2	0.90	0.03	0.06	0.0017	0.2
750	9	0.67	0.21	0.11	0.0015	1.0
749	8	0.74	0.16	0.09	0.0015	0.9
750	20	0.28	0.39	0.31	0.0012	2.7
751	20	0.41	0.44	0.15	0.0012	2.6
751	20	0.48	0.38	0.13	0.0013	2.6
751	40	0.22	0.55	0.23	0.0011	5.8
750	40	0.24	0.55	0.20	0.0011	5.8
751	40	0.21	0.53	0.25	0.0011	5.8

12.9.2 The predicted formation rates of TFE, HFP, and OFCB

In an effort to investigate the differences in results for HFP and OFCB in sections 12.6 and 12.7 with the results of Meissner *et al* (2004) and van der Walt (2007) further; the formation rates of TFE, HFP, and OFCB were predicted using the kinetic data available in the literature. The rates were determined using the differential equations in section 11.3.3. To relate the actual measured mole fractions of TFE, HFP, and OFCB with the predicted formation rates, the fractions in Table 24 were plotted against the residence time shown in the same table. The predicted rates and the actual measured fractions of TFE, HFP, and OFCB at the three reaction temperatures (650 °C, 700 °C, and 750 °C) are indicated in Figure 75, Figure 76, and Figure 77.

When the results of the TFE, HFP, and OFCB mole fractions in sections 12.2 to 12.4 for a specific temperature is considered, it is clear that there exists a trend regarding the formation of these products. Initially, at low pressures, a high concentration of TFE is present in the system with very low levels of OFCB and HFP. With an increase in pressure, and hence residence time, the TFE concentration starts to decrease. As the TFE concentration decreases the OFCB concentration increases, with small amounts of HFP in the system. The OFCB concentration increases to above that of TFE and seems to plateau out after a while. If the results in section 12.8 are considered; with a further increase in residence time, the OFCB and TFE concentration decrease rapidly coupled with a sharp increase in the HFP concentration. This is almost the same trend as seen from the predicted rates in the above mentioned figures.

The predicted reaction rates in Figure 75, for a reaction temperature of 650 °C, follow the same trend as the experimental data except for the HFP fractions. This could be due to the differential equations not accounting for the production of difluorocarbenes directly from PTFE, as described by reactions (20) and (21); and by assuming the reaction constant k_5 is small enough to be negligible. It is also assumed that the production of HFP is only from the dissociation of OFCB. Atkinson and Atkinson (1957) proved that the dominant route of HFP production is through this pathway, however, reaction (24) cannot be neglected. The same reasons can explain the deviation between the experimental data and the predicted data at high temperatures (Figure 76 and Figure 77). The deviations could also be due to the assumption made, regarding the depolymerisation of the PTFE fed per second, to estimate the residence time; the fact that the product specific kinetics were determined from the pyrolysis of TFE; and the fact that the system was modelled as a plug flow reactor (PFR). The system would more likely resemble a combination between a PFR and a continuous stirred tank reactor (CSTR). Nevertheless, the kinetics do indicate that at an extended residence time the HFP concentration will ultimately increase to above that of TFE and OFCB, also seen in section 12.8.

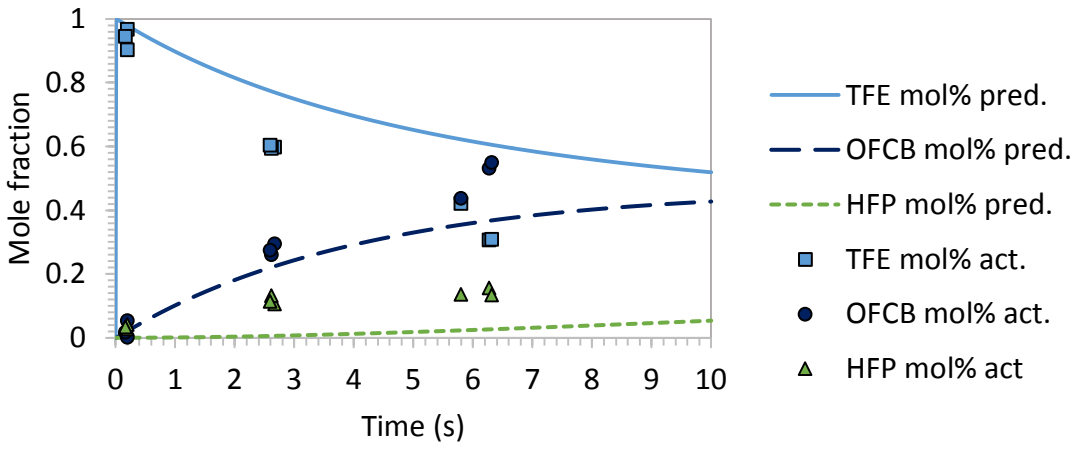

Figure 75: The predicted and actual mole fractions of TFE, HFP, and OFCB over time for a reaction temperature of 650 °C.

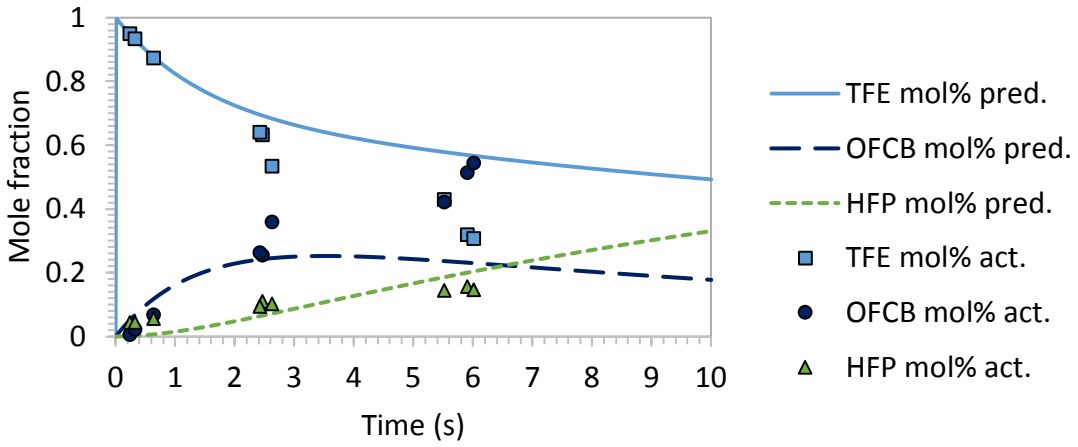

Figure 76: The predicted and actual mole fractions of TFE, HFP, and OFCB over time for a reaction temperature of 700 °C.

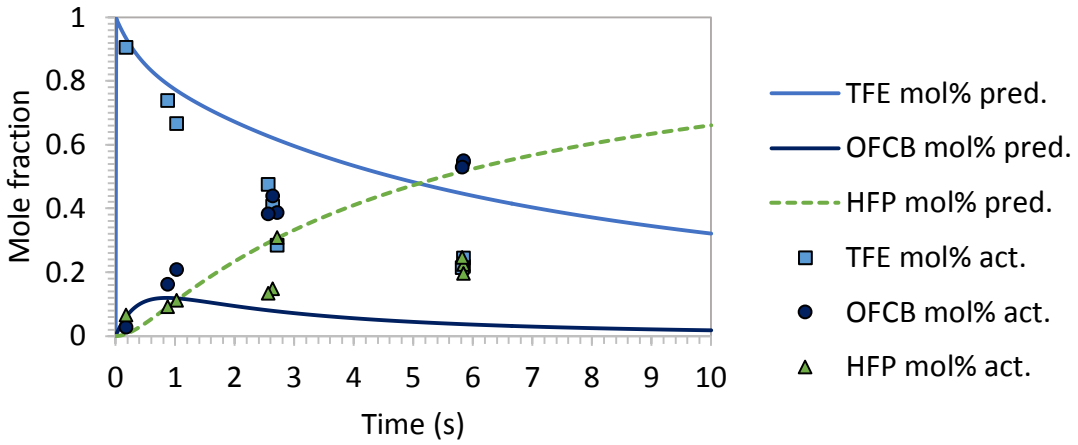

Figure 77: The predicted and actual mole fractions of TFE, HFP, and OFCB over time for a reaction temperature of 750 °C.

The results provided by Meissner *et al* (2004) and van der Walt (2007) had higher concentrations of HFP and lower concentrations of OFCB compared to the results presented in this investigation. This could be explained by the predicted formation rates in Figure 75, Figure 76, and Figure 77. In the depolymerisation experiments of Meissner *et al* (2004), PTFE was first pyrolysed in a vertical reactor (520 °C and 13.33 kPa – 101.32 kPa), similar to the reactor used in this investigation (refer to section 10.2.1 and Appendix C.4.1 for comparison). The product gas was then subjected to a second and third heated in a horizontal reactor where the gas was heated further (600 °C – 800 °C). The residence time and reactor temperature in the vertical reactor in addition to the residence time and increased temperature in the first section of the horizontal reactor could have caused the products to react further. Therefore, leading to higher HFP mole fractions and lower OFCB fractions than reported in this investigation. This same reason could explain why the contour plots (see sections 12.5, 12.6, and 12.7) of TFE, HFP, and OFCB differ from those presented by Meissner *et al* (2004).

These results show that higher HFP concentrations can be achieved if the residence time of the gas in the reactor is increased. The residence time can be increased in two ways: either by increasing the operating pressure, or by increasing the reactor volume. However, both of these options could lead to the increased production of PFIB, as seen in the experimental runs in section 12.8.

12.10 Determination of the product specific kinetics from the experimental data

The product specific kinetics of the system were investigated to study the effects of reactions (24), (25), and (34) on the production of HFP. In section 12.9.2, it was assumed that reactions (24) and (34) can be neglected, as proposed by Atkinson and Atkinson (1957), and that the main and only pathway of HFP production was through the dissociation of OFCB. It was also assumed that all of the difluorocarbenes produced during PTFE depolymerisation, combines to produce TFE. It is important to note that some of the product specific kinetics were determined via calculations using only a few experimental data points.

To determine the product specific kinetics the reaction equations in Table 25 were assumed. In the table, reaction (44) is the overall reaction that includes reactions (20) and (21) (page 61), where PTFE depolymerises to produces difluorocarbenes during the initiation step. It was assumed that this reaction will have the same reaction rate as the overall PTFE depolymerisation kinetics determined in the literature (see page 18), and that all of the PTFE fed in one second (0.183 $g \cdot s^{-1}$) is converted to difluorocarbenes. The differential equations

(equations (45) – (49)) were derived assuming that the reactions in Table 25 are all elementary. In contrast to the differential equations used in section 12.9.2 (also see section 12.9.2), equations (24) and (34) were not assumed to be negligible. The product specific kinetics were determined via solving the differential equations in GNU Octave. The reaction rate constants were adjusted until the predicted formation rates of TFE, HFP, and OFCB fit the experimental data in sections 12.2, 12.3, and 12.4. The pre-exponential constants and activation energies were determined by plotting $\ln k_i$ as a function of $\frac{1}{T}$. The depolymerisation system was modelled as a PFR.

Table 25: The reaction equations used to determine the product specific kinetics for this system.

Rate constant symbol	Reaction	Rate constant units	
k_1	$PTFE \rightarrow \bullet\bullet CF_2$	s^{-1}	(44)
k_2	$2 \bullet\bullet CF_2 \rightarrow CF_2 = CF_2$	$mol^{-1} \cdot s^{-1}$	(22)
k_3	$2CF_2 = CF_2 \rightarrow OFCB$	$mol^{-1} \cdot s^{-1}$	(23)
k_4	$OFCB \rightarrow 2CF_2 = CF_2$	s^{-1}	(33)
k_5	$OFCB \rightarrow CF_3 — CF = CF_2 + \bullet\bullet CF_2$	s^{-1}	(25)
k_6	$CF_2 = CF_2 + \bullet\bullet CF_2 \rightarrow CF_3 - CF = CF_2$	s^{-1}	(24)
k_7	$CF_3 - CF = CF_2 \rightarrow CF_2 = CF_2 + \bullet\bullet CF_2$	s^{-1}	(34)

$$\frac{dW_{PTFE}}{dt} = -k_1 W_{PTFE} \tag{45}$$

$$\frac{dN_{TFE}}{dt} = 0.5k_2 N_{CF_2}^2 - k_3 N_{TFE}^2 + 2k_4 N_{OFCB} - k_6 N_{TFE} N_{CF_2} + k_7 N_{HFP} \tag{46}$$

$$\frac{dN_{OFCB}}{dt} = 0.5k_3 N_{TFE}^2 - k_4 N_{OFCB} - k_5 N_{OFCB} \tag{47}$$

$$\frac{dN_{HFP}}{dt} = k_5 N_{OFCB} + k_6 N_{TFE} N_{CF_2} - k_7 N_{HFP} \tag{48}$$

$$\frac{dN_{CF_2}}{dt} = \frac{k_1 W_{PTFE}}{50} - k_2 N_{CF_2}^2 + k_5 N_{OFCB} - k_6 N_{TFE} N_{CF_2} + k_7 N_{HFP} \tag{49}$$

The formation rates determined for each of the reaction temperatures (650 °C, 700 °C and 750 °C) are indicated in Figure 78, Figure 79 and Figure 80, respectively. The determined pre-exponential constant and activation energy for each of the reactions are summarised in Table 26, with the corresponding Arrhenius plots in Appendix B.6.

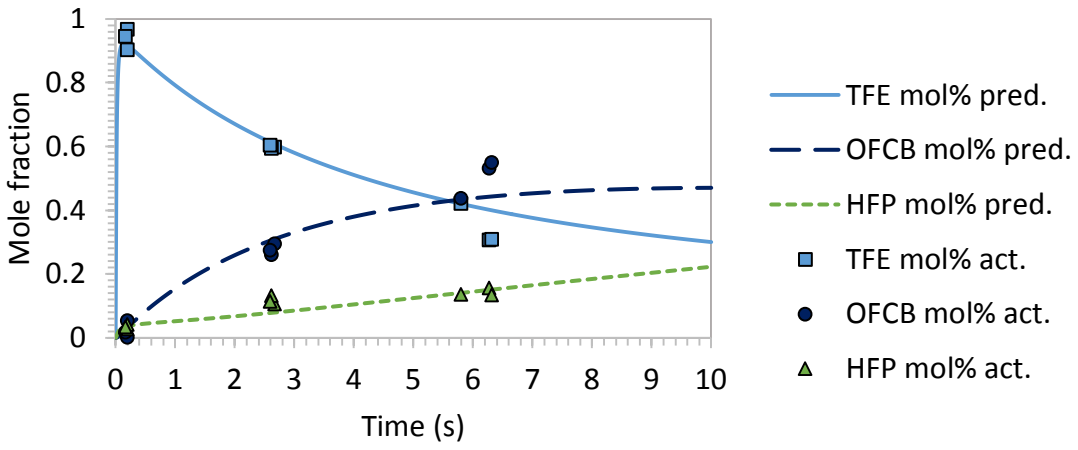

Figure 78: The determined formation rates of TFE, HFP, and OFCB over time compared to the actual product fractions at a temperature of 650 °C.

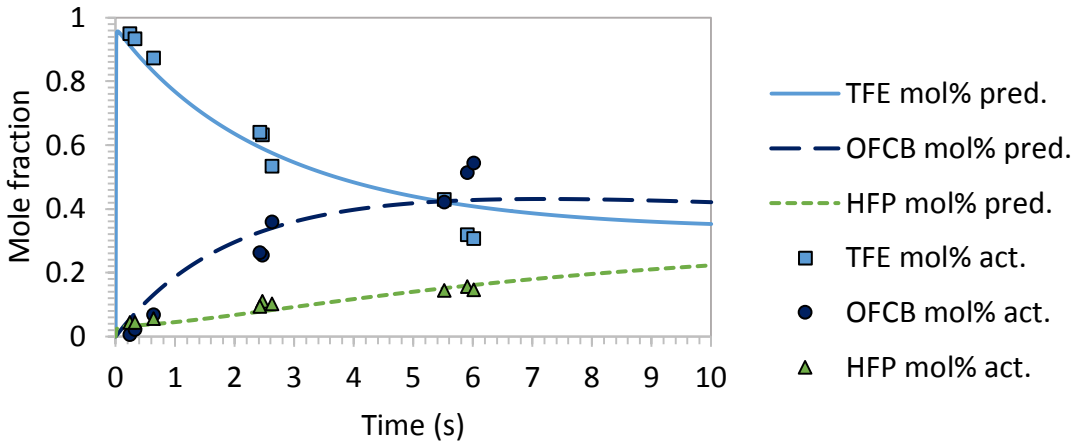

Figure 79: The determined formation rates of TFE, HFP, and OFCB over time compared to the actual product fractions at a temperature of 700 °C.

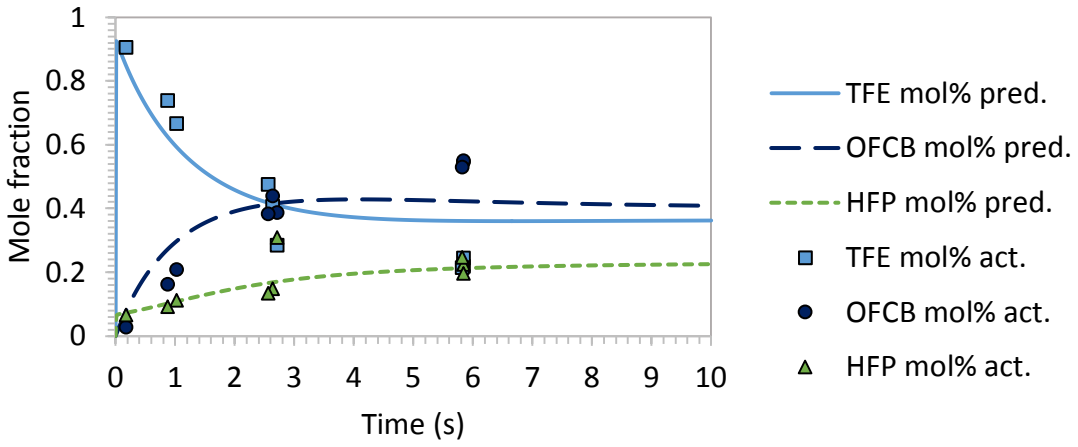

Figure 80: The determined formation rates of TFE, HFP, and OFCB over time compared to the actual product fractions at a temperature of 750 °C.

Table 26: The calculated activation energies and pre-exponential constants for each of the reactions in Table 25.

	Rate constant						
	k_1 s^{-1}	k_2 $mol^{-1}{\cdot}s^{-1}$	k_3 $mol^{-1}{\cdot}s^{-1}$	k_4 s^{-1}	k_5 s^{-1}	k_6 s^{-1}	k_7 s^{-1}
Pre-exponent	1.47×10^{21}	3.2×10^{17}	6.28×10^{6}	2.74×10^{15}	1.7×10^{2}	5.11×10^{18}	1.25×10^{22}
Activation energy ($kJ{\cdot}mol^{-1}$)	339.39	214.25	79	323.79	66.43	274.91	436.01

Comparison of the pre-exponential constants of the various reactions in Table 26, indicate that the reaction rates of reactions (24) and (34) (k_6 and k_7) are not small enough to be neglected, as assumed in the previous section. Atkinson and Atkinson (1957) proposed that the main formation pathway of HFP is through OFCB dissociation. However, this reaction cannot account for the HFP concentrations measured at residence times of 0.2 s and 2.7 s. At these residence times, the OFCB concentration is not high enough to enable reaction (25) to produce these fractions of HFP. Therefore, the HFP concentrations measured at residence times lower than 3 s should mainly be from TFE reacting with difluorocarbenes. Hence, it can be deduced that at low residence times (< 3 s) the main route of HFP production is through reaction (24). With an increase in residence time, the dominant HFP formation pathway shifts to reaction (25).

The calculated kinetics for reactions (23) and (33) (k_3 and k_4 in Table 26) are in line with the data proposed by Atkinson and Atkinson (1957). The pre-exponential constant and activation energy of reaction (25) (k_5) do not correspond with the data proposed by Atkinson and Atkinson (1957); however, they determined the kinetic data from the pyrolysis of TFE and assumed that all of the HFP is produce via OFCB dissociation. They did not account for the production of HFP via reaction (24).

The formation rates in Figure 78, Figure 79, and Figure 80 slightly deviate from the actual mole fraction data points. This could be due to the system being modelled as a PFR. By modelling the system as a PFR, the continuous addition of PTFE into the reactor and the effects thereof on product formation is neglected. Therefore, it is recommended to model the system in future as a PFR/CSTR system to account for these effects. The deviation could also be attributed to the assumptions made in calculating the residence times or the error in determining the mole fractions via the FTIR analysis method. Improving the FTIR calibration for the system and including a flow meter in the system should improve the accuracy of product specific kinetics.

13 Conclusions and recommendations

Statistical analysis of the TFE response function indicate that the production of TFE is highly sensitive to changes in pressure. An increase in pressure leads to lower fractions of TFE. This, however, is the complete opposite for the production of HFP and OFCB. An increase in both temperature and pressure leads to higher concentrations of HFP and OFCB. The production OFCB is highly sensitive to pressure; whereas the formation of HFP is equally affected by pressure and temperature changes. However, changes in pressure have a larger effect on the HFP production than temperature at pressures lower than approximately 20 kPa. At higher pressures the sensitivity has the inverted affect, with temperature having a larger effect. The statistical result of HFP and OFCB completely contradict the results determined by Meissner *et al* (2004).

The highest mole fraction of OFCB (55 mol %) was observed at operating conditions of 40 kPa and 750 °C. Compared to the literature, this is the highest concentration of OFCB achieved at these operating conditions, with both van der Walt (2007) and Meissner *et al* (2004) only achieving a maximum of 25 mol %. In contrast to the data of both Meissner *et al* (2004) and van der Walt, the maximum observed HFP mole fraction was 25 mol % during this investigation. The inverted maximum OFCB and HFP concentrations observed by Meissner *et al* (2004) and van der Walt (2007) compared to the maximum concentrations observed during this investigation, could be due to a difference in residence time of the gas products in the reactor. A brief kinetic analysis of the system, using the relevant kinetic data available in the literature, confirms that the HFP concentration will increase with an increase in residence time. This was also observed in three failed experiments where the residence time of the gas in the reactor increased due to abnormal or no PTFE flow from the feeder. During these experimental runs the HFP concentration increased and the OFCB concentration decreased to values similar to those observed by Meissner *et al* (2004) and van der Walt.

TFE mole fractions of 95 mol % and higher can be achieved with operating temperatures in the range of 650 °C to 720 °C, together with a system pressure of 2 kPa or less. To produce a single component product gas stream with higher than 96 mol % TFE, operating conditions of ± 675 °C and < 10 kPa are recommended.

A mole fraction of 19 mol % and higher can be expected for HFP within the operating range of 744 °C to 750 °C and 32 kPa up to 40 kPa. To maximise this fraction (> 20 mol %), without changing the residence time, an operating temperature and pressure of 750 °C and 40 kPa are recommended. However, at these conditions the OFCB fraction would be maximised at 50 mol % or higher. Hence, these conditions would not be optimal if distillation is to be used to separate the mixture due to the small difference in the HFP and OFCB relative volatility.

With the current system as is, without increasing the residence time, no set of operating conditions will produce a product gas containing more HFP than OFCB as determined in this investigation.

In future, if the need arise to produce a product gas containing mostly TFE and OFCB with a HFP concentration less than 10 mol %, an operating temperature range of 660 °C – 695 °C and operating pressure range of 14 kPa – 20 kPa is recommended. At these conditions a TFE concentration of ± 65 mol %, an OFCB concentration of ± 25 mol %, and a HFP concentration of ± 9 mol % can be expected.

The results from the three failed experiments substantiate the work presented by Atkinson and Atkinson (1957) in that the dominant reaction path for the formation of HFP is the dissociation of OFCB and not the pyrolysis of TFE. However, analysis of the product specific kinetics indicate that OFCB dissociation is the dominant HFP production pathway only at residence times higher than 3 s. At lower residence times the dominant HFP production pathway is through the reaction of TFE with difluorocarbenes. It was concluded that to increase the HFP concentration and decrease the OFCB concentration, the residence time of the gas in the reactor should be increased. This can be achieved via two methods: either increase the reaction pressure or increase the reactor heated section volume. It is recommended that a more in-depth study into the exact effects of residence time on the OFCB and HFP formation be performed.

The product specific kinetics determined for the reversible reaction of $TFE \leftrightarrow OFCB$, are in line with the kinetics proposed by Atkinson and Atkinson (1957). To improve the accuracy of the product specific kinetics the following is recommended: Re-determine the kinetics by modelling the system as a combined PFR/CSTR system instead of just a PFR system; improve the calibration of the FTIR analysis method and insert a flow meter in the system to improve the residence time calculation.

References

Anderson, HC (1964) "Thermogravimetry of Polymer Pyrolysis Kinetics", *Journal of Polymer Science,* 6, 175 – 182.

Amoros, JL, Mallol, G, Sanchez, E and Garcia, J (2000) "Design of bins and hoppers for the storage of particulate materials. Problems associated with the discharge operation", *Castellon (Spain),* 41 – 58.

Atkinson, B and Atkinson, VA (1957) "The Thermal Decomposition of Tetrafluoroethylene", *Journal of the Chemical Society*, 2086 – 2094.

Babenko, YI, Lisochkin, YA and Poznyak, VI (1993) "Explosion of tetrafluoroethylene during nonisothermal polymerization", *Combustion, explosion, and shock waves*, 5(29), 603 – 609.

Bates, L (2000) *Guide to the Design, Selection, and Application of Screw Feeders,* Professional Engineering Publishing Limited, UK.

Bhadury, PS, Singh, S Sharma, M and Palit, M (2007) "Flash pyrolysis of polytetrafluoroethylene in a quartz assembly", *Journal of Analytical and Applied Pyrolysis,* 78, 288 – 290.

Chase, GG (sa) "Hopper design", Slide Notes 10, The University of Akron, *www.inti.gob.ar/cirsoc/pdf/silos/Solids**Notes10**HopperDesign.pdf* [2014, August 14].

Collins, RD, Fiveash, P and Holland, L (1969) "A mass spectrometry study of the evaporation and pyrolysis of polytetrafluoroethylene", *Vacuum,* 19(3), 113 – 116.

Conesa, JA and Font, R (2001) "Polytetrafluoroethylene decomposition in air and nitrogen", *Polymer Engineering and Science*, 41(12), 2137 – 2147.

Cox, JM, Wright, BA and Wright, WW (1964) "Thermal degradation of fluorine-containing polymers. Part I. Degradation in vacuum", *Journal of Applied Polymer Science,* 8, 2935 – 2950.

Diamondback Technology (2005) "Eliminating arching hangups in hopper", Whitepapers, http://www.chemicalprocessing.com/whitepapers/2005/8/ [25 September 2015].

Drobny, JG (2009) *Technology of Fluoropolymers, Second Edition,* CRC Press, Taylor & Francis Group, Florida, USA.

DuPont (*sa*) *Product information: Teflon 807-N PTFE granular moulding resin.*, Switzerland.

Eaton, JW, Bateman, D, Hauberg, S, Wehbring, R (2016) "GNU Octave A high-level interactive language for numerical computations", Free Software Foundation, Boston, USA.

Ebnesajjad, S (2000) *Fluoroplastics: Volume 1: Non-Melt Processable Fluoroplastics: The Definitive User's Guide and Databook*, Plastics Design Library, New York, USA.

Eilers, A (2003) "A perfect smoother", *Analytical Chemistry*, 75(14), 3631 – 3636.

Ferrero, F, Meyer, R, Kluge, M, Schroder, V and Spoormaker, T (2013) "Self-ignition of tetrafluoroethylene induced by rapid valve opening in small diameter pipes", *Journal of Loss Prevention in the Process Industries,* 1(26), 177 – 185.

Fernandez, JW, Cleary, PW and McBride, W (2011) "Effect of screw design on hopper drawdown of spherical particles in a horizontal screw feeder", *Chemical Engineering Science,* 66, 5585 – 5601.

Ferse, A, Lunkwitz, K, Grimm, H, Dietrich, P, Engler, G, Gross, U, Prescher, D and Schulze, D (1978) "Degradation of polytetrafluoroethylene to low molecular products by means of energy-rich radiation", *Z. Chem.*, 18(2).

Ganesan, K, Raza, SK, Vijayaraghavan, R (2010) "Chemical warfare agents", J. Pharm. Bioallied Sci. 2010, 2, 166–178.

Gangal, SV (*sa*) "Fluorine-containing polymers, polytetrafluoroethylene" in *Kirk-Othmer Encyclopedia of Chemical Technology*, John Wiley & Sons, Inc.

Hercules, DA, DesMarteau, DD, Fernandes, RE, Clark, JL Jr. and Thrasher, JS (2014) "Evolution of Academic Barricades for the use of Tetrafluoroethylene (TFE) in the Preparation of

Fluoropolymers", *Handbook of Fluoropolymer Science and Technology*, Wiley & Sons, 413 – 431.

Hori, KS and Shizuoka-ken, JP (1997) "Method for granulation of polytetrafluoroethylene powder", *European Patent 0794213 A2,* assigned to DuPont-Mitsui Fluorochemicals Co. Ltd., Tokyo.

Ichida, T and Homoto, Y (2008) "Process for producing fluoromonomer", *US Patent 7,317,071 B2,* assigned to Daikin Industries, LTD, Osaka.

Jenike, AW (1964) *Storage and flow of solids*, Bulletin 123, Utah Engineering Experiment Station, University of Utah, Salt Lake City.

Jenike (1964) as quoted by Bates, L (2000) *Guide to the Design, Selection, and Application of Screw Feeders,* Professional Engineering Publishing Limited, UK.

Jun, HS, Kim, KN, Park, KY and Woo, SI (1995) "Thermal degradation of polytetrafluoroethylene in flowing helium atmosphere I. Degradation rate", *Korean Journal of Chemical Engineering,* 12(2), 156 – 161.

Lewis, EE and Naylor, MA (1947) "Pyrolysis of Polytetrafluoroethylene", *Journal of the American Chemical Society,* 68, 1968 – 1970.

Lonfei, J, Jingling, W and Siiuman, X (1986) "Mechanism of pyrolysis of fluoropolymers", *Journal of Analytical and Applied Pyrolysis,* 10, 99 – 106.

Matheson TriGas (2008) "Material Safety Data Sheet: Tetrafluoroethylene", https://www.mathesongas.com/pdfs/msds/MAT22980.pdf [2014, October, 13].

McGlinchey, D (2008) *Bulk Solids Handling: Equipment selection and Operation,* Blackwell Publishing Ltd., UK.

Meissner, E, Wroblewska, A and Milchert, E (2004) *"*Technological parameters of pyrolysis of waste polytetrafluoroethylene*", Polymer Degradation and Stability*, 83, 163 – 172.

Mesowicz (1987) as quoted by Simon, CM and Kaminsky, W (1998) "Chemical recycling of polytetrafluoroethylene by pyrolysis", *Polymer Degradation and Stability,* 62, 1 – 7.

Michaelsen, JD and Wall, LA (1957) "Further studies on the pyrolysis of polytetrafluoroethylene in the presence of various gases", *Journal of Research of the National Bureau of Standards,* 58(6), 327 – 331.

Morisaki, S (1978) "Simultaneous thermogravimetry-mass spectrometry and pyrolysis-gas chromatography of fluorocarbon polymers", *Thermochimica Acta*, 25, 171 – 183.

NAC/AEGL Committee (2010) "Acute exposure guideline levels (AEGLs) for perfluoroisobutylene (PFIB)", National Advisory Committee for Acute Exposure Guideline Levels for Hazardous Substances, Interim report, http://www.epa.gov/oppt/aegl/pubs/perfluoroisobutylene_interim_sept_2010.pdf [2014, June 30].

NIST/SEMATECH (2012) "e-Handbook of Statistical Methods", http://www.itl.nist.gov/div898/handbook/, [2015, October 18].

Patil, KD (2009) *Mechanical Operations: Fundamental principles and applications*, Nirali Prakashan.

Rae, PJ and Dattelbaum, DM (2004) "The properties of poly(tetrafluoroethylene) (PTFE) in compression" *Polymer*, 45, 7615–7625.

Raymond, AK (1985) *Materials handling handbook,* John Wiley & Sons.

Reza, A and Christiansen, E (2007) "A case study of a TFE explosion in a PTFE manufacturing facility", *Process Safety Progress*, 26(1), 77 – 82.

Schottle, T, Hintzer, K, Staudt, HJ and Weber, H (1995) "Process for the preparation of fluorinated monomers", *US Patent 5,432,259,* assigned to Hoechst Aktiengesellschaft, Frankfurt am Main, Germany.

Schulze, D (2008) *Powders and Bulk Solids,* Springer Berlin Heidelberg, New York.

Schulze, M, Bolwin, K, Gulzow, E and Schnurnberger, W (1995) "XPS analysis of PTFE decomposition due to ionizing radiation", *Fresenius Journal of Analytical Chemistry,* 353, 778 – 784.

Siegle, JC, Muus, LT, Lin, T and Larsen, HA (1964) "The molecular structure of perfluorocarbon polymers. II. Pyrolysis of polytetrafluoroethylene", *Journal of Polymer Science,* 2, 391 – 404.

Simon, CM and Kaminsky, W (1998) "Chemical recycling of polytetrafluoroethylene by pyrolysis", *Polymer Degradation and Stability,* 62, 1 – 7.

Sonnendecker, PW (2016) *Quantitative Analysis of Inline, Time-Resolved FTIR Spectra: Steps towards Automation*, MEng Thesis, University of Pretoria, Pretoria, South Africa.

The Engineering ToolBox (sa) "Friction and Friction Coefficients", http://www.engineeringtoolbox.com/friction-coefficients-d_778.html [2015, January 30]

Van Bramer, DJ (1999) "Tetrafluoroethylene shipping/storage mixtures", *US Patent 5,866,727,* assigned to E. I. du Pont de Nemours and Company, Wilmington, Delaware, USA.

Van Bramer, DJ, Shiflett, MB and Yokozeki, A (1994) "Safe Handling of Tetrafluoroethylene", *US Patent 5,345,013,* E. I. du Pont de Nemours and Company, Wilmington, Delaware, USA.

Van der Walt, IJ (2007) *Recovery of valuable products from polytetrafluoroethylene (PTFE) waste,* Ph.D. Thesis, North West University, Potchefstroom, South Africa.

Van der Walt, IJ (2015) "Ribbon feeders", Personal Communication, Department of Chemical Engineering, University of Pretoria, South Africa.

Zion Research (2015) "Polytetrafluoroethylene (PTFE) (Granular, Fine Powder, Dispersion, Micronized Powder) Market for Automotive & Transportation, Electrical & Electronics, Chemical Processing, Industrial Equipment and Other Applications: Global Industry Perspective, Comprehensive Analysis, Size, Share, Growth, Segment, Trends and Forecast, 2014 – 2020", http://www.marketresearchstore.com/report/polytetrafluoroethylene-market-z39861 [2016, June 22].

Appendix

Appendix A Screw feeder design results

A.1 Experimental results for the addition of an external vibrator to the hopper surface

Table 27: The vibration setting intervals for each run. "Rest of run" indicates that the vibrator will vibrate for a second in intervals as indicated in the table, until the run is stopped after the total run time has been reached.

Run number	No vibration period at start	Vibrate for a second every:				
		120 (s)	90 (s)	30 (s)	15 (s)	10 (s)
Run 1	0 min			Rest of run		
Run 2	15 min			10 min	12 min	Rest of run
Run 3	12 min			10 min	18 min	Rest of run
Run 4	10 min			10 min	15 min	Rest of run
Run 5	5 min			10 min	15 min	Rest of run
Run 6	7 min			10 min	15 min	Rest of run
Run 7	7 min			10 min	15 min	Rest of run
Run 8	5 min			Rest of run		
Run 9	Rest of run					
Run 10	5 min	Rest of run				
Run 11	5 min		Rest of run			
Run 12	5 min		Rest of run			
Run 13	5 min	Rest of run				
Run 14	5 min	Rest of run				
Run 15	5 min	Rest of run				

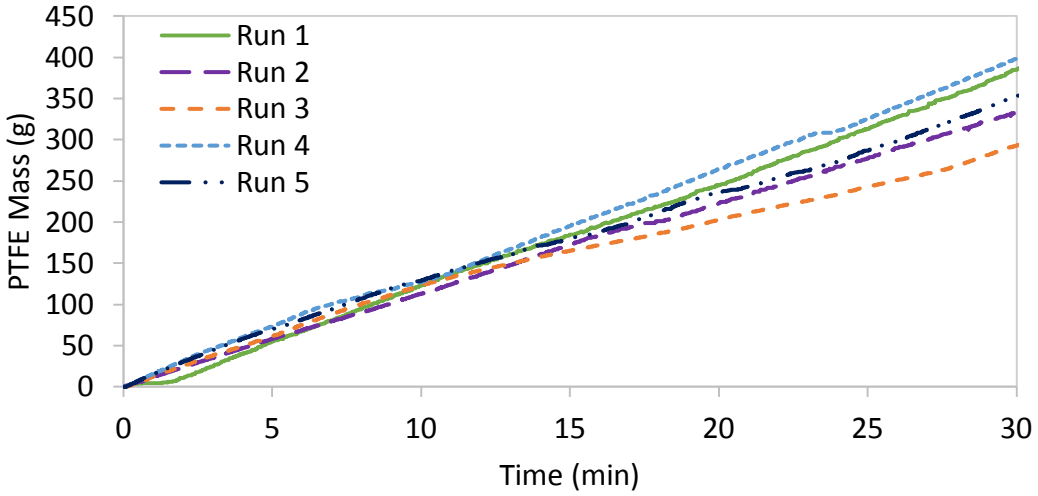

Figure 81: The first five runs of the hopper system with a vibrator attached at a motor speed of 37 rpm (50 Hz). The vibrating intervals can be seen in Table 27.

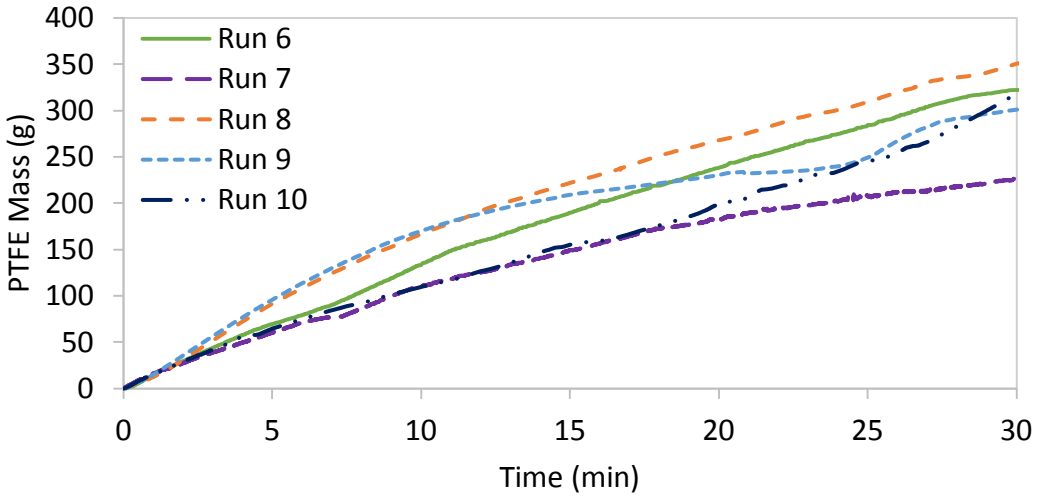

Figure 82: The second set of five runs of the hopper system with the vibrator attached at a motor speed of 37 rpm (50 Hz). The vibrating intervals can be seen in Table 27.

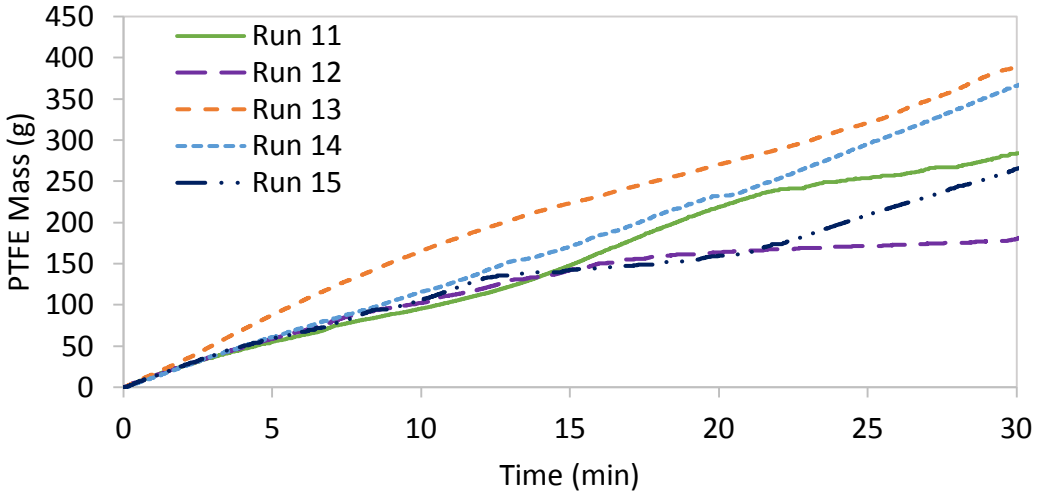

Figure 83: The last five runs of the hopper system with the vibrator attached at a motor speed of 37 rpm (50 Hz). The vibrating intervals can be seen in Table 27.

A.2 Final hopper calibration experimental results

A.2.1 Calibration under atmospheric conditions

A.2.1.1 Hopper calibration run at 37 rpm

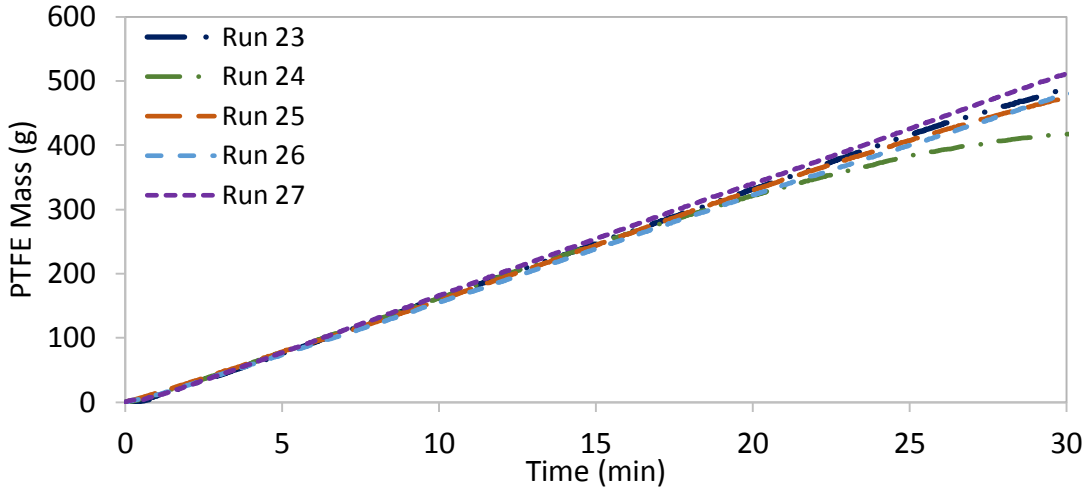

Figure 84: Five calibration runs performed with Teflon® PTFE 807N at a VFD setting of 50 Hz corresponding to a motor speed of 37 rpm.

Table 28: Average flow rate calculation results at 37 rpm.

Run number	Calculated slope ($g \cdot min^{-1}$)	Intercept (g)	Standard Slope error	R^2
23	16.404	0	5.97E-05	0.99
24	14.894	0	2.64E-04	0.99
25	16.063	0	8.26E-05	0.99
26	15.921	0	4.67E-05	0.99
27	16.978	0	4.96E-05	0.99
Average	16.342	0		

A.1.1.1. Hopper calibration runs at 30 rpm

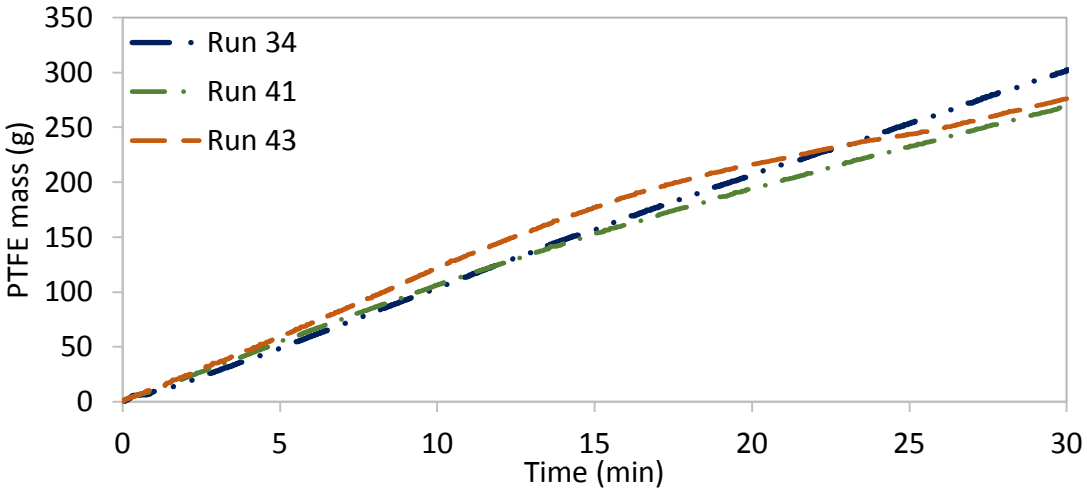

Figure 85: Three calibration runs performed with Teflon® PTFE 807N at a VFD setting of 40 Hz corresponding to a motor speed of 30 rpm.

Table 29: Average flow rate calculation results at 30 rpm.

Run number	Calculated slope ($g \cdot min^{-1}$)	Intercept (g)	Standard Slope error	R^2
34	10.16	0	3.84E-05	1.00
41	9.37	0	1.19E-04	1.00
43	10.00	0	2.42E-04	0.99
Average	9.843	0		

A.1.1.2. Hopper calibration runs at 30 Hz

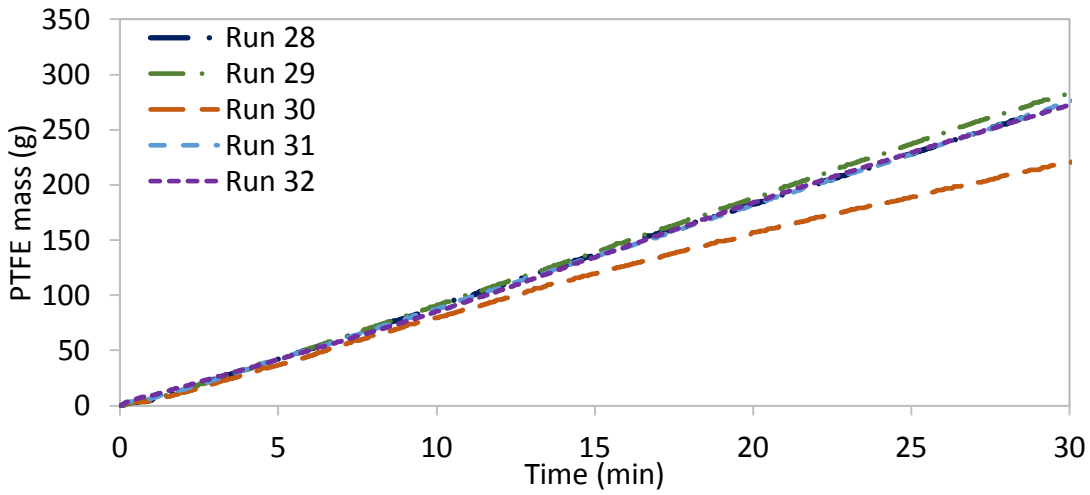

Figure 86: Five calibration runs performed with Teflon® PTFE 807N at a VFD setting of 30 Hz corresponding to a motor speed of 22 rpm.

Table 30: Average flow rate calculation results at 22 rpm.

Run number	Calculated slope ($g \cdot min^{-1}$)	Intercept (g)	Standard Slope error	R^2
28	9.11	0	2.33E-05	1.00
29	9.40	0	3.51E-05	1.00
30	7.56	0	5.81E-05	1.00
31	9.11	0	2.92E-05	1.00
32	9.08	0	3.66E-05	1.00
Average	9.175	0		

A.1.1.3. Hopper calibration runs at 15 rpm

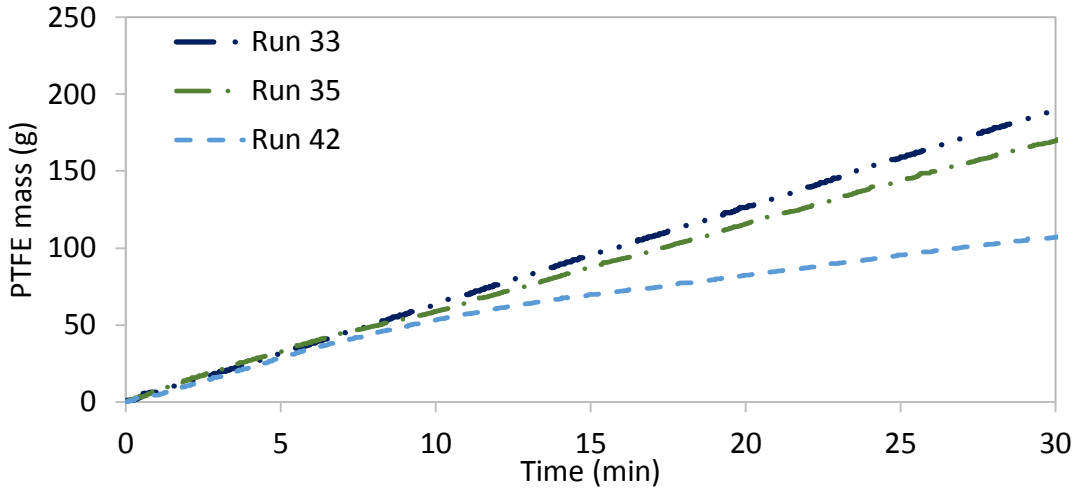

Figure 87: Three calibration runs performed with Teflon® PTFE 807N at a VFD setting of 20 Hz corresponding to a motor speed of 15 rpm.

Table 31: Average calculated flow rate at 15 rpm.

Run number	Calculated slope ($g \cdot min^{-1}$)	Intercept (g)	Standard Slope error	R^2
33	6.33	0	6.34E-06	1.00
35	5.73	0	3.00E-05	1.00
42	3.92	0	1.26E-04	0.98
Average	6.032	0		

A.1.2. Calibration under atmospheric conditions

Table 32: Flow rate calculations at four different VFD frequencies for the system under vacuum conditions.

Mass (g)	Time (min)	Flow rate ($g \cdot min^{-1}$)	Standard deviation	Average flow rate ($g \cdot min^{-1}$)
		37 rpm		
200.6	10	20.06	0.64	19.61
191.6	10	19.16		
		30 rpm		
151.2	10	15.12	0.52	14.94
153.4	10	15.34		
143.5	10	14.35		
		22 rpm		
112.7	10	11.27	0.43	10.97
106.6	10	10.66		
		15 rpm		
72	10	7.2	0.36	6.94
70.8	10	7.08		
65.3	10	6.53		

Appendix B Continuous PTFE depolymerisation results

B.1 Response surface equations presented by Meissner *et al* (2004)

$$Y_i = Y(Y_k)$$

$$Y_i = b_0 + b_1 \cdot X_1 + \cdots + b_i \cdot X_i + b_{11} \cdot X_1^2 + \cdots + b_{ii} \cdot X_i^2 + b_{12} \cdot X_1 X_2 + \cdots + b_{i-1,1} \cdot X_{i-1} X_i$$

for $X_k \in [-2,2]$; $X_1 - Temperature$; $X_2 - Pressure$; $X_3 - Nitrogen\ flow\ rate$; $X_4 - PTFE\ feeding\ rate$

Table 33: Coefficient values for the response surface equations of TFE, HFP and OFCB as calculated by Meissner *et al* (2004).

Corresponding variable		Coefficient values					
		First section of reactor			Second section of the reactor		
		Y_2 (TFE)	Y_3 (HFP)	Y_4 (OFCB)	Y_7 (TFE)	Y_8 (HFP)	Y_9 (OFCB)
	b_0	6.26	74.11	5.54	6.01	75.16	4.58
X_1	b_1	-9.03	11.43	-5.90	7.95	10.64	-5.39
X_2	b_2	-5.70	2.31	-0.71	-5.70	2.60	-0.76
X_3	b_3	-1.02	1.15	-0.40	-0.77	0.01	-0.14
X_4	b_4	1.22	1.25	-1.61	1.45	1.69	-1.51
X_1^2	b_{11}	3.96	-5.27	1.37	3.92	-5.71	1.41
X_1X_2	b_{12}	4.27	-9.20	0.91	3.77	-7.88	0.91
X_1X_3	b_{13}	0.26	-0.75	1.40	-0.26	-0.59	1.37
X_1X_4	b_{14}	-2.11	0.71	2.61	-2.12	-1.19	2.67
X_2^2	b_{22}	5.44	-6.11	1.62	5.30	-5.52	1.51
X_2X_3	b_{23}	1.14	-0.49	-0.09	0.37	-0.36	0.17
X_2X_4	b_{24}	0.21	-1.37	0.80	0.21	-2.29	0.87
X_3^2	b_{33}	0.72	-1.12	1.04	0.50	-1.58	1.00
X_3X_4	b_{34}	0.87	-0.37	0.09	0.75	0.01	0.08
X_4^2	b_{44}	0.22	-2.27	0.66	-0.14	-2.35	0.58

B.2 Experimental data produced at 650 °C.

B.2.1 Product distribution at < 10 kPa

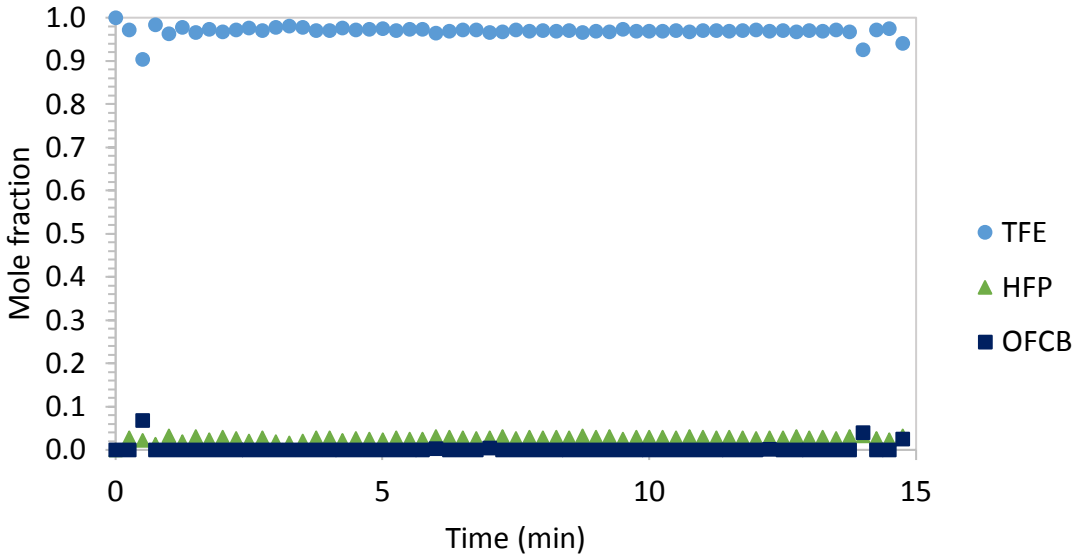

Figure 88: Mole fraction distribution of TFE, HFP, and OFCB for run number 1 at 2 kPa.

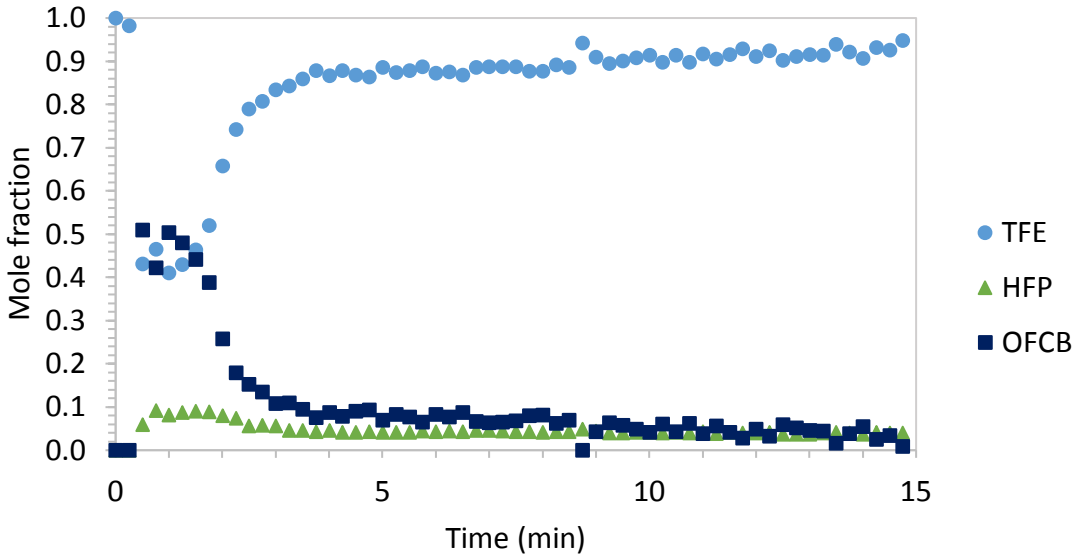

Figure 89: Mole fraction distribution of TFE, HFP, and OFCB for run number 12 at 1.8 kPa.

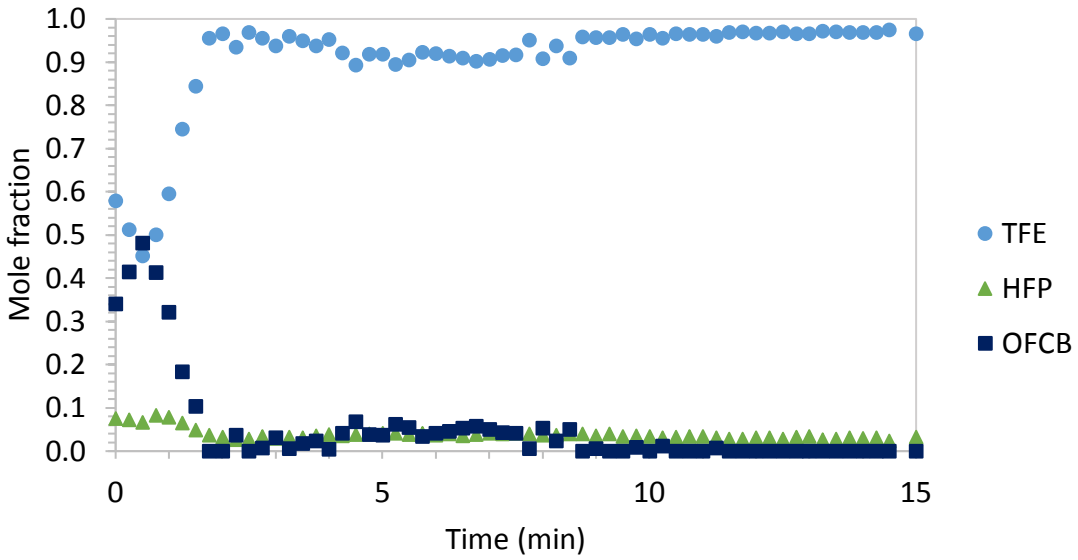

Figure 90: Mole fraction distribution of TFE, HFP, and OFCB for run number 20 at 1.6 kPa.

B.2.2 Product distribution at 20 kPa

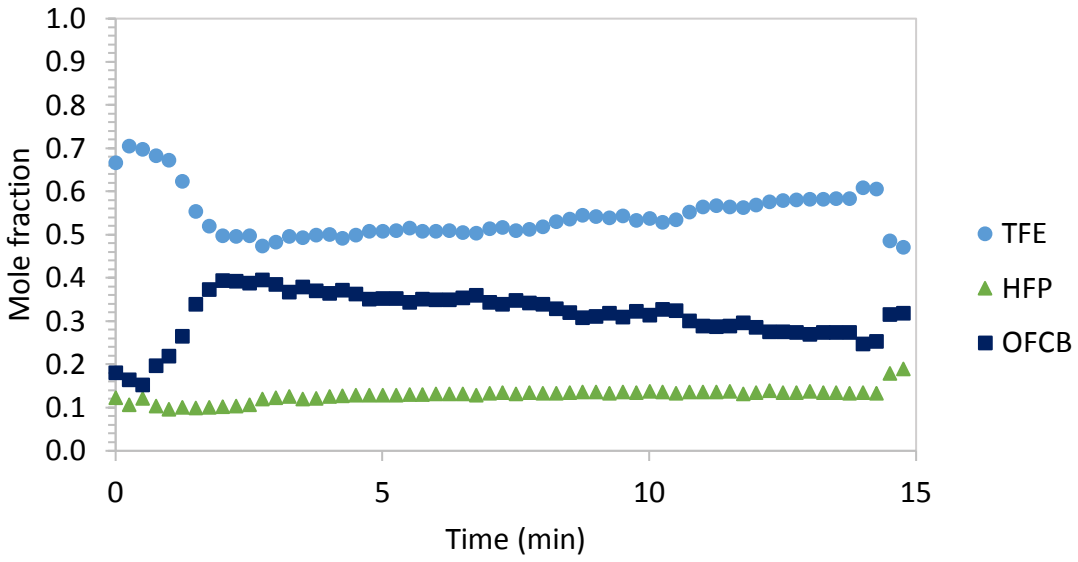

Figure 91: Mole fraction distribution of TFE, HFP, and OFCB for run number 7.

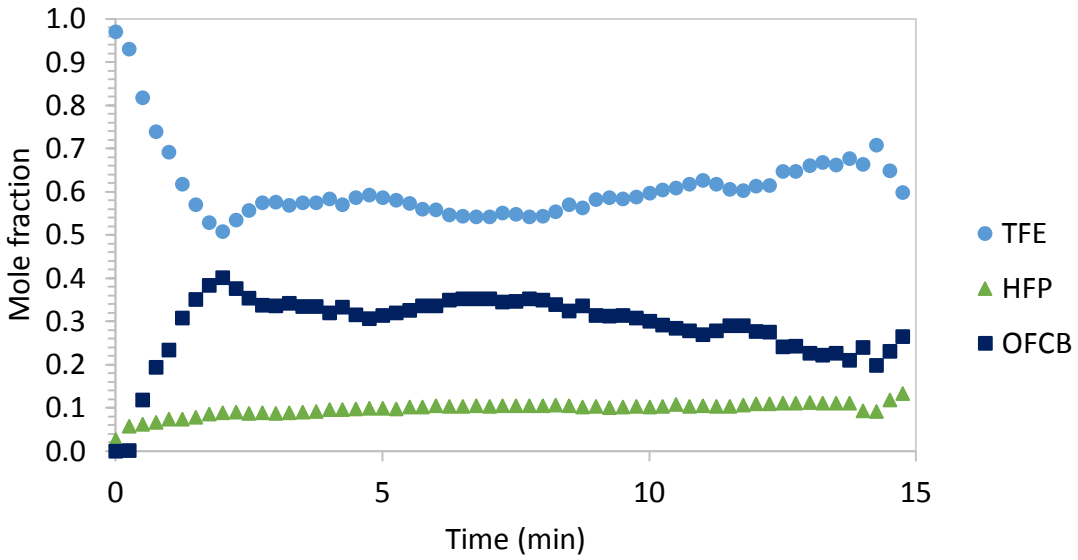

Figure 92: Mole fraction distribution of TFE, HFP, and OFCB for run number 18.

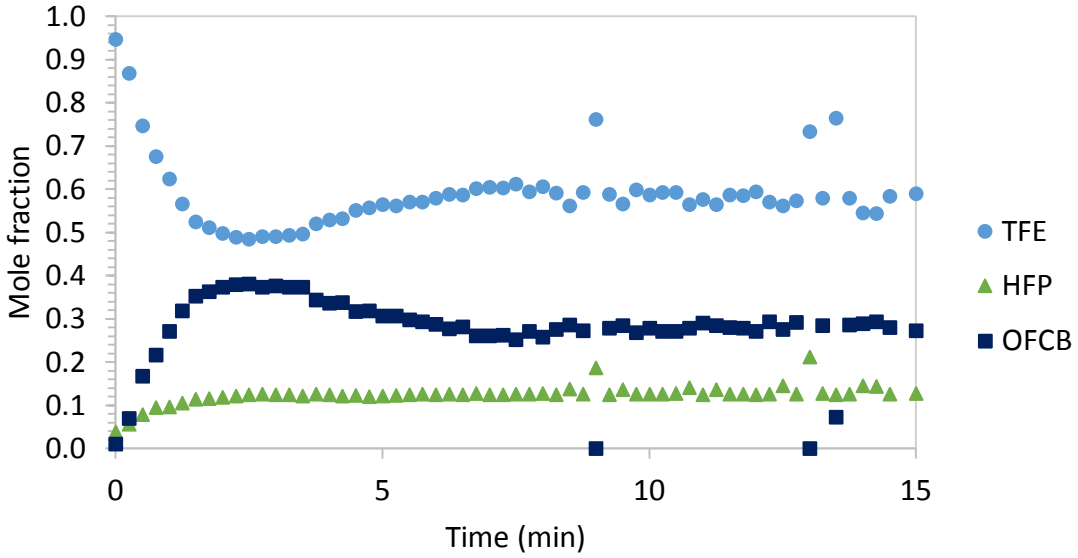

Figure 93: Mole fraction distribution of TFE, HFP, and OFCB for run number 26.

B.2.3 Product distribution at 40 kPa

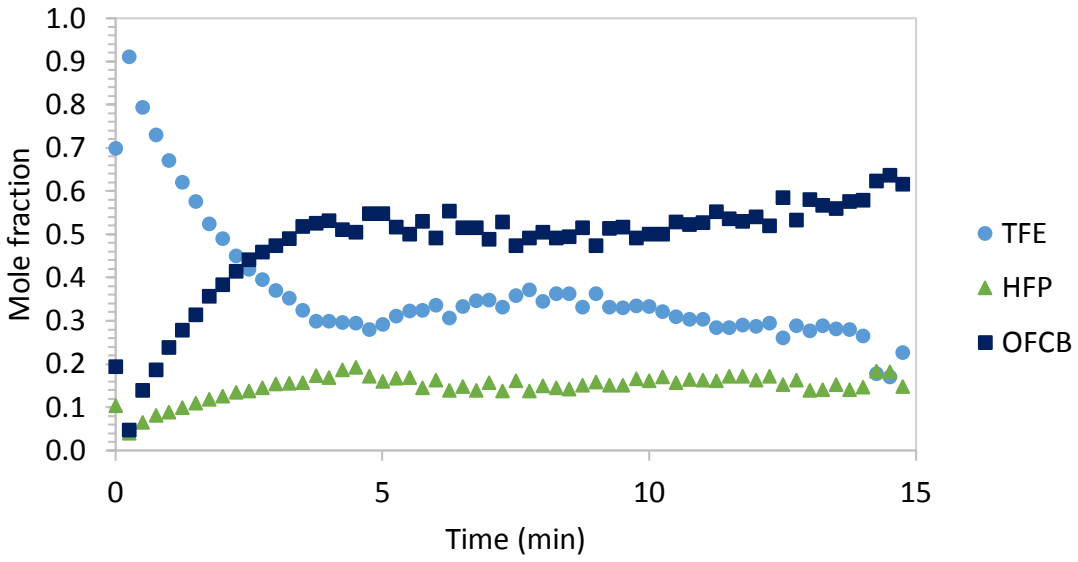

Figure 94: Mole fraction distribution of TFE, HFP, and OFCB for run number 2.

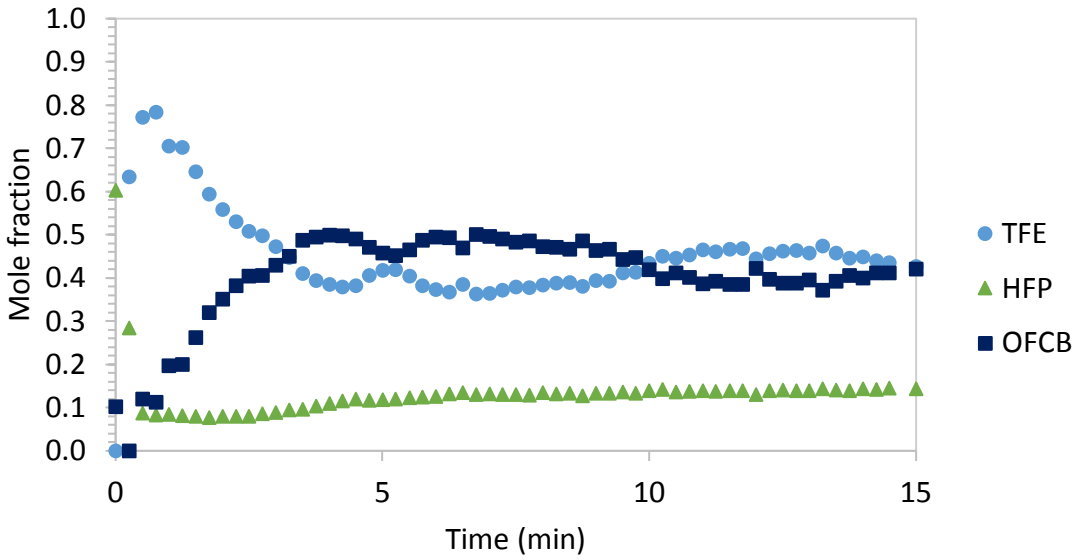

Figure 95: Mole fraction distribution of TFE, HFP, and OFCB for run number 13.

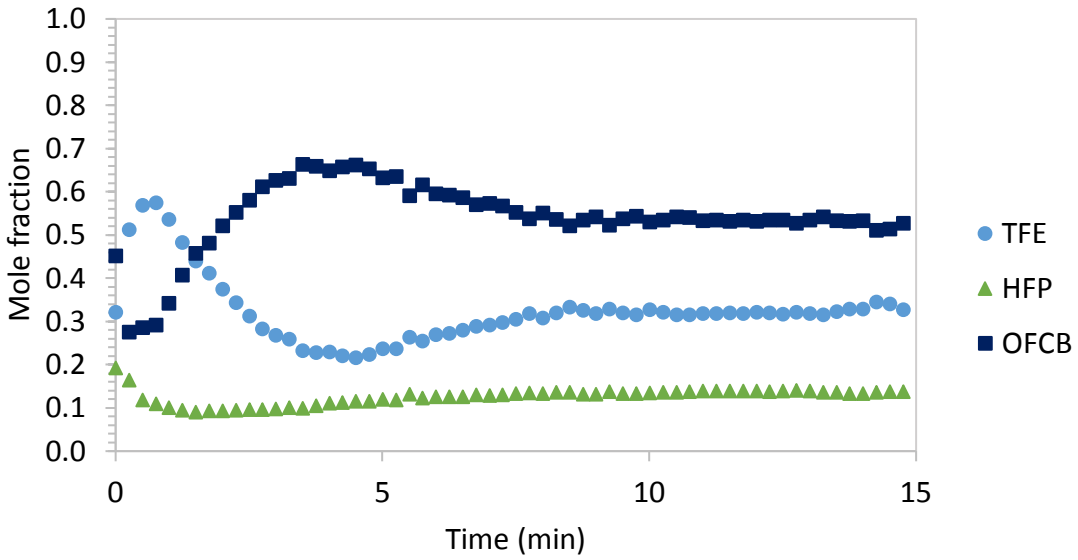

Figure 96: Mole fraction distribution of TFE, HFP, and OFCB for run number 21.

B.3 Experimental data produced at 700 °C.

B.3.1 Product distribution at < 10 kPa

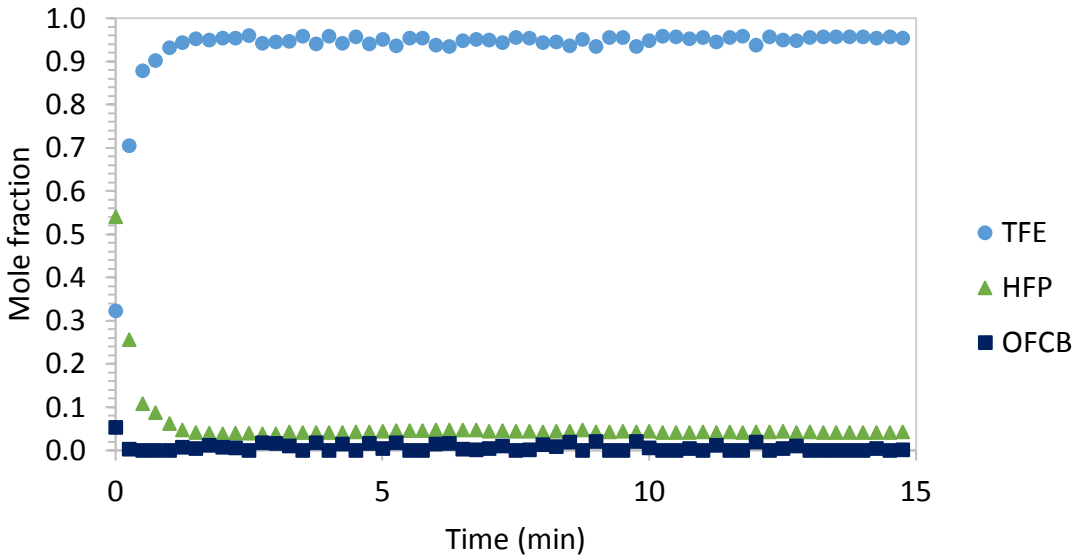

Figure 97: Mole fraction distribution of TFE, HFP, and OFCB for run number 5.

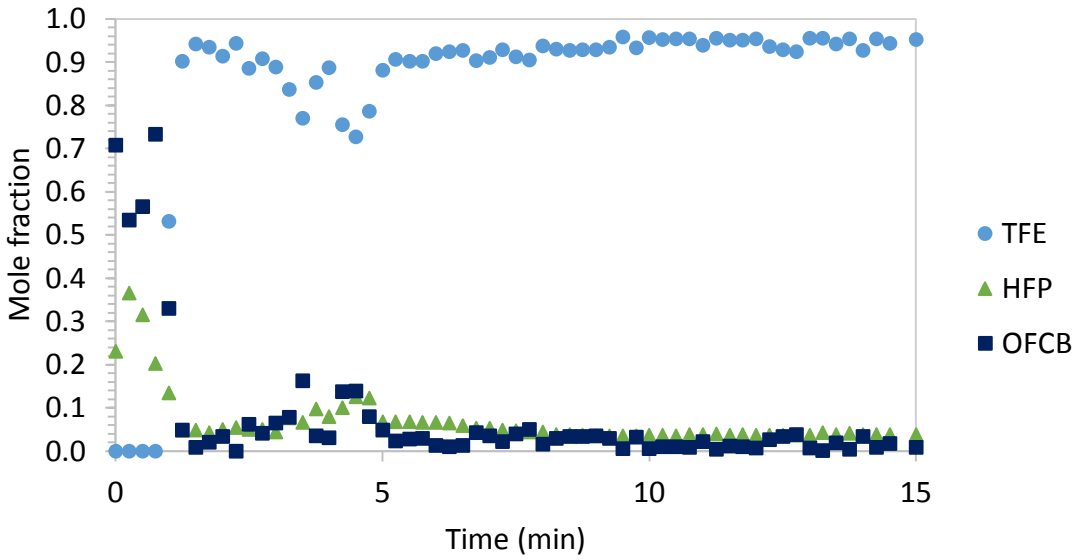

Figure 98: Mole fraction distribution of TFE, HFP, and OFCB for run number 16.

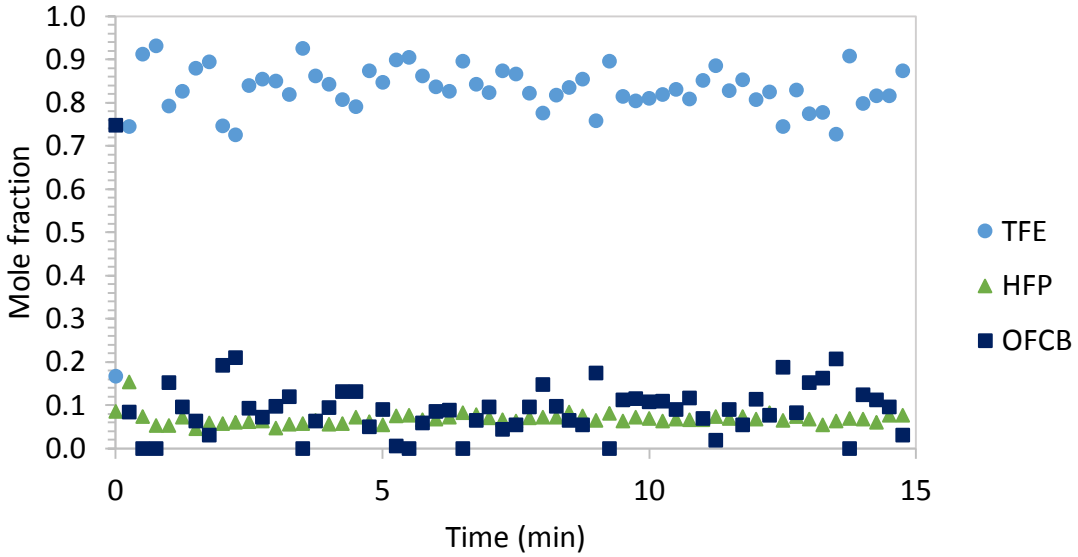

Figure 99: Mole fraction distribution of TFE, HFP, and OFCB for run number 24.

B.3.2 Product distribution at 20 kPa

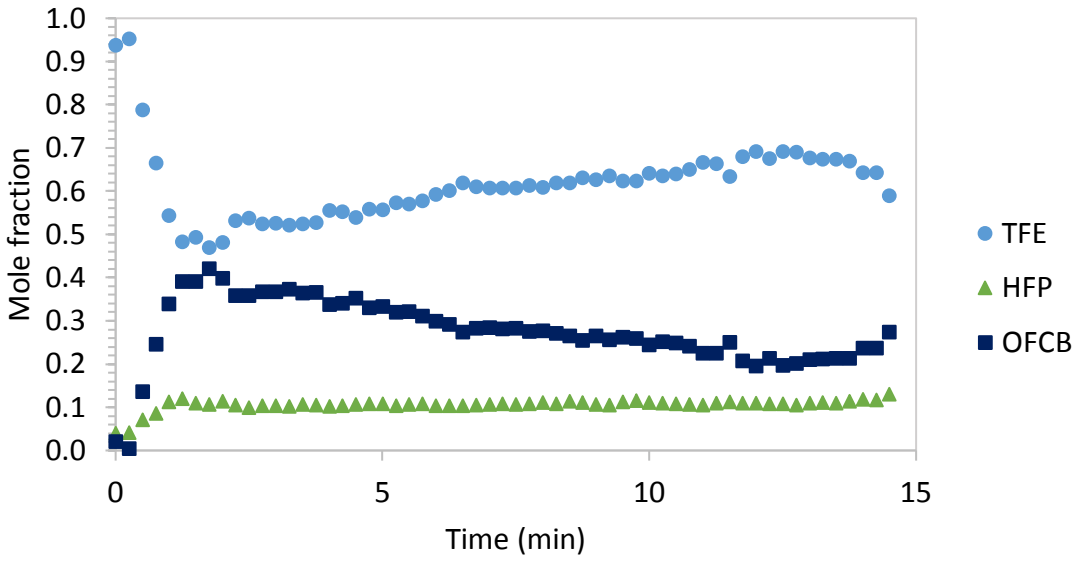

Figure 100: Mole fraction distribution of TFE, HFP, and OFCB for run number 9.

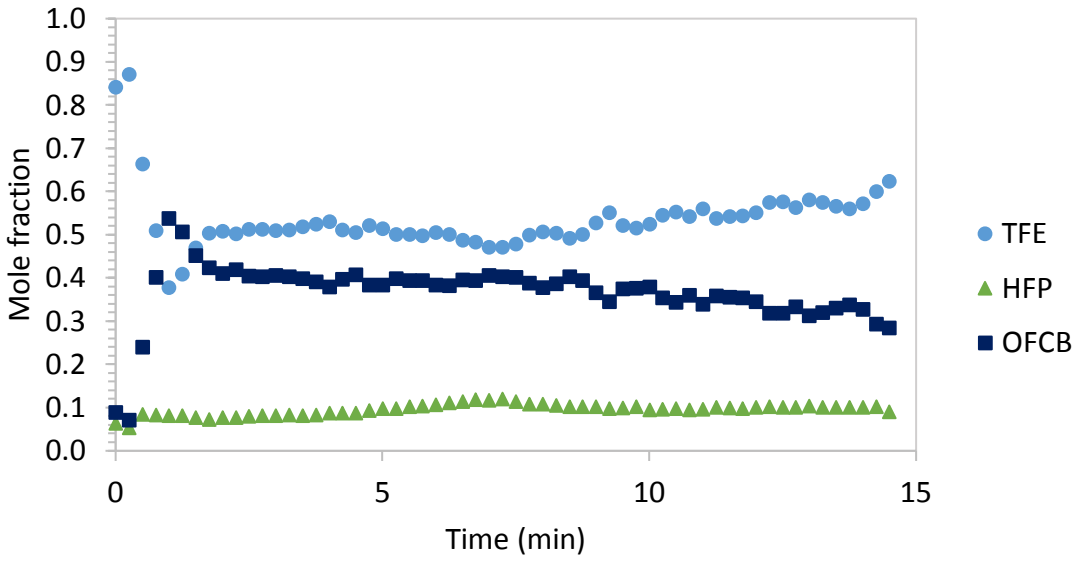

Figure 101: Mole fraction distribution of TFE, HFP, and OFCB for run number 10.

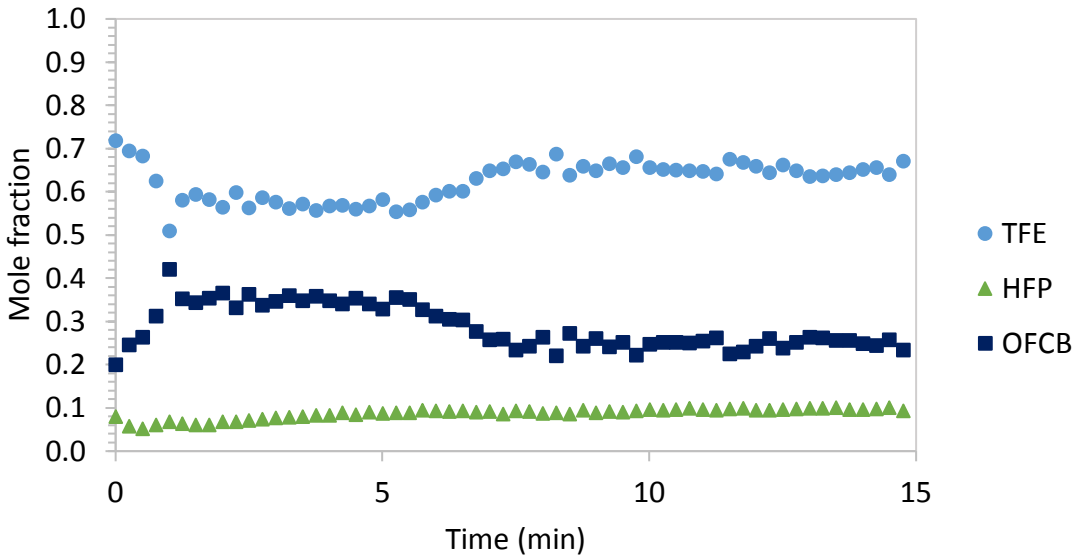

Figure 102: Mole fraction distribution of TFE, HFP, and OFCB for run number 11.

B.3.3 Product distribution at 40 kPa

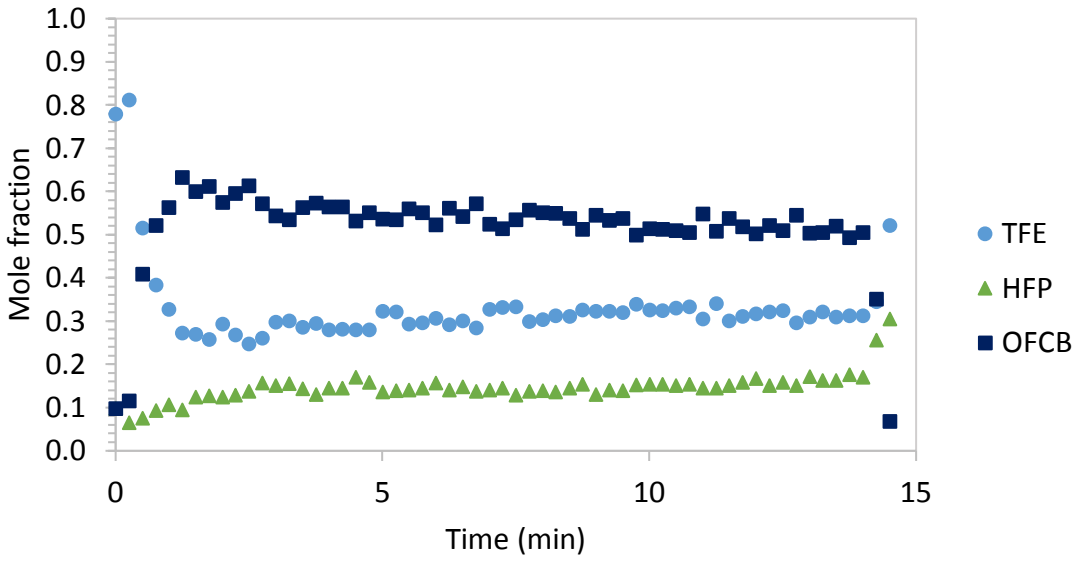

Figure 103: Mole fraction distribution of TFE, HFP, and OFCB for run number 6.

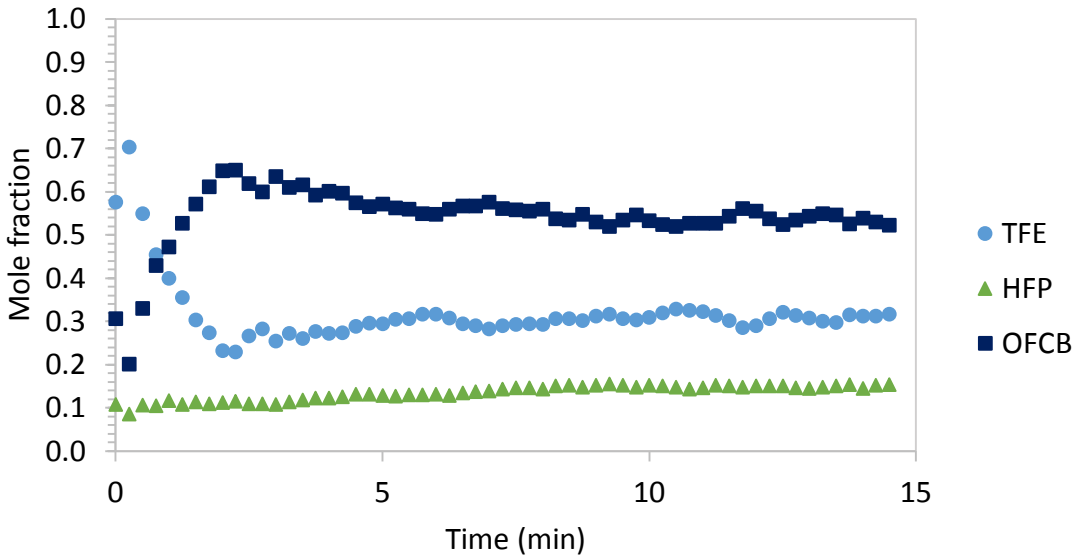

Figure 104: Mole fraction distribution of TFE, HFP, and OFCB for run number 17.

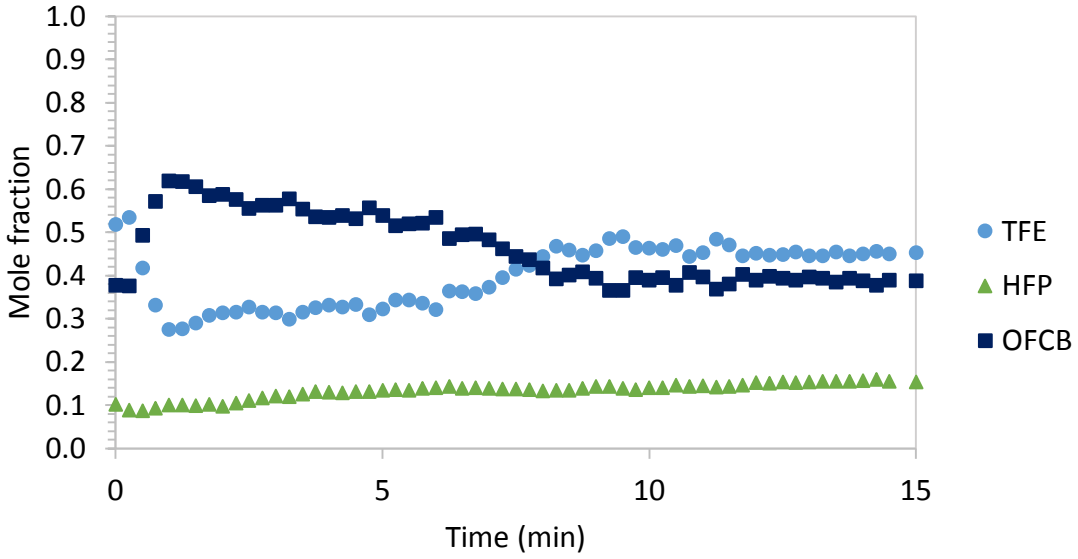

Figure 105: Mole fraction distribution of TFE, HFP, and OFCB for run number 25.

B.4 Experimental data produced at 750 °C.

B.4.1 Product distribution at < 10 kPa

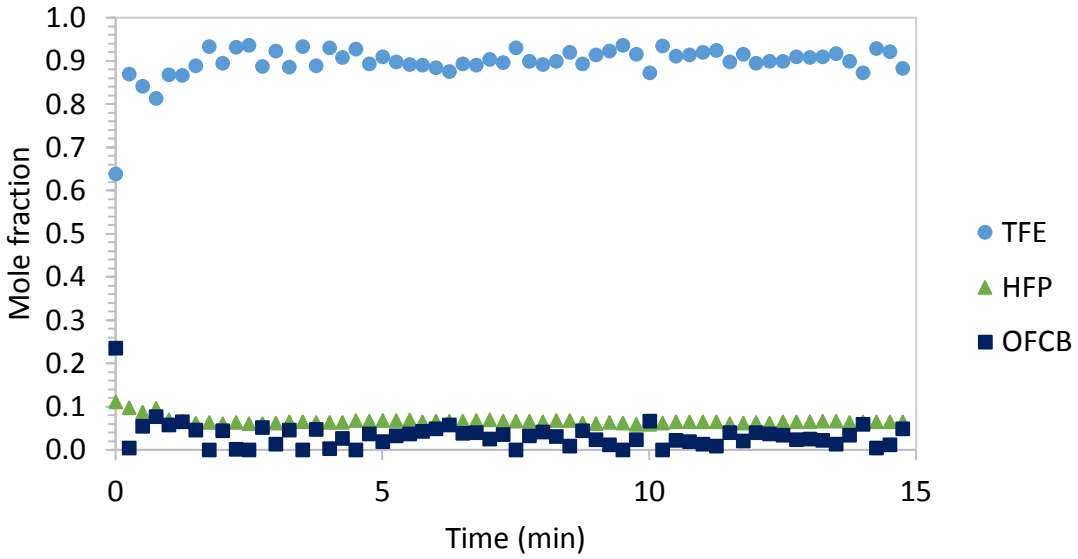

Figure 106: Mole fraction distribution of TFE, HFP, and OFCB for run number 3.

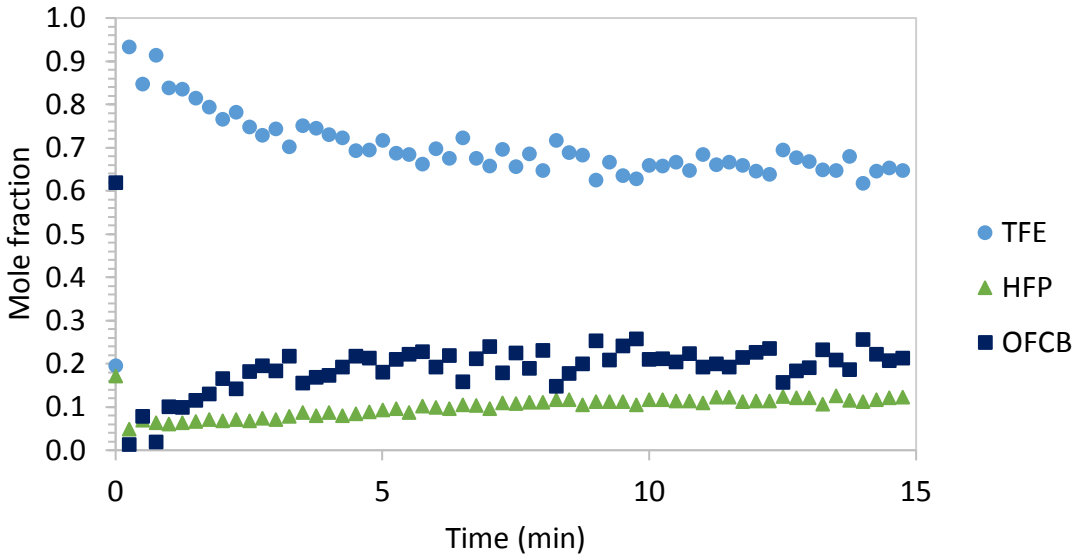

Figure 107: Mole fraction distribution of TFE, HFP, and OFCB for run number 14.

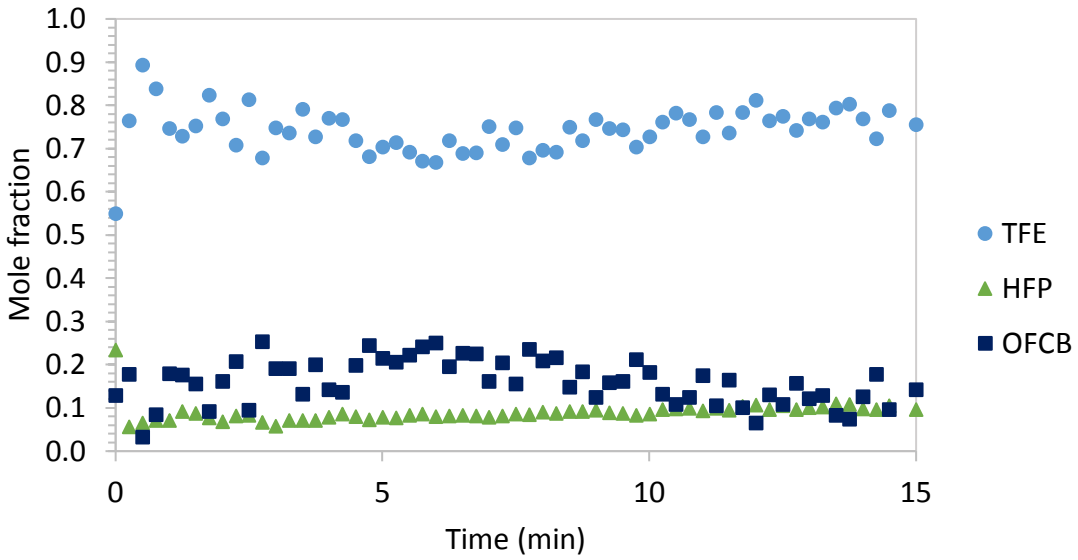

Figure 108: Mole fraction distribution of TFE, HFP, and OFCB for run number 22.

B.4.2 Product distribution at 20 kPa

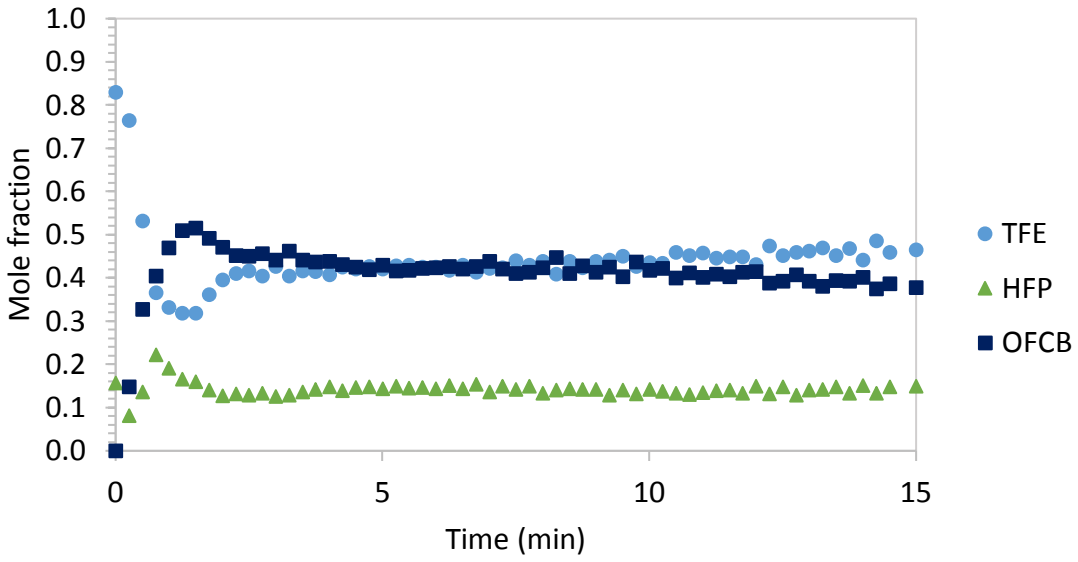

Figure 109: Mole fraction distribution of TFE, HFP, and OFCB for run number 8.

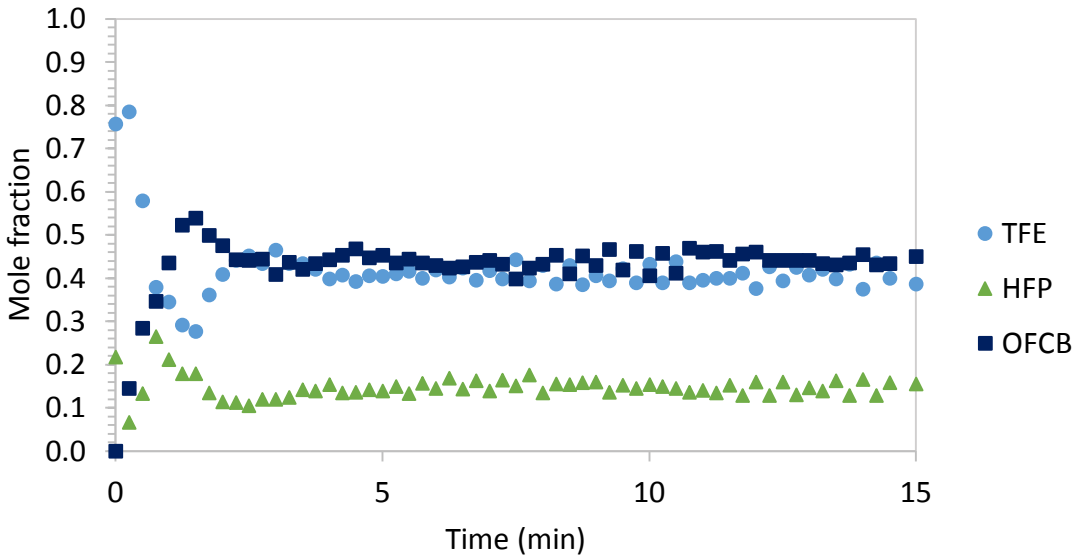

Figure 110: Mole fraction distribution of TFE, HFP, and OFCB for run number 19.

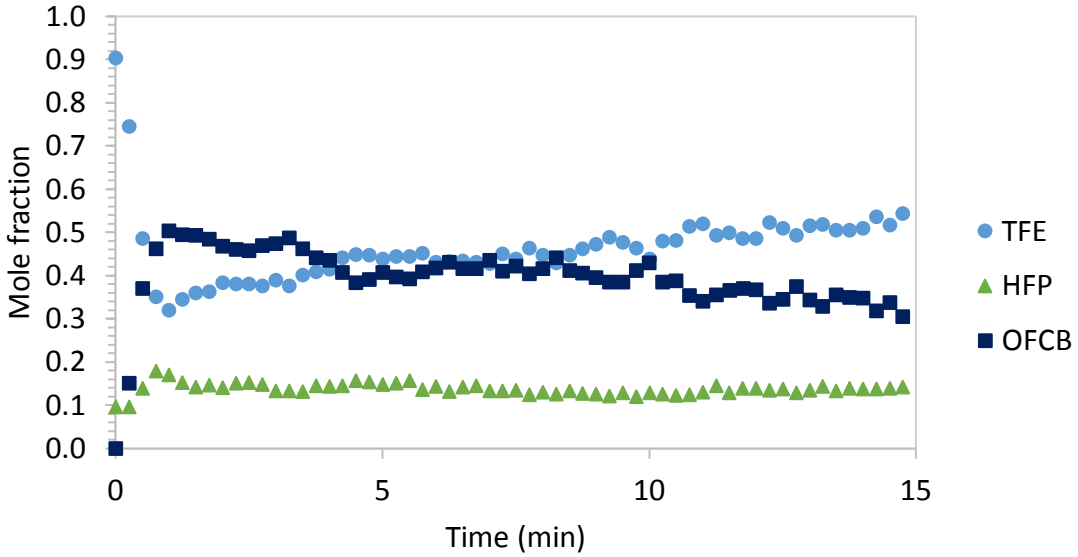

Figure 111: Mole fraction distribution of TFE, HFP, and OFCB for run number 27.

B.4.3 Product distribution at 40 kPa

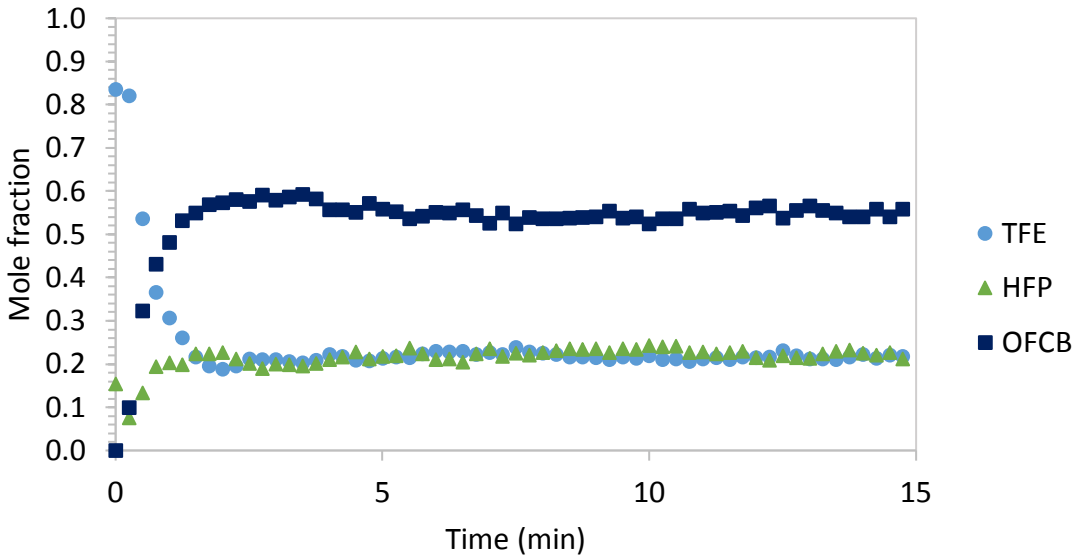

Figure 112: Mole fraction distribution of TFE, HFP, and OFCB for run number 4.

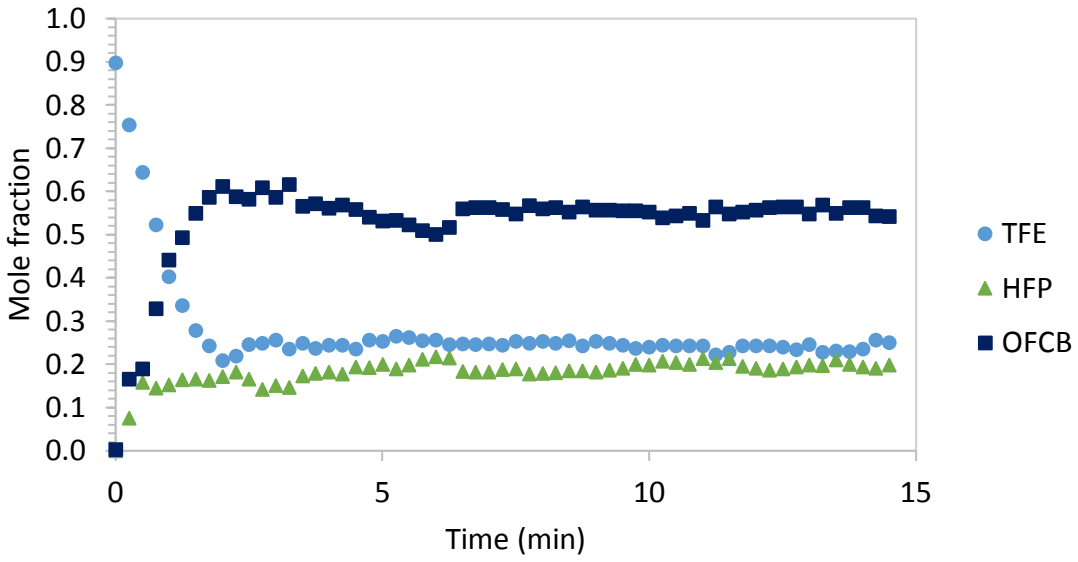

Figure 113: Mole fraction distribution of TFE, HFP, and OFCB for run number 15.

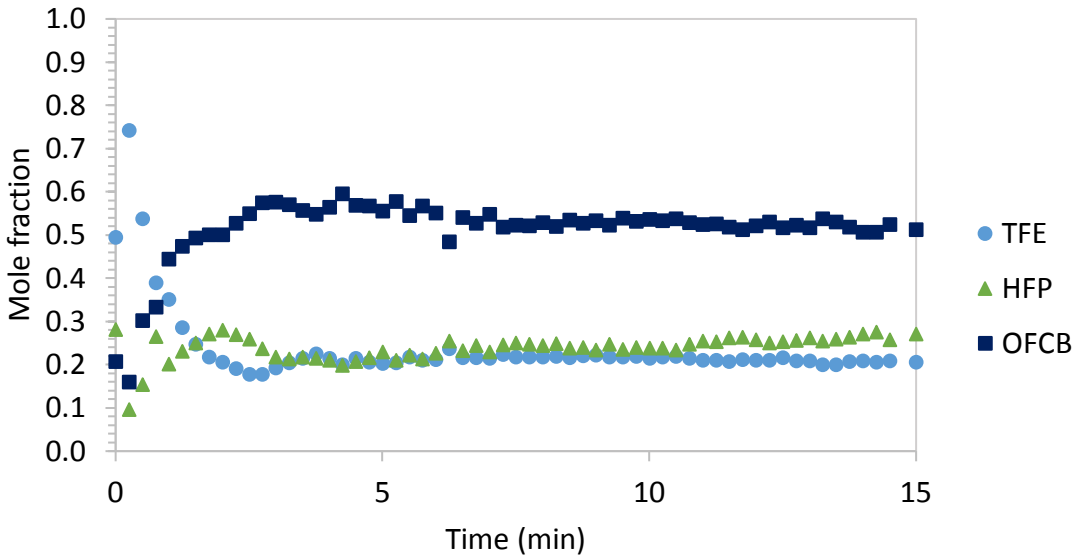

Figure 114: Mole fraction distribution of TFE, HFP, and OFCB for run number 23.

B.5 Experimental response function values

Table 34: The experimental values of response functions $Y_1 - Y_3$.

Run number	Y_1	Y_2	Y_3
		Mole fraction	
1	0.968	0.028	0.0018
2	0.307	0.156	0.532
3	0.904	0.065	0.028
4	0.218	0.225	0.546
5	0.950	0.044	0.005
6	0.319	0.157	0.513
7	0.598	0.106	0.295
8	0.284	0.308	0.388
9	0.633	0.110	0.255
10	0.533	0.102	0.360
11	0.641	0.094	0.263
12	0.903	0.041	0.053
13	0.421	0.135	0.437
14	0.666	0.111	0.208
15	0.245	0.195	0.550
16	0.934	0.044	0.022
17	0.306	0.146	0.544
18	0.594	0.132	0.261
19	0.408	0.148	0.439
20	0.946	0.035	0.017
21	0.309	0.134	0.549
22	0.739	0.092	0.161
23	0.213	0.246	0.529
24	0.873	0.055	0.067
25	0.429	0.144	0.422
26	0.605	0.115	0.274
27	0.476	0.135	0.383

B.6 Arrhenius graphs of the rate constants

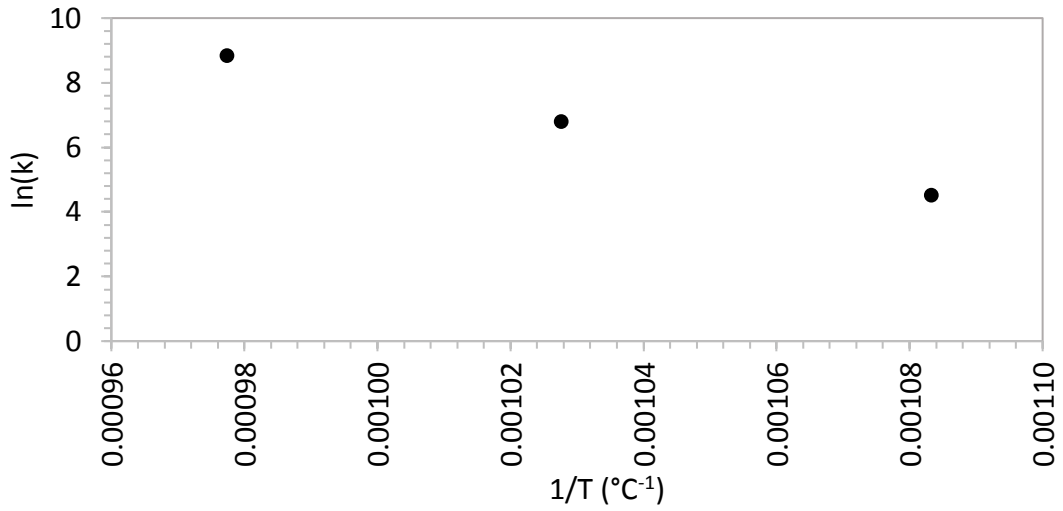

Figure 115: The Arrhenius plot for reaction constant k_1 (reaction (44)).

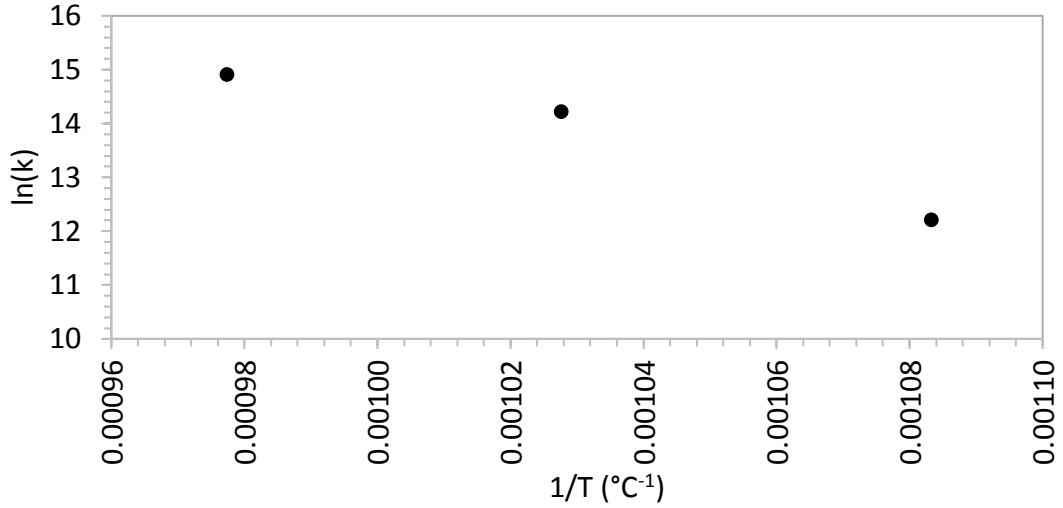

Figure 116: The Arrhenius plot for reaction constant k_2 (reaction (22)).

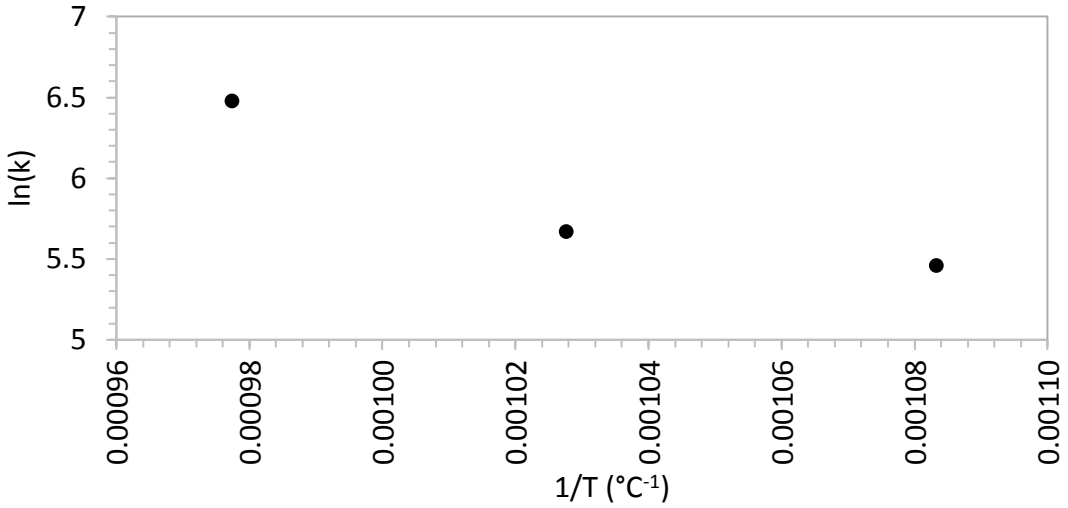

Figure 117: The Arrhenius plot for reaction constant k_3 (reaction (23)).

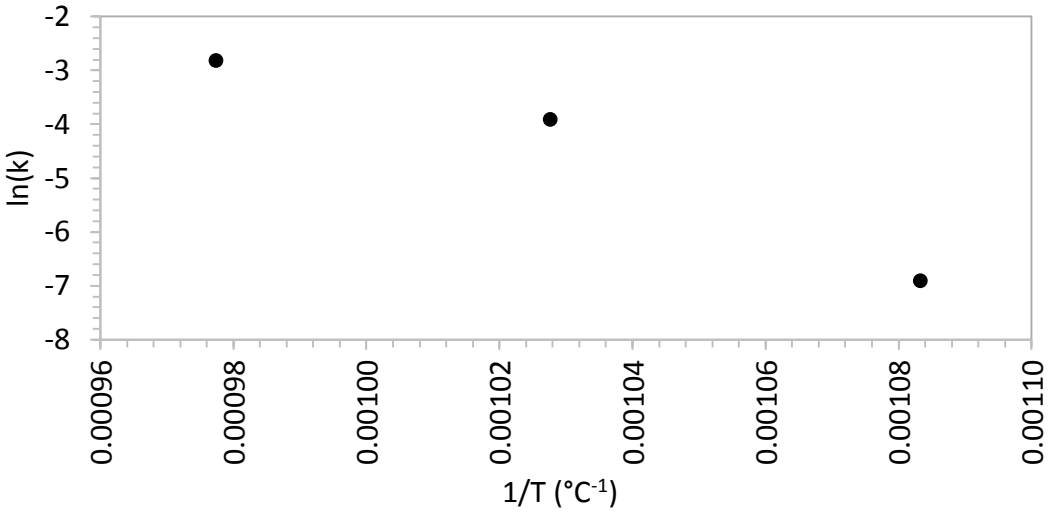

Figure 118: The Arrhenius plot for reaction constant k_4 (reaction (33)).

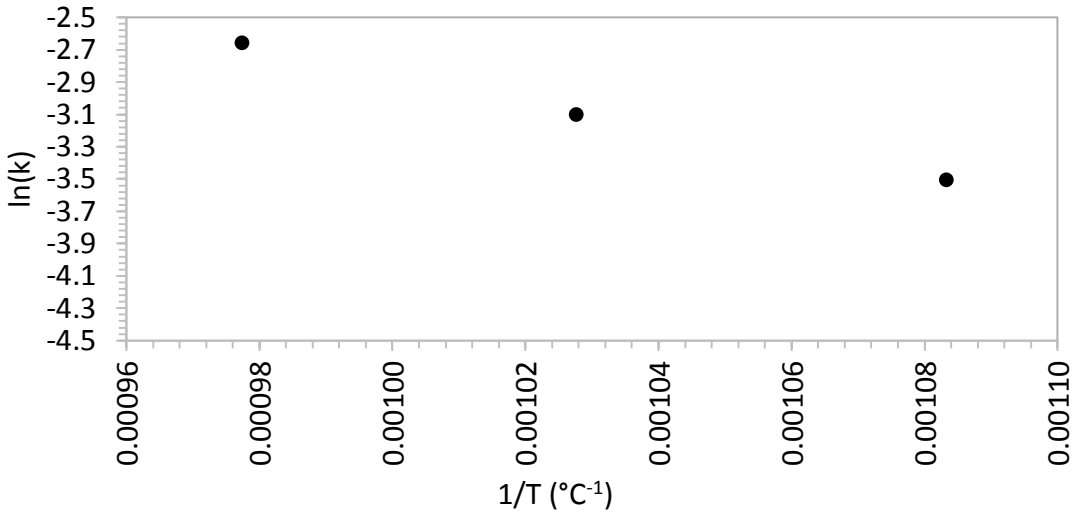

Figure 119: The Arrhenius plot for reaction constant k_5 (reaction (25)).

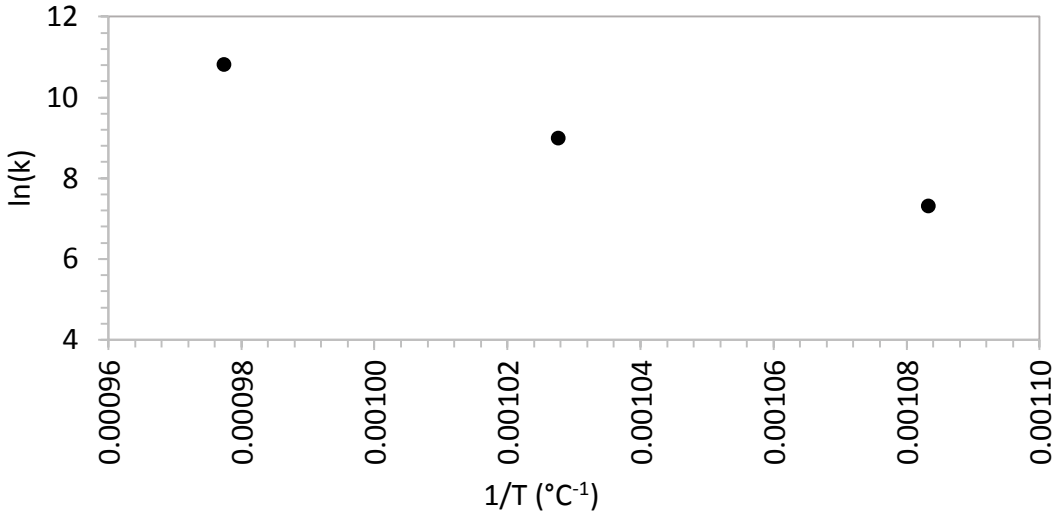

Figure 120: The Arrhenius plot for reaction constant k_6 (reaction (24)).

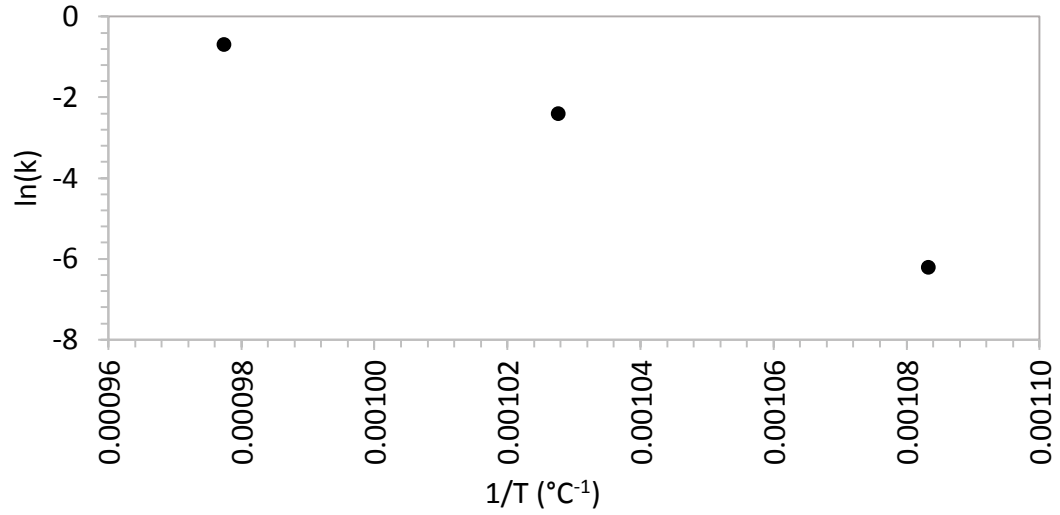

Figure 121: The Arrhenius plot for reaction constant k_7 (reaction (34)).

Appendix C Safety review and standard operating procedure

The following safety review pertains to the newly commissioned, semi-automated, pilot plant scale, continuous PTFE depolymerisation system available in the Fluoropolymer Laboratory at the University of Pretoria. The depolymerisation system has the capacity to depolymerise 11 g PTFE·min^{-1} at various temperatures and pressures. This safety review focuses on the operational procedures and precautions put in place to manage any foreseeable hazards associated with this system. Especially those pertaining to the production of TFE and PFIB, the two most dangerous products of PTFE depolymerisation.

C.1 Engineering data

The operational temperature and pressure limits for the system were determined experimentally and are listed in Table 35 below.

Table 35: Maximum and minimum operating limits of the continuous PTFE depolymerisation system.

Operational limits	Temperature (°C)	Pressure (kPa (abs.))	PTFE flow rate (g·min^{-1})
Steady state operation without a flow of inert gas in the system to promote gas flow			
Maximum	750	40	11
Minimum	650	0	N/A
Steady state operation with a steady inert gas flow.			
Maximum	800	70	11
Minimum	650	0	N/A

C.2 Hazards, safety and first aid.

There are various hazards and safety considerations to be taken into account when working with TFE and the other by-products associated with thermal decomposition of PTFE. Few hazards exist around the handling of PTFE as it is inert, stable, non-toxic and unreactive. However, the same does not hold for the monomer, TFE, as it is highly reactive with oxygen, halogens and oxidising agents such as perchlorates, peroxides, permanganates, chlorates and nitrates (MSDS, Matheson TriGas). TFE is a known deflagrant which could cause the backpropagation of an explosion into storage cylinders, *etc* (Ebnesajjad, 2000). The two main reactions that are of concern when working with TFE are dimerisation and decomposition (Equation (50) and (51)) (Babenko, Lisochkin, and Poznyak, 1993; Hercules *et al*, 2014).

The dimerisation reaction of TFE, that produces octafluorocyclobutane (OFCB), starts at temperatures of about 200 °C and can act as a precursor to the second decomposition reaction (Equation (51)) due to the energy released. TFE usually polymerises above its critical temperature of 33.3 °C and below its critical pressure of 3.94 MPa. In the absence of air, TFE violently decomposed to yield tetrafluoromethane and carbon as indicated in Equation (51). This reaction is usually initiated by hot spots in equipment and can be initiated by the sudden adiabatic compression or expansion of TFE gas (Reza and Christiansen, 2007; Ferrero *et al*, 2013). As Equation (52) indicates, the reaction of TFE with oxygen is highly exothermic, which is why it is imperative that any system containing TFE gas is sealed from the atmosphere to prevent oxygen from leaking in. All of the equipment and piping should be flushed and evacuated thoroughly before an experimental run commences.

$$2C_2F_{4\,(g)} \rightarrow c\text{–}C_4F_{8\,(g)} \qquad \Delta H_R = -206\ kJ{\cdot}mol^{-1} \qquad (50)$$

$$C_2F_{4\,(g)} \rightarrow CF_{4\,(g)} + C_{(s)} \qquad \Delta H_R = -273\ kJ{\cdot}mol^{-1} \qquad (51)$$

$$C_2F_{4\,(g)} + O_{2\,(g)} \rightarrow 2COF_{2\,(g)} \qquad \Delta H_R = -628\ kJ{\cdot}mol^{-1} \qquad (52)$$

Due to its instability, TFE should never be stored without an inhibitor or diluent that prevents auto polymerisation and reduces the TFE explosive hazard. Suitable inhibitors include terpenes, such as α-pinene, terpene B, and D-limonene (Drobny, 2009: 9 - 10). Some suitable diluents include hydrochloric acid, carbon dioxide (Van Bramer, Shiflett, and Akimichi, 1994) and hexafluoropropylene (Van Bramer, 1999). To prevent any storage hazards associated with the handling of TFE, the gas produced during PTFE depolymerisation will not be stored for any length of time. The gas is pumped into a holding cylinder which is transferred to other downstream processes to be used for other research purposes.

Apart from the reactivity and polymerisation hazards mentioned above, TFE is highly flammable and must be kept away from sources of ignitions, oxygen, and/or heat. Fires caused by TFE could produce hydrogen fluoride and should therefore not be extinguished with water. In such an event, the source should be shut off, if it can be done safely, and the fire should be allowed to burn out by itself. Hydrogen fluoride is extremely hazardous and corrosive when in contact with water.

All gases produced by the thermal decomposition of PTFE are asphyxiants and respiratory equipment should be worn in the event of exposure. Apart from TFE and PFIB, none of the other possible products show hazards other than pulmonary oedema or pulmonary congestion. Long term exposure may cause damage to the liver, kidneys, lungs or heart. Little, if any, toxicity information exists for all but PFIB. Acute Exposure Guideline Levels (AEGLs) for PFIB are shown in Table 36 (NAC/AEGL Committee, 2010).

Table 36: AEGL-3 limits for rats exposed to PFIB

10 min	30 min	1 hour	4 hours	8 hours
2.0 ppm	0.67 ppm	0.33 ppm	0.083 ppm	0.042 ppm

C.3 Safety checklist

The following system checks should always be completed before an experimental run is executed:

- Is the compressor operational?
- Is there sufficient inert gas pressure to the system?
- Is there sufficient air pressure to the valve distribution box?
- Is the hopper cleaned and filled with the correct mass of PTFE?
- Was the hopper replaced and all of the fittings connected and fastened?
- Has the holding cylinder been replaced with a clean empty cylinder?
- Is the valve connected to the holding cylinder open?
- Is the table top area surrounding the system clear of any clutter or potentially dangerous substances?
- Is the fume hood above the system switched on and operational?

C.4 Procedures

C.4.1 Equipment layout

The configuration of the equipment in the depolymerisation system is depicted in Figure 122.

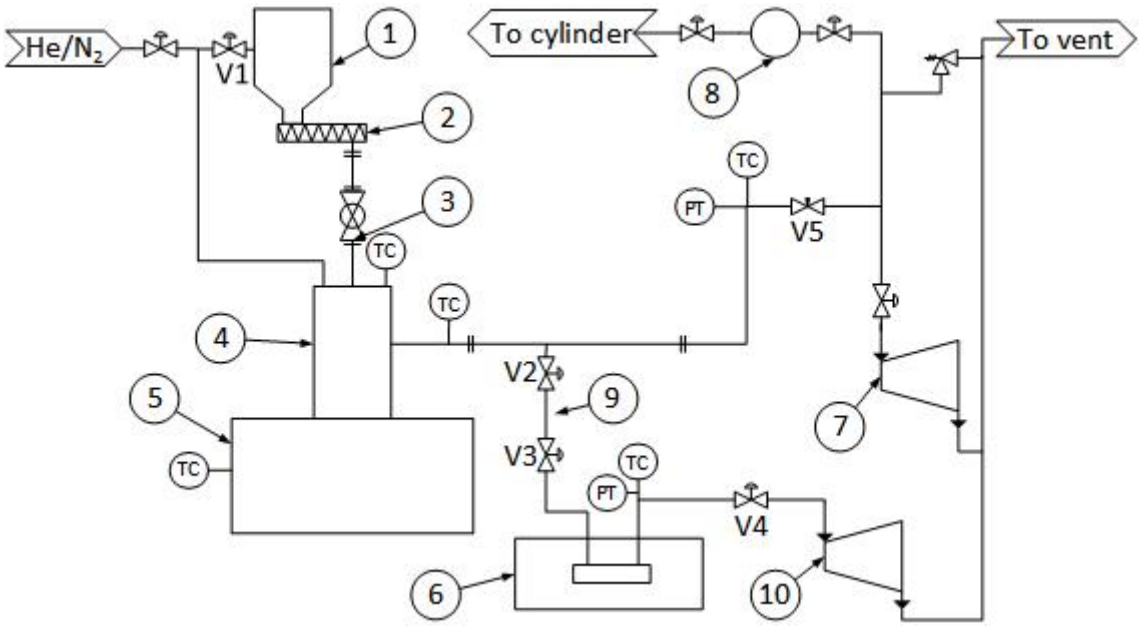

Figure 122: Layout of the continuous depolymerisation setup: (1) hopper, (2) screw feeder, (3) ball valve, (4) pyrolysis reactor, (5) furnace, (6) FTIR spectrometer, (7 and 10) vacuum pump, (8) diaphragm pump, (9) sampling tube.

C.4.2 Analytical equipment

C.4.2.1 PerkinElmer Spectrum Two™ IR Spectrometer

A PerkinElmer Spectrum Two™ Infrared Spectrometer was used to collect all of the experimental infrared spectra. The Spectrum Two™ was configured as follows:

- Scan range: 3000 cm^{-1}–500 cm^{-1}
- Resolution: 4 cm^{-1}
- Data interval: 1 cm^{-1}
- Accumulations: 1
- Scan speed: 0.20 $cm \cdot s^{-1}$
- Source: MIR
- Beamsplitter: Optical KBr
- Detector: $LiTaO_3$
- Windows: KBr
- Optimum range: 7800 cm^{-1} – 450 cm^{-1}

For this system a new custom built gas cell was used. The cell was constructed out of aluminium and has an internal diameter of 30 mm with an optical path length of 90 mm. A detailed design of the gas cell is described in Sonnendecker (2016).

C.4.2.2 PerkinElmer Clarus SQ8 GC-MS

Samples from the depolymerisation system was analysed qualitatively by means of a PerkinElmer Clarus 680 gas chromatograph (GC), coupled to a PerkinElmer Clarus SQ8 C mass spectrometer (MS).

The GC was fitted with an 1 m x 1 mm ID Restek® Hayesep Q™ polymer packed column with a 100/200 mesh size. An electron ionization source (PerkinElmer Marathon Filament, N6470012D) was used for sample ionization. The instrument maintained a system pressure of below 1.5 x 10^{-5} Torr and an injection line temperature of 150 °C (Sonnendecker, 2016). Helium flow was maintained at 20 ml·min^{-1}. The MS transfer line and source were kept at 120 °C. The NIST Mass Spectral Program for NIST/EPA/NIH Mass Spectral Library, version 2.0g (built 19 May 2011) was used for component identification.

The following GC method was used to produce well resolved peaks:

- Hold at starting temperature of 50 °C for 1 min.
- The temperature is then ramped at a rate of 100 °C·min^{-1} to 150 °C.
- The system is then held at 150 °C for 8 min.

C.4.3 Normal operating procedure

Disclaimer: Caution, this procedure/process should ONLY be carried out/operated by a trained person/persons with the proper equipment. The author/s or anyone associated with this project cannot be held liable for practicing anything herein contained.

The following step by step guide provides an in-depth description of the standard operating procedure to follow when operating the continuous depolymerisation system at steady state under no inert gas flow conditions.

- Complete the safety checklist (see Appendix C.3) before starting with this procedure.
- Open National Instruments™ LabVIEW and run the vi files required to operate and control the depolymerisation system.
- In National Instruments™ LabVIEW, enter the required experimental parameters (temperature, pressure, flow rate and experimental run time).
- Start Vacuum Pump 2 (see Figure 122).
- Setup the web camera in front of the viewing glass of the feeder system.
- Start the system by clicking the "Start" button.

- The system will now start with the flush and evacuation cycle. First, the system is evacuated and then pressurised to atmospheric pressure. The system is then evacuated three times, with a waiting period of 30 s between every evacuation to ensure the PTFE bed in the hopper is completely evacuated. After this, a system vacuum check is initialised. If the system is deemed vacuum tight, the reactor is heated to the specified reaction temperature. If the system does not pass the vacuum test, an error message will be displayed and the system will stop automatically.

- While the reactor is being heated, setup the FTIR.
- When the reactor reaches temperature, start the reaction by clicking "Start Run".
  - The ball valve connecting the reactor and the feeder system will open and the system will be evacuated one last time before the feeder motor is turned on. If the reaction pressure is selected to be larger than zero, close the manually operated pressure control valve (V5 in Figure 122). If the reaction pressure is selected to be < 10 kPa (abs.), ensure that valve V5 is fully open.
- PTFE depolymerisation will start as soon as the feeder motor is activated. If the reaction pressure is selected to be higher than < 10 kPa (abs.), wait for the pressure to increase in the reactor as the product gas evolves. Control the reaction pressure throughout the entire run by manipulating valve V5. The FTIR sampling system will start taking samples of the product gas as soon as the feeder motor starts. Monitor the displayed temperature and pressure profiles of the system to ensure that the reaction runs smoothly. Monitor the web camera display to ensure that PTFE is fed continuously throughout the run.
- When the reaction time is reached the feeder motor will stop. Open valve V5 completely.
  - The system will operate for another 10 min at temperature without PTFE flow to ensure than all of the PTFE in the reactor is depolymerised.
- When the reaction stops, the ball valve will close and the furnace will switch off. The system will enter a flush and evacuation cycle to remove any product gas left in the system. Lastly, the system is pressurised with nitrogen gas to atmospheric pressure.

C.4.4 Safety precautions and procedures

To determine the operational hazards associated with the system and the corresponding consequences, a HAZOP analysis of the system was performed. The full HAZOP analysis table is available in Appendix C.5.

The HAZOP analysis revealed that all of the major hazards associated with the depolymerisation system can be minimised by optimal temperature and pressure control. Run away temperatures could lead to the production of PFIB, which is highly undesirable. The reactor temperature will only increase if the furnace controller malfunctions. However, the furnace used in the system heats at a very slow rate, meaning increases in temperatures

beyond that specified will be noticed immediately by the operator. When a temperature increase is noticed, the furnace can be deactivated immediately.

Pressure increases are far more dangerous since a sudden increase in pressure can happen instantaneously. To prevent the pressure from reaching dangerous levels, a pressure relief valve is installed in the system. The system is also monitored continuously throughout an experimental run by an operator, with pressure profile plots displayed for the entire system on the computer screen. Pressure deviations in the system will be detected immediately by the operator. A pressure increase can occur either due to a valve failure, caused by a loss of air pressure to the air-operated valves, or due to pump failure. In the case of air pressure loss the following procedure should be followed:

- Stop the entire system by selecting the "Stop" button. Ensure that the furnace is switched off.
- Switch the gas input connection from the compressed air supply, provided by the compressor, to the inert gas supply provided by the gas cylinders.
- Open all the valves and evacuate the system to remove any evolved product gas.

In the case of a pressure increase due to pump failure, the following procedure should be followed:

- Stop the entire system by selecting the "Stop" button. Ensure that the furnace is switched off.
- Open the three valves of the FTIR sampling system and use the FTIR vacuum pump to evacuate the system.

In the case of a power failure, a backup generator is available and will automatically switch on within minutes. Open all of the required valves and evacuate the system.

Leakages in the system could lead to TFE reacting explosively with oxygen. Since this is a major hazard, it is necessary to prevent this from happening instead of managing the problem when it occurs. Therefore, the entire system should be vacuum checked manually and pressure checked on a regular basis. The system will also be vacuum checked before every experimental run. The entire depolymerisation system, except for the holding cylinder, is situated under and extraction hood as an extra precaution. In case a leak does occur, switch off the furnace and leave the laboratory immediately. The system will automatically be switched off after the reaction time has lapsed.

C.4.5 Waste disposal

The gas produced during a PTFE depolymerisation reaction is pumped to a holding cylinder.

C.4.6 Clean-up procedures

After an experimental run, the system will go into a flush and evacuation cycle to remove any gas product left in the system. The hopper and screw system should be dismantled and cleaned after every five consecutive experimental runs or when the hopper is close to empty. Always ensure that the reactor has cooled down to ambient temperature before removing the feeding system.

To clean the feeding system properly, remove the screw by removing the screw flange. Remove any PTFE left in the hopper and scrape off any PTFE on the sides of the hopper or screw tube. Before refilling the hopper, replace the screw, the screw flange, and the stirrer. Replace the feeder system and ensure that all of the fittings are connected and fastened.

The reactor should be cleaned at least once a month to remove any build-up of PTFE or char.

The valves in the system could experience fine particle build-up due to TFE polymerisation, consequently, the valves should be dismantled and cleaned thoroughly at least once a month to avoid valve failure.

C.5 HAZOP analysis

Item	Study node	Process parameter	Deviation (guide word)	Possible cause	Sub cause	Possible consequences	Action required/followed	Precautions
1A	Screw feeder	Pressure	Higher	The valve failed to open during evacuation cycle.	No gas flow due to compressor shutdown.	1. Cause sudden pressure increase in the reactor when ball valve opens. 2. Could cause PTFE to flow into reactor uncontrollably, causing a very high volume of product gas to be produced if the reactor is at temperature.	1. Stop reaction completely. Switch to inert gas in the cylinder. 2. Stall feeding of PTFE until most of the product gases have been removed.	1. Before the feeder is activated, the ball valve connecting the reactor and feeder will open and the evacuated.
1A	Screw feeder	Pressure	Higher	Pump malfunction or failure	1. Power failure. 2. Pump failure.	1. Cause sudden pressure increase in the reactor when ball valve opens. 2. Could cause PTFE to flow into reactor uncontrollably, causing a very high volume of product gas to be produced if the reactor is at temperature.	1. Stop reaction completely. Wait for back-up generator to start. 2. Stop reaction completely. Repair or replace the pump.	Back-up generator available.
1A	Screw feeder	Pressure	Lower	The valve failed to open during reaction causing pressure difference between reactor and hopper.	No gas flow due to compressor shutdown.	Could affect PTFE flow into the reactor.	1. Stop reaction and switch over to inert gas from cylinders.	

HAZOP analysis cont.

Item	Study node	Process parameter	Deviation (guide word)	Possible cause	Sub cause	Possible consequences	Action required/followed	Precautions
1A	Screw feeder	Pressure	Feeder starts sooner than expected	Malfunction in programming		If the ball valve between the reactor and hopper is not open, PTFE will start to pile up in the feed tube.	Stop the process and clean the feed tube before proceeding.	
1B	Screw feeder	Flow	None	PTFE compaction in hopper		No reaction	Clean and refill the hopper.	
1B	Screw feeder	Flow	Higher			Too much PTFE into the reactor. Overproduction of product gas. PTFE build-up in the reactor.	Stop screw feeder motor and allow the PTFE in the reactor to react completely.	
1C	Screw feeder	Agitation	None	Failure of stirrer motor		Rat-hole formation in hopper occurs. Could cause irregular PTFE flow rate	Stop reaction and replace the motor.	
1C	Screw feeder	Agitation	High	Stirrer malfunction		Over agitation could lead to compression of PTFE in the hopper leading to an irregular flow rate or no flow rate.	Disconnect the stirrer relay and operate stirrer manually.	
2A	Reactor	Temperature	Higher	Malfunctioning of furnace controller		Too high temperatures could lead to the production of dangerous product gases (PFIB), especially at high operating pressures.	Stop reaction by switching off the furnace.	Constantly monitor the temperature profile data during the reaction.

HAZOP analysis cont.

Item	Study node	Process parameter	Deviation (guide word)	Possible cause	Sub cause	Possible consequences	Action required/followed	Precautions
2B	Reactor	Pressure	Higher	Pump malfunction or failure	1. Power failure. 2. Pump failure.	At high pressures, the production of toxic product gases increase. With increasing pressure, the risk of TFE auto polymerisation increases.	1. Stop reaction completely. Wait for back-up generator to kick in. 2. Stop reaction completely. Repair or replace the pump.	Pressure relieve valve installed in the system to ensure that the pressure never exceeds atmospheric.
2B	Reactor	Pressure	Higher	Valve failure	No gas flow due to compressor shutdown.	1. Cause sudden pressure increase in the reactor when ball valve opens. 2. Could cause PTFE to flow into reactor uncontrollably, causing a very high volume of product gas to be produced if the reactor is at temperature.	Stop reaction and switch over to inert gas from cylinders.	
2C	Reactor	Flow	Higher	VFD control failure		Too high a PTFE flow rate could cause a build-up of melted PTFE in the reactor disrupting the flow of gases and PTFE.	Stop screw feeder motor and allow the PTFE in the reactor to react completely.	.